Monazite geochronology and pressure-temperature constraints on Early Neoproterozoic and Caledonian-aged metamorphism in the Shetland Islands

Kathryn A. Cutts
Supervisor: Martin Hand
Honours student, Continental Evolution Research Group
Geology and Geophysics, School of Earth and Environmental Sciences,
The University of Adelaide, Adelaide, SA 5005, Australia

2010

Table of Contents

Abstract

EMPA U-Th-Pb and LA-ICPMS U-Pb monazite data and pressure-temperature calculations on lower to upper amphibolite facies rocks in the Shetland Islands constrain the evolution of Caledonian metamorphism and have identified an early Neoproterozoic metamorphic basement to the Dalradian Supergroup. EMPA monazite and LA-ICPMS data suggest that peak metamorphism occurred at *c.* 460 Ma in the central and northern Shetland Islands, and at *c.* 910 Ma in the basement sequences. These Neoproterozoic age samples have no evidence of Caledonian aged monazite and have been interpreted to be a metamorphic basement to the Dalradian, possibly forming part of the Moine Supergroup. Low-grade rocks immediately beneath the Shetland ophiolite on the island of Unst are characterised by garnet-staurolite-chloritoid-chlorite assemblages with up-P prograde paths culminating in peak conditions of *c.* 550°C and 7-8 kbars. In the slightly higher-grade rocks on Yell, prograde staurolite-biotite-muscovite assemblages have been replaced by peak garnet-kyanite assemblages that formed at *c.* 650°C and 8 kbar. At Lunna Ness on North-eastern Mainland, metapelites had peak assemblages of garnet-sillimanite-biotite-rutile-quartz, which replaced the earlier garnet-biotite-muscovite-kyanite-quartz assemblages. In mafic lithologies, the peak assemblages are defined by garnet-hornblende-plagioclase-quartz. Peak assemblages were associated with partial melting and local granite emplacement and formed at around 700-800°C and 9-10 kbar. Based on available data, the thickness of the Shetland ophiolite is insufficient to have generated the peak metamorphic pressures via obduction. It is therefore likely that peak Caledonian metamorphism predates the ophiolite obduction event.

The Caledonian Orogen (Fig. 1A) marks the collision of Baltica and Laurentia in an event that produced an orogenic belt of Himalayan scale. The products of this orogenic event are preserved in east Greenland (Kalsbeek *et al.* 2000; Watt *et al.* 2000; Watt & Thrane 2001; Gilotti & Elvevold 2002), western Scandinavia (Schwab *et al.* 1988; Daly *et al.* 1991; McKerrow *et al.* 2000; Roberts 2003), the British Isles (Noble *et al.* 1996; Highton *et al.* 1999; Millar 1999; Soper *et al.* 1999; Strachan 2000; Strachan *et al.* 2002) and in the Appalachian belt of the eastern United States (Schwab *et al.* 1988; McKerrow *et al.* 2000; Murphy *et al.* 2004; Murphy *et al.* 2004).

In recognition of the importance of the Caledonian Orogeny in shaping the tectonic architecture of northern Scotland and Ireland (e.g. Highton *et al.* 1999; Soper *et al.* 1999; Strachan 2000;

Strachan *et al.* 2002), there has been an enormous amount of work undertaken to understand the stratigraphic development of the basins and their basement, which were deformed in the Caledonian Orogeny, the timing of events, the structural architecture and evolution and the metamorphic conditions that accompanied deformation (e.g. Schwab *et al.* 1988; Millar 1999; Soper *et al.* 1999; McKerrow *et al.* 2000; Strachan 2000; Strachan *et al.* 2002). In many ways, the early work on the Caledonian marked the birth of modern tectonic analysis and was pivotal in seminal works such as Ramsay (1963).

The Caledonian is defined by two phases of orogenesis. The earliest event is the Grampian Event, which occurred between about 480 to 460 Ma with probable peak metamorphism at *c.* 470 Ma (Soper *et al.* 1999; Oliver *et al.* 2000; Strachan *et al.* 2002). In the Scottish Highlands, the Grampian orogenic event caused deformation in the Grampian Highlands (the region between the Great Glen Fault and the Highland Boundary Fault; (Fig. 1B) an area consisting primarily of Dalradian Supergroup sequences). Deformation in the Dalradian Supergroup consists of the formation of large-scale recumbent folds such as the Kinlochleven antiform. Folding was accompanied by shear zone formation. Several generations of folding occurred, deformation was accompanied by regional prograde metamorphism to amphibolite facies (Phillips *et al.* 1999). The Grampian orogenic event is thought to have been caused by the onset of closure of the Iapetus Ocean, specifically by the collision between an oceanic arc and Laurentia (Dewey & Ryan 1990; Soper *et al.* 1999; Phillips *et al.* 1999; Strachan 2000; Strachan *et al.* 2002).

The later Scandian Event (435-410 Ma; Strachan *et al.* 2002; Kinny *et al.* 2003) is thought to mark the completion of closure of the Iapetus Ocean with the collision between Baltica and Laurentia. The Scandian Event principally affected the Moine Supergroup, creating the tectonic form surface within the Moine metasediments (Friend *et al.* 1997; Kinny *et al.* 1999; Strachan *et al.* 2002; Kinny *et al.* 2003) and generating west-vergent basement-cored nappe systems (Friend *et al.* 1997; Rogers *et al.* 1998; Storey *et al.* 2004). It was probably also at this time that most of the movement occurred along the large thrusts and sinistral strike slip faults in the region (Strachan *et al.* 2002; Storey *et al.* 2004). These structures include the Moine Thrust, which transported the orogen for up to 150 km westwards across Cambrian limestones and Palaeoproterozoic basement in the Caledonian foreland (Friend *et al.* 1997; Rogers *et al.* 1998; Strachan *et al.* 2002; Friend *et al.* 2003). It is thought that the strike slip faults have taken up to 2000 km of slip, with the Great Glen Fault taking up to 200 km alone and juxtaposing the

Northern Highland and Grampian terranes. For this reason the effects of the Scandian Event are restricted to the Northern Highland terrane since the two regions were not in close proximity during the Scandian. In the Northern Highland terrain, the Scandian Event was associated with Barrovian metamorphism with the development of garnet-staurolite-kyanite-bearing assemblages that formed at around 8 kbar and 650°C (Strachan *et al.* 2002).

The vast bulk of the work on the Caledonian of the British Isles has focussed on Scotland and Northern Ireland (Highton *et al.* 1999; Phillips *et al.* 1999; Robertson & Smith 1999; Smith *et al.* 1999; Strachan 2000; Strachan *et al.* 2002). In contrast, comparatively little effort has been focussed on the part of the orogen preserved in the Shetland Islands (e.g. Flinn & Pringle 1976; Flinn 1985; Prichard 1985; Fig. 2). This is despite the Shetland Islands containing an equivalent stratigraphic architecture to the Northern Highland and Grampian terranes (Flinn 1985; Strachan *et al.* 2002), which are separated by the interpreted extension of the Great Glen Fault (Flinn 1985; Ritchie *et al.* 1987; Flinn & Oglethorpe 2005). The western margin of the orogen in the Shetland region is bounded by the extension of the Moine Thrust, which carries the orogen across an undeformed Palaeoproterozoic foreland (Ritchie *et al.* 1987). Additionally the Shetland Islands contain a well-preserved ophiolite package sitting at the top of the structural section (Flinn 1985; Prichard 1985; Spray 1988; Spray & Dunning 1991; Strachan *et al.* 2002; Flinn & Oglethorpe 2005). Therefore the Shetlands arguably preserves the best cross section of the Caledonian Orogen in the British Isles. Despite easy accessibility and extensive outcrop there has been comparatively little work done to constrain the timing of tectonic events and the P-T evolution associated with Caledonian deformation.

In this study an integrated approach using metamorphic pressure-temperature calculations and EMPA U-Th-Pb and LA-ICPMS U-Pb monazite dating is used to determine the physical conditions and evolution of metamorphic assemblages in the Shetland Islands, and to constrain the timing of tectonism. This represents one of the few studies of this type undertaken in the Shetland section of the Caledonian Orogeny, and is the first study to directly date the timing of peak metamorphism in that part of the orogen. The results of this study show that Barrovian prograde Caledonian metamorphism at *c.* 465 Ma was associated with up-pressure P-T paths culminating in burial depths of around 30 km under modest geothermal gradients. This metamorphic expression is consistent with crustal thickening in a convergent orogen. The geochronological data has also identified the presence of an early Neoproterozoic metamorphic basement to the Dalradian sequences.

Geological setting

The geology of the Shetland Islands can be roughly divided into five time slices (Fig. 2):

1. Lewisian >1800 Ma,
2. Moine Superoup sedimentary succession *c.* 950-850 Ma,
3. Dalradian Supergroup sedimentary succession *c.* 600-480 Ma,
4. Caledonian Orogenesis (including emplacement of the Shetland Ophiolite) *c.* 480-410 Ma,
5. Silurian to recent units (post 430 Ma)

Lewisian

In the west of the Shetland Islands are the Archaean to Paleoproterozoic rocks that comprise the foreland to the Caledonian Orogen. These are exposed in North Mainland and parts of Yell (Fig. 2). There are two types of basement gneiss, the western and the eastern. The western gneisses are banded orthogneisses with some interbanded amphibolites, which are cut by foliated pegmatites (Flinn 1985). A zone of mylonitization and shearing is present within these gneisses. Hornblende grains taken from an intrusion into these gneisses have given K-Ar ages of 2873-2661 Ma (Flinn *et al.* 1979; Flinn 1985). The eastern gneisses are very similar to the Lewisian inlier of Scotland (Flinn 1985). These gneisses are schistose, feldspathic rocks with bands of amphibolite and contain lenses of serpentinite ranging in size from a few cm to tens of metres. A large body of serpentinised ultrabasic rock gave K-Ar ages ranging from 2313-1043 Ma (Flinn *et al.* 1979; Flinn 1985).

Moine Supergroup

Directly to the east of the Archaean-Palaeoproterozoic Lewisian is the Moine Supergroup, which outcrops in North Mainland and makes up all of the island of Yell, where it is locally known as the Yell Sound Division (Fig. 2; Flinn 1985; Flinn 1994). The Moine sequences of North Mainland are interleaved with the Lewisian basement gneisses discussed above (Fig. 2; Flinn 1985; Strachan *et al.* 2002). The rocks of North Mainland are predominantly silicious psammites however, garnet-mica psammites and metapelites are also present. The entire sequence is highly schistose and this increases near contacts with the basement gneisses. Bands of pelitic garnet-mica schists occur frequently in the sequence but are more common near contacts with the basement gneisses (Flinn 1985).

The Yell Sound Division lies to the east of the Walls Boundary Fault in the Shetland Islands and has also been equated with the Moine Supergroup of Scotland, which was deposited between *c.* 1000 and 900 Ma (Noble *et al.* 1996; Millar *et al.* 1999; Tanner & Bluck 1999; Strachan *et al.* 2002). This sequence may have been separated by 200 km laterally from the Moine rocks of North Mainland (Flinn *et al.* 1972; Flinn 1985; Strachan *et al.* 2002). The Yell Sound Division consists of steeply dipping silicious psammites and interbedded hornblende schists with occasional, widely scattered pelites containing staurolite and kyanite. Garnet is present throughout the Yell Sound Division (Flinn 1985; Flinn 1994). The division contains a number of gneissic belts up to several hundred metres wide. These have developed by recrystallization of the psammite or by tectonism of early granitic intrusions (Flinn 1985). Thin slices of Lewsian-type basement gneiss are also interleaved with the rocks of the Yell Sound Division (Strachan *et al.* 2002). Lithologiocally the Moine rocks on North Mainland bears a strong resemblance to the Morar Group in the Scottish Highlands (Flinn 1988; Strachan *et al.* 2002). Conceivably the Yell Division correspond to the Glenfinnan Group, which overlies the Morar Group in Scotland (Flinn 1985; Flinn 1988; Strachan *et al.* 2002). The total stratigraphic thickness of the Moine sequences is difficult to estimate due to the intensity of deformation, however it is thought to be around 10 km (Tanner & Evans 2003; Cawood *et al.* 2004).

The interpreted Morar Group equivalents on North Mainland have been thrust westward across the Lewisian basement along a gently to moderately east-dipping zone of mylonites up to 1 km thick (Flinn 1985; Ritchie *et al.* 1987; Strachan *et al.* 2002). This mylonite zone almost certainly represents a continuation of the Scandian-aged Moine Thrust, which separates the same lithological divisions in the Northwestern Highlands terrain (Ritchie *et al.* 1987).

The Morar Group and possible Glenfinnan equivalents on Yell are separated by the Walls Boundary Fault, which is interpreted (Ritchie *et al.* 1987; Strachan *et al.* 2002; Flinn & Oglethorpe 2005) to be the extension of the Great Glen Fault. If this interpretation is correct, then the sequences on either side may record distinctly different Scandian histories, as is the case in the Scottish Highlands (Strachan *et al.* 2002).

Dalradian Supergroup

The Dalradian sequences make up most of Mainland and the western half of the islands of Unst and Fetlar (Fig. 2). The boundary between the correlative Moine sediments of the Yell Sound Division and the Dalradian Supergroup of Shetland is represented by the Boundary Zone on the

eastern edge of Yell. The Boundary zone is a narrow zone a few hundred meters wide made up of a combination of laminated and coarsely bedded psammitic rocks. On the eastern side of the boundary zone is a sequence of mylonites known as the Harcosay Slide and on its western side is the Valayre Gneiss. The Valayre Gneiss is an augen gneiss containing porphyroblasts of K-feldspar up to 4 cm in size, which separates the inferred Dalradian and Moine sequences throughout the Shetland Islands. The Valayre gneiss runs from the top of the island of Yell, south along the eastern edge of Yell, through the peninsula of Lunna Ness on Mainland where it is truncated by the Nesting Fault and then also along the western side of mainland, separating the Dalradian and Moine units there (Flinn 1985; Flinn 1994).

In the Shetlands, the Dalradian Supergroup has been split into three divisions. The Scatsca Division which outcrops on eastern Unst and Fetlar along with central Mainland directly east of both the Nesting and Walls boundary faults. This division is probably the equivalent of the Lower Dalradian (or Appin Group) of Scotland, and consists of impure quartzites interlayered with psammopelitic schists and metapelitic schists, which contain staurolite, kyanite and garnet. In some localities mafic layers of hornblende schist are present (Flinn 1985). The Whiteness Division outcrops in central Mainland between the Walls Boundary and Nesting Faults and consists predominantly of limestone units with interlayered laminated psammites and semipelites. This division is probably the equivalent of the Argyll Group of Scotland. The Clift Hills Division outcrops in Southern Mainland and consists of metavolcanic-clastic units followed by a 3km thick sequence of psammopelitic phyllites with some interbedded quartzite and limestone bands (Flinn 1985). It is probably equivalent to the Southern Highland Division of Scotland (Miller & Flinn 1966; Flinn 1985; Strachan *et al.* 2002).

The Dalradian Supergroup has an apparent total thickness of 25 km, although this complete vertical thickness was probably not deposited in one place. Age constraints on Dalradian sedimentation are poor. Sedimentation started some time after *c.* 800 Ma. This is the age of pegmatites that intrude the Glen Banchor sucession, which underlies the Grampian Group in Scotland (Highton *et al.* 1999; Strachan *et al.* 2002). Sr/Sr whole rock isotope data from metacarbonate rocks from the Grampian Group have values consistent with the global strontium seawater signature between 800 Ma and *c.* 670 Ma (Strachan *et al.* 2002). The Port Askaig Tillite at the base of the Argyll Group in Scotland is thought to correlate with either Sturtian glaciation (720 Ma) or the Varangerian tillites of Norway that are 620-590 Ma in age (Condon & Prave 2000; Gorokhov *et al.* 2001; Brasier & Sheilds 2000; Strachan *et al.* 2002). Deposition of the

Dalradian Supergroup is thought to have lasted between 300 and 150 Ma depending on the onset of deposition (between 800 and 670 Ma) and the reliability of age indicators in the upper Dalradian (Strachan *et al.* 2002)

Caledonian Orogenesis

The Shetland Ophiolite was emplaced during Caledonian Orognesis. It outcrops on Unst and Fetlar but is best preserved on the island of Unst. It consists of two thrust sheets that represent an original structural thickness around 8-10 km each (Spray 1988; Spray & Dunning 1991; Strachan 2000; Strachan *et al.* 2002). The ophiolite does not display a full sequence of oceanic crust, rather a partial section through the crust. Four distinct rock units are present: a basal serpentinised harzburgite tectonite (up to 2 km thick), a dunite-wehrlite-clinopyroxenite cumulate unit (up to 3 km thick), a gabbro unit (up to 1.5 km thick) and a discontinuously exposed basic dyke sequence (usually greater than 500 m in thickness; Spray 1988). A sequence of sedimentary rock is present between the two thrust sheets. These packages were thought to have been deposited after the obduction of the first ophiolite thrust sheet due to erosion of the thrust sheet and nearby metamorphic basement forming a sequence of fine-grained laminated silicious sediments locally conglomeratic (an example of which is the Funzie comglomerate, a thick sequence, mostly consisting of quartzite pebbles but with some pebbles of ophiolite affinity, which is exposed on the island of Fetlar; Flinn 1985; Flinn & Oglethorpe 2005).

U-Pb dating of a zircon from a plagiogranite within the gabbro unit of the ophiolite has yielded an age of 492 ± 3 Ma (Spray & Dunning 1991). This plagiogranite was formed by the partial melting of amphibolitized gabbros near the spreading centre, and is likely to constrain the age of the oceanic crust, which makes up the ophiolite (Spray & Dunning 1991). Age data has also been gathered from the metamorphic sole sequence of the ophiolite, a sequence of hornblendic and graphitic schists known as the Norwick hornblendic schists. K-Ar dating of hornblende from this unit has yielded ages of 465 ± 6 Ma, 471 ± 3 Ma, 473 ± 6 Ma, 476 ± 6 Ma and 479 ± 6 Ma (Spray 1988). These ages are interpreted as the age of obduction of the ophiolite (Spray 1988; Flinn *et al.* 1991; Spray & Dunning 1991; Flinn & Oglethorpe 2005).

The deformation in the Shetland Islands during the Caledonian Orogeny occured in two phases. During the Grampian Event (470-460 Ma), the Shetland Ophiolite nappe was thrust westward over Moine and Dalradian sequences that are now exposed on the islands of Unst and Fetlar.

These Moine and Dalradian sediments underwent Barrovian metamorphism along with regional folding (Strachan *et al.* 2002).

The later Scandian Event (435-410 Ma) resulted in the formation of strike-slip faults such as the Walls Boundary Fault, the Nesting Fault and its splays, the Arisdale Fault and the Bluemull Sound Fault. Additionally the extension of the Moine Thrust is interpreted to pass through North Mainland, carrying Morar Group sequences westward across the Caledonian Foreland. Packages in the hanging wall of the Moine Thrust are highly deformed by regional-scale mylonite fabrics that interleave cover and basement (Strachan *et al.* 2002).

The Moine and Dalradian sequences east of the Walls Boundary Fault have undergone lower to upper amphibolite-grade metamorphism (Flinn 1985; Strachan *et al.* 2002). In general, there is westward increase in metamorphic grade from chloritoid-bearing assemblages in the immediate footwall of the ophiolite sequence on Unst and Fetlar to kyanite-bearing assemblages on Yell and Mainland (Flinn 1994; Flinn *et al.* 1996). In aluminous metapelitic rocks, peak assemblages generally contain garnet and kyanite, and in mafic rocks garnet-hornblende. West of the Walls Boundary Fault, the Morar Group has undergone amphibolite-grade metamorphism producing coarse-grained garnet-bearing assemblages that have subsequently been deformed by an intense greenschist-grade west-directed mylonitic fabric, which is probably Scandian in age, based on structural correlations with the NW highland terrain in Scotland (Flinn 1985).

Existing P-T data from the Shetlands is limited to the metamorphic sole of the ophiolite, and rocks belonging to the Yell Sound Division (Spray 1988; Flinn *et al.* 1991; Flinn 1994). P-T estimates using garnet-clinopyroxene thermobarometry from assemblages in the ophiolite sole give *c.* 750°C and an estimated pressure of 3 kbars (Spray 1988). In contrast Flinn *et al.* (1991), using similar assemblages and an assumed plagioclase composition suggested that ophiolite sole conditions were around 750°C and 10 kbar (Flinn *et al.* 1991). On Yell, conventional thermobarometry from metapelitic assemblages and interlayered garnet-bearing mafic rocks give conditions between 620-680°C and 7-10 kbar (Flinn 1994). However, aside from limited petrological descriptions (Spray 1988; Flinn 1994; Flinn *et al.* 1996) there has not yet been a systematic attempt to understand the textural evolution of the metamorphic rocks in the Shetland Islands. Additionally there has been no attempt to directly date high-T minerals associated with peak or near peak metamorphism in the Shetland Islands. The goal of this work is to constrain the timing of metamorphism in the Shetland Islands, and to determine the P-T evolution associated with Caledonian tectonism.

Analytical Methods

Mineral Chemistry

Mineral compositions for selected samples were obtained using a Cameca SX51 Electron Microprobe at Adelaide Microscopy, located at the University of Adelaide. The analyses were obtained using wavelength dispersive spectrometers. Quantitative analyses were run at an accelerating voltage of 15 kv and a beam current of 20 nA, with a beam diameter of 2-3 μm. Representative mineral compositions are given in Appendix 1. For selected garnet grains, compositional maps were also run. These were conducted by setting each of the four spectrometers to measure the peaks of Mg, Ca, Fe and Mn. Mapping conditions were an accelerating voltage of 15 kv and a beam current of 100 nA. To quantify the maps, a traverse of each garnet was also conducted.

PT Calculations

Pressure and temperature calculations were conducted using analyses obtained from the electron microprobe (Appendix 1). All samples chosen for analysis were garnet bearing. P-T calculations were conducted using two assemblages for each sample. The first assemblage consists of core compositions from minerals that experience zoning such as garnet, hornblende and plagioclase along with matrix minerals such as muscovite and biotite. The second assemblage uses the rim compositions of zoned minerals. This was done in order to discern the P-T evolution of the sample during mineral growth.

Pressures and temperatures for the formation of metamorphic mineral assemblages present in Shetland Islands samples were calculated utilising the average-P and average-T approach (Powell & Holland 1994) using the computer program THERMOCALC v3.21 (Powell & Holland 1988) and the updated internally consistent dataset of Holland and Powell (1998).

The average P, average T, average PT approaches are multiple equilibria techniques which utilise a least-squares method to calculate the optimal P-T conditions from the thermodynamic data of end-members involved in a series of independent reactions that entirely specify the thermodynamics of the system (Powell & Holland 1994). The average-P approach allows the calculation of pressure for a chosen temperature, while the average-T approach calculates the temperature for a given pressure. The average-PT approach is the most powerful in estimating metamorphic conditions, calculating pressure and temperature simultaneously. This approach

however, cannot always be used as some assemblages or assemblage compositions may not allow an average-PT calculation due to an insensitivity to either pressure or temperature. In these cases, the average-P or average-T must be used.

P-T calculations done with THERMOCALC include uncertainties on the activities and enthalpys of mineral end-members, which are propagated through to the final results (Powell & Holland 1994). Each independent reaction is enclosed in an uncertainty envelope, the width of which plays a crucial role in determining the optimal P-T conditions. Thus a reaction with a large uncertainty envelope will contribute relatively little to the final result. As the reactions in the independent set involve overlapping subsets of end-members, the equilibria are constrained to move in a correlated way that results in the P-T intersection moving in a predictable manner. The results are subject to a χ^2 test. If this is passed it means that a solution has been found that is consistent with input data and their uncertainties. These calculations allow the identification of end-members, which strongly influence the result as well as activities, which are not well fitted by the average result. Samples that fail the χ^2 tests will usually pass once outlying end-members have been identified and either omitted from the dataset or down played by increasing the uncertainty on their activities. The ability to identify end-members that either strongly influence the results or are significant outliers means that the robustness of the P-T results and the degree of equilibrium between the chosen mineral compositions can be assessed.

All samples used in this study had ≥ 4 independent reactions utilised during the average P-T calculations. Some samples had low variance assemblages with up to 11 independent reactions being found. If an end-member was a significant outlier, it was removed from the dataset and the calculations were redone. Only one end-member was removed in one sample. This did not obviously change the P-T estimate but it did improve the χ^2 fit of the result such that it passed at 95% confidence. Reasons why end-members occur as outliers include 1) inadequacies in activity models for particular ranges of mineral compositions and 2) analytical problems derived from the microprobe (e.g. Mawby 2000).

A variable that is difficult to constrain using the average P-T approach is that of fluid composition. Since all the samples used in this study contain hydrous minerals such as biotite, muscovite and hornblende, it is likely there was a free fluid phase present during the metamorphism of these rocks (Guiraud *et al.* 2001). In this case it is possible that the composition of the fluid may exert a strong influence on the apparent P-T stability of the

observed mineral assemblages (e.g Spear 1993; White *et al.* 2003). In order to understand this dependency, P-T calculations were undertaken using a range of assumed fluid compositions that were modelled as H_2O-CO_2 mixtures defining XH_2O in the fluid (Fig. 3).

The samples collected from the Lunna Ness region on Mainland contain the products of partial melting, which means that in general, all available fluid in the rock would have been incorporated into the melt. Calculations on these samples were conducted using an activity for water, which was determined using a similar process to that outlined above for XH_2O.

Electron Microprobe Monazite Geochronology

This geochronological technique is based on the chemical dating of monazite using an electron microprobe to measure the amounts of U, Th and Pb. Monazite is typically very rich in the radioactive elements U and Th, and therefore radiogenic Pb accumulates at a rate such that measurable quantities (>300 ppm) of Pb are reached in about 100 Ma (Montel *et al.* 2000). Previous studies (e.g. Parrish 1990) have demonstrated that monazite contains negligible common lead compared with the radiogenic component, therefore it can be assumed that all measured lead in monazite is the result of the radiogenic breakdown of U and Th. The most recent estimate of the closure temperature for lead diffusion in monazite is ~900°C at a cooling rate of 10°C/Ma in a 10 μm grain (Pyle *et al.* 2005). This means that monazite dating should be an effective tool for the amphibolite facies rocks of the Shetland Islands as it will almost certainly record growth ages.

Analyses of monazite were undertaken using a Cameca SX51 Electron Microprobe at Adelaide Microscopy in the University of Adelaide. The analyses were run at an accelerating voltage of 20 kV and a beam current of 100 nA. Th, U and Pb were analysed concurrently with PET crystals using Mα lines for Th and Mβ lines for Pb and U. The standards used were huttonite (Th), UO_2 and a synthetic Pb glass. The full range of elements which are typically partitioned into monazite were analysed (Table 1). Analyses below 97% total concentration were rejected for age determination and all analyses had their background lead concentrations corrected with respect to the known standard. Offline corrections were made to account for the overlap of the second order Ce Lα escape peak with the required Pb Mβ peak (Pyle *et al.* 2005). The ages for each spot were then determined using the U-Th-Pb concentrations and the statistical methods outlined in Montel *et al.* (1996). Probe performance was monitored by comparison with a standard 514 Ma monazite of known U-Th-Pb concentrations. Reproducibility of the standard (n = 140) was 511 ± 8 Ma.

LA-ICPMS Monazite Geochronology

Single grain U-Pb monazite dating was carried out using the LA-ICPMS at the University of Adelaide. A few grains were imaged using BSE and CL imaging on a Phillips XL20 SEM with attached Gatan CL. Grains were also mapped during analysis by the electron microprobe to ensure that probe points did not lie between two growth zones. Monazite grains were taken from the matrix or garnet grains of most samples and considered to be metamorphic in origin.

U-Pb isotopic analyses were acquired using a New Wave 213 nm Nd-YAG laser in a He ablation atmosphere, coupled to an Agilent 7500cs ICP-MS. For monazite analysis, a spot size of 15 μm is used, a 50 second gas blank is analysed first, followed by 10 seconds where the laser is on but shuttered, then 60 seconds of actual sample analysis. The laser is fired for 10 seconds with the shutter closed to allow crystal and beam stabilisation.

U-Pb fractionation was corrected using the Madel monazite standard (TIMS normalisation data $^{207}Pb/^{206}Pb$=495.7 Ma, $^{206}Pb/^{238}U$=513.8 Ma and $^{207}Pb/^{235}U$=510.6 Ma; Payne *et al.* submitted) and accuracy was checked using an internal standard of known age. Over the duration of this study, the average normalisation ages were $^{207}Pb/^{206}Pb$=490.2 Ma, $^{206}Pb/^{238}U$=523.7 Ma and $^{207}Pb/^{235}U$=518.2 Ma (n=26). If Pb 204 (or common lead) is present in the monazite grains, they are plotted on a Terra-Wasserberg plot to get a correct age (Payne *et al.* 2006).

Sm-Nd Analysis

Garnets were separated from the whole rock using a diamond saw, the two grains used in the analysis had their edges ground off to remove any remaining rock and also to remove any possible outer growth zone. The garnet depleted whole rock was then crushed and milled while the garnets were crushed using a mortar and pestle. The garnet separates were sieved, to a grainsize between 75 and 150 microns and then put through magnetic and heavy liquid separation techniques to remove impurities such as oxide, quartz and epidote.

Between 160-190 mg and approximately 45 mg of sample was used for garnet separates and whole rocks respectively. To further reduce the risk of inclusions, before isotopic analysis was carried out, the garnet separates were leached in either 6M HCl or 50% HF and left on a hotplate at 150°C for approximately one hour. The leachate was pipetted from the residual solid material and the solid material washed three times in deionised water separately to remove any trace of

the leachate fraction. Following this the leached garnet fractions and the whole rock fractions were spiked with a mixed ^{147}Sm-^{150}Nd spike prior to dissolution. Both the garnet separates and the whole rocks were dissolved in HNO_3 – HF acid mixtures for periods between 2 and 18 days. Sm and Nd isotopic compositions were measured on a Finnigan MAT 262 TIMS with Sm being measured in static mode while Nd was measured in both static and dynamic mode. The isotopic ratios were corrected for fractionation to $^{146}Nd/^{144}Nd = 0.7120903$ and to a $^{152}Sm/^{149}Sm$ ratio of 1.9347. Reported errors on the measured $^{143}Nd/^{144}Nd$ are 2 standard error analytical uncertainties. Throughout the duration of this study blanks ranged from 104 to 240 pg Nd, and the long term average for the La Jolla standard is 0.511838 ± 0.000008 (1σ, n =6).
Age calculations were conducted using Isoplot v. 3.00 (Ludwig 2001) with values (reported at 95% confidence) based on a decay constant for Sm of $6.54 \times 10^{-12} y^{-1}$.

Metamorphic Petrology

The samples used in this study were collected from several regions of the Shetland Islands (Fig. 4).

Unst

The major geological feature of this island is the large ophiolite complex that sits structurally on top of the Dalradian sequences (Fig. 5A). Samples SH-13 and FRQ-1 were collected directly to the west of this from a muscovite-chlorite-garnet schist sequence (Fig. 5B). Both of these samples are characterised by a lack of biotite with the foliation being predominantly defined by muscovite and chlorite. The minerals in SH-13 are muscovite, chlorite, garnet, plagioclase, quartz and ilmenite with some minor tourmaline. Garnets are small (around 2 mm in diameter at most) and generally appear to be shattered or broken (Fig. 6A). A foliation in this sample is defined by muscovite, ilmenite and chlorite and this is interpreted as a retrograde assemblage on the basis that it overprints the peak assemblage.

FRQ-1 contains garnet, staurolite, chlorite, chloritoid, muscovite, ilmenite and quartz (Fig. 6B). Garnet grains are large (up to 1 cm in diameter) and contain inclusions of staurolite, chlorite, chloritoid and muscovite, suggesting a prograde staurolite-chloritoid association. Garnet grains along with staurolite (around 2 mm long) are enclosed by a finer grained foliated fabric of muscovite, chlorite, chloritoid and quartz (Fig. 6B). Based on its fine-grain size and evidence that the peak garnet-staurolite porphyroblasts are wrapped by the fabric, the matrix assemblage is interpreted to be a retrograde feature.

The island of Unst is split down the middle (north-south) by the Burra Firth Lineament which separates the eastern part of Unst (dominated by the ophiolite) from sequences to the west that are interpreted to be Dalradian. Samples SH-10, SH-11 and SH-14 were collected from the garnet-biotite-plagioclase-quartz-muscovite ± kyanite schists of Western Unst (Fig. 5C).

Sample SH-10 contains a mineral assemblage of garnet-quartz-biotite-muscovite-chlorite-plagioclase-ilmenite. Garnet grains are up to 3 mm in size, most are broken up and partially replaced by chlorite (Fig. 6C). The foliation in this sample wraps garnet grains and is defined by chlorite, biotite, muscovite and ilmenite. This is interpreted as a retrograde assemblage since chlorite resorbs peak metamorphic garnet. Some plagioclase grains are also partially to completely replaced by unfoliated, fine-grained muscovite (Fig. 6D).

The minerals present in SH-11 are biotite-garnet-muscovite-kyanite-plagioclase-ilmenite-rutile-quartz. Garnets are large (up to 1.5 cm in diameter), and in places are partially replaced by biotite. Garnet grains contain inclusions of sillimanite, muscovite and biotite, which suggest a prograde assemblage of sillimanite-muscovite-biotite-plagioclase-quartz (Fig. 6E). The foliation in this sample is defined by biotite, muscovite, ilmenite and kyanite this is interpreted as the retrograde assemblage.

Sample SH-14 has a peak assemblage of muscovite-biotite-garnet-plagioclase-ilmenite-quartz (Fig. 6F). Porphyroblasts of muscovite are present with grains up to 5 mm in size (Fig. 6F). These grains generally lie within the foliation plane but are wrapped by smaller foliated grains. Garnet grains are up to 3 mm in size and contain inclusions of muscovite, biotite, quartz and ilmenite, this is interpreted as a prograde assemblage. The foliation is defined by retrograde muscovite and biotite.

Yell

Samples SH-9 and SH-24 were collected from kyanite-garnet-staurolite-quartz-muscovite-biotite ± plagioclase-bearing metapelitic schist (Fig. 5D) in eastern Yell (Fig. 4). These samples have similar mineral assemblages except that SH-9 contains plagioclase. Both contain the minerals garnet, quartz, muscovite, biotite, kyanite ilmenite, rutile and relict staurolite armoured in either large quartz grains (SH-24, Fig. 6G) or large plagioclase grains (SH-9, Fig. 6H). In SH-24, staurolite in quartz is present as an inclusion in garnet, suggesting a prograde assemblage of

garnet, staurolite, muscovite, biotite and quartz. The foliation is defined by biotite, muscovite and kyanite. In both samples kyanite is poorly lineated. Garnet grains are up to 1cm in diameter in SH-24 and about 3mm in diameter for sample SH-9.

Lunna Ness

Lunna Ness is a narrow peninsula off of central Mainland. The rocks in this region are both felsic and mafic in composition, with minor pelitic layers and have undergone migmatisation (Fig. 5E).

SH-30a, and SH-31 were sampled from the mafic rocks with an assemblage of garnet-hornblende-plagioclase-ilmenite-quartz-titanite ± biotite. Sample SH-30a has an assemblage of hornblende-garnet-plagioclase-titanite-quartz-ilmenite (Fig. 6I). Hornblende is anhedral in appearance, garnet grains are up to 1cm in diameter and garnets contain inclusions of ilmenite, quartz and titanite indicating a prograde assemblage. SH-31 contains an assemblage of hornblende-biotite-garnet-plagioclase-titanite-ilmenite-quartz. The foliation in SH-31 is defined by biotite and hornblende, although biotite-rich and hornblende-rich domains are restricted to separate layers (Fig. 6J). The garnets in this sample are large (up to 1.5 cm in diameter) and contain abundant inclusions of quartz, ilmenite and biotite, giving the prograde assemblage for this sample.

Sample SH-29 is granitic with an assemblage of biotite-garnet-plagioclase-K-feldspar-muscovite-quartz (Fig. 6K). Garnet grains (up to 2 mm in size) have inclusions of muscovite, biotite and quartz indicating the prograde assemblage of the sample. Fine-grained muscovite replaces K-feldspar in places (Fig. 6K).

Samples SH-31c and FRQ-20a and b were collected from migmatised metapelites. Sample SH-31c has the assemblage garnet-biotite-plagioclase-quartz-ilmenite. A foliation is present defined by biotite; ilmenite also appears to follow this foliation. Garnet grains are about 3mm in size, many containing inclusions of ilmenite, quartz and biotite. Some garnets also appear to be reacting to produce biotite (Fig. 6L). From this it is apparent that the prograde assemblage of this sample is plagioclase, biotite, quartz and ilmenite. The peak metamorphic assemblage is garnet, biotite, plagioclase, ilmenite and quartz. The retrograde assemblage is biotite, plagioclase, quartz and ilmenite.

The FRQ-20 samples come from the same outcrop but have slightly different mineral assemblages. FRQ-20b contains the assemblage garnet-biotite-kyanite-sillimanite-plagioclase-K-feldspar-rutile-ilmenite, which represents the peak assemblage of this sample (Fig. 6M). Garnet in sample FRQ-20b is up to 2 mm in size and contains inclusions of kyanite, muscovite and biotite. FRQ-20a contains the same assemblage as FRQ-20b, however foliated muscovite has replaced sillimanite (Fig. 6N). Garnet in sample FRQ-20a is up to 3 mm in size and also contains inclusions of kyanite, muscovite and biotite, indicating a prograde assemblage of kyanite, muscovite, biotite, garnet and plagioclase (Fig. 6N). In sample FRQ-20a, kyanite appears to have been partially replaced by muscovite (Fig. 6O). The replacement of sillimanite by muscovite indicates a retrograde assemblage of garnet-kyanite-plagioclase-biotite-muscovite. A foliation defined by sillimanite (muscovite in FRQ-20a) and biotite is present in these samples.

North Mainland

The rocks of this region are possible equivalents of the Morar Group of the Moine Supergroup in Scotland. Sample SH-16 was taken from highly schistose rocks (Fig. 5F) and contains the assemblage garnet-muscovite-quartz-chlorite-biotite-ilmenite. Garnets are large with most being greater than 1cm in diameter, and contain abundant inclusions of quartz and minor ilmenite that define helitical inclusion trails (Fig. 6P). This is interpreted as the prograde assemblage of the sample. The garnets are enclosed in an intense foliation defined by chlorite-muscovite-quartz. Chlorite partially to completely replaces garnet, suggesting that the matrix fabric is a retrograde feature.

Mineral Chemistry

Mineral compositions were analysed in samples FRQ-1, FRQ-20b, SH-9, SH-11, SH-13, SH-14, SH-24, SH-30a, SH-31 and SH-31c. The procedure for mineral composition analysis is given above and representative mineral compositions are given in Appendix 1.

Garnet

Garnets from samples SH-9, SH-11, SH-14, SH-16, SH-31c and FRQ-1 were analysed and mapped.

The remaining samples (SH-13, SH-24, SH-30a, SH-31 and FRQ-20b) had core and rim analyses conducted on the garnets. Garnet cores have an XFe from 0.54 to 0.72 and an XMn of 0.01 to 0.13, rims have an XFe between 0.55 to 0.76 and an XMn of 0.0005 to 0.2. Samples FRQ-1, SH16, SH-9 and SH-31c were quite Fe rich (Table 2).

Compositional mapping of garnets (Fig. 7) reveal three distinct styles of garnet zonation in the metamorphic rocks of the Shetland Islands. Samples SH-16 (Figs. 7A and 7B) and FRQ-1 (Fig. 7C) display characteristic growth zonation, with cores rich in Mn, decreasing dramatically toward the rim. This decrease in XMn is mirrored by increasing XFe and modest increases in XMg, consistent with growth during increasing temperature (e.g. Spear 1993). Sample FRQ-1 shows a narrow enrichment of Mn at the rim of the garnet, suggesting minor garnet resorption by Mn-poor matrix minerals. This rim enrichment in Mn is consistent with the petrological evaluation (above) that the matrix assemblage in FRQ-1 is a retrograde feature. The second type of garnet zonation is shown by samples SH-31c (Fig. 7D) and SH-9 (Fig. 7E). These samples contain essentially homogenous compositions for most cations.

These homogenous compositions can be interpreted in several ways. One alternative is that they represent compositions that have been homogenised an extended duration (> 5-10 Ma) at high (> 700°C) temperatures (e.g. Spear 1993). This explanation is plausible for SH-31c which comes from a region of migmatisation in the Lunna Ness area. However existing thermobarometry from Yell (Flinn 1994; Flinn *et al.* 1996), suggests that Sample SH-9 was subject to temperatures < *c.* 650°C. For temperatures in this range, diffusion is extremely inefficient (e.g. Spear 1993), suggesting that diffusional modification is unlikely to have homogenized the garnet compositions. In this case the homogeneous compositions may result from the garnet-producing reaction being overstepped, with fast garnet growth being unable to record changes in P-T and hence compositional zoning (e.g. Spear 1993). The third variety of garnet zonation is shown by SH-11 (Fig. 7F) and SH-14 (Fig. 7G). In SH-11, garnets are fractured with the fragments showing rim-ward compositional modification as though they were separate grains. In SH-14, garnet shows a distinct overgrowth of high-Ca garnet that is also enriched in Mn and depleted in Mg. The rim-ward enrichment in Mn suggests that prior to the growth of new high Ca garnet, the original garnet had been partially resorbed, leading to a rimward enrichment in Mn. Subsequent growth of new garnet inherited the Mn-rich composition. The compositional patterns in both SH-11 and SH-14 suggest that these samples experienced a polymetamorphic history that contrasts with the simple garnet zoning patterns in the remainder of the samples.

Staurolite

Staurolite is present in samples SH-9, SH-24 and FRQ-1. XFe from samples SH-9 and SH-24 is similar with values for SH-9 being 0.65-0.7 and XFe for SH-24 being 0.67-0.7. XZn values for

these samples are fairly different with values ranging between 0.01-0.05 for SH-24 and 0.09-0.15 for SH-9. Sample FRQ-1 is slightly different with XFe~0.79 and XZn~0.05.

Muscovite

Muscovite is present in samples SH-9, SH-11, SH-13, SH-14, SH-24 and FRQ-1. Overall, XFe (Fe/(Fe+Mg)) varies from 0.3-0.7 with the highest values (of 0.7) in sample FRQ-1. Values for XNa vary between 0.05 to 0.33. While values for Al^{vi} are between 3.55 to 3.81 (based on 11 oxygens).

Biotite

Biotite occurs in samples SH-9, SH-11, SH-14, SH-24, SH-31, SH-31c and FRQ-20b. Biotites have XFe^{2+} values that range between 0.40 to 0.54, XNa values which range between 0.01 to 0.07, titanium contents up to 3.1 wt% (sample FRQ-20b) and an Al^{vi} of 0.43 to 0.78 (based on 11 oxygens).

Chlorite

Chlorite is present in samples FRQ-1 and SH-13. Chlorite has XFe^{2+} ($Fe^{2+}/(Fe^{2+}+Mg)$ values that range between 0.36 to 0.52, XMg ($Mg/(Fe^{2+}+Mg)$ values range between 0.48 to 0.63 and an Al^{vi} of 2.7 to 3.0 (based on 14 oxygens).

Feldspars

Plagioclase is present in samples SH-9, SH-11, SH-13, SH-14, SH-30a, SH-31, SH-31c, FRQ-20. Compositions range from albite 0.23-0.83 and anorthite 0.17-0.76 (based on 8 oxygens). The most Ca rich samples are SH-9, SH-13 and SH-14. In SH-9 rims are more Na rich, while in SH-13 and SH-14, cores have higher XNa than rims. Sample SH-30a shows rim-ward enrichment in Ca. However in contrast, SH-31 shows the opposite zonation.

FRQ-20 contains K-Feldspar, this has a composition of orthoclase 0.85-0.91 and albite 0.09-0.15.

Hornblende

Hornblende occurs in samples SH-30a and SH-31. Hornblende from these samples is not very aluminous with Al^{vi} varying from 0.59-0.64 in SH-30a and 0.92-1.15 in sample SH-31. XFe ($Fe^{2+}/(Fe^{2+}+Mg)$) of hornblende varies in SH-31 (0.48-0.52) but not in SH-30a (0.37-0.38). Hornblende cores seem to have slightly lower XFe contents than rims with 0.37 (core)-0.38 (rim)

in SH-30a and 0.48(core) -0.50(rim). Garnet grains from both of these samples also have slightly lower XFe contents in the cores (Table 2).

Chloritoid

Only sample FRQ-1 contains chloritoid. XFe (Fe/(Fe+Mg)) varies between 0.77-0.79. A chloritoid grain sampled from inside a garnet grain had an XFe of 0.77 while those sampled from the matrix gave XFe around 0.78.

P-T Calculations

Activity and composition relationships for mineral end-members used in THERMOCALC v3.21 were calculated using the software AX2000 (Powell *et al.* 1998). Appendix 2 contains an example of an output file from AX2000 while Appendix 3 contains an example of a THERMOCALC v3.21 output file. The results of the PT calculation are summarized in Table 3.

PT calculations were undertaken on samples SH-9, SH-11, SH-13, SH-14, SH-24, SH-30a, SH-31, SH-31c, FRQ-1 and FRQ-20b. From the results of these calculations (Table 3) it was apparent that different parts of the Shetland Islands had experienced different PT conditions, and that the samples could be split on this basis into four groups: East Unst, West Unst (separated by the Burra Firth Lineament), Yell and Lunna Ness. The pressures experienced by all of these groups is similar, with most around the 8-9 kbar region. Only the samples from Lunna Ness are slightly higher, with pressures around 10 kbar. The calculated temperatures show a variation between groups with samples from eastern Unst giving temperatures of *c.* 550°C and those from Lunna Ness giving 700-800°C.

P-T pseudosection Interpretation

While the P-T calculations give an estimate of the peak metamorphic conditions, the metamorphic evolution (P-T path) can be inferred using calculated P-T pseudosections (Powell *et al.* 1998). These are forward modelled phase diagrams that show what mineral assemblages will develop in different parts of P-T space for a rock of specified composition. In the present study, whole rock major oxide compositions were determined for a number of samples. These compositions were then used as a basis to select published P-T pseudosections for similar compositions in order to evaluate the P-T evolution of selected samples.

Several samples were chosen for representation of their metamorphic evolution using published P-T pseudosections calculated for compositions appropriate to Shetlands metapelites. These samples were SH-9, SH-24, FRQ-1 and FRQ-20. These samples were chosen due to their large assemblage of minerals that give constrained P-T conditions using the program THERMOCALC.

Sample SH-9 was modelled using a P-T pseudosection from Tinkham *et al.* (2001; Fig. 8A). Based on the mineralogy discussed above, the prograde mineral assemblage for SH-9 consists of staurolite-garnet-plagioclase-biotite-muscovite-quartz. This is based on the presence of relict staurolite grains armoured inside of large grains of plagioclase. The peak assemblage of SH-9 is garnet-plagioclase-kyanite-muscovite-biotite-quartz. These two assemblages define P-T path that tracks out a significant increase in pressure for a relatively small increase in temperature. This style of P-T path indicates burial to approximately 30 km of material (based on the peak pressure of ca. 8 kbar), with a burial segment of around 10 km (3 kbar), recorded by the mineral textures.

Sample FRQ-1 was modelled using a P-T pseudosection from Tinkham & Ghent (2005; Fig. 8B). The prograde assemblage in this sample is defined by the association chloritoid-muscovite-chlorite-ilmenite-quartz which occurs as inclusions in garnet. Staurolite, which is also included in garnet grains is interpreted to have grown at the same time as garnet.
The peak assemblage of the sample is interpreted to be the assemblage of garnet-staurolite-muscovite-chlorite-chloritoid-ilmenite-quartz. The foliation, which wraps both the garnet and staurolite grains, is interpreted to be a retrograde assemblage of chlorite-muscovite-chloritoid-ilmenite-quartz, consistent with the presence of rim resorption of garnet (above). These three mineral assemblages define the P-T path for this sample. The prograde and peak assemblages define a burial path with a larger increase in pressure than temperature, once again indicating burial to approximately 30 km (based on peak pressures around 8 kbar). The retrograde P-T path tracks out a P and T decreasing evolution.

Sample SH-24 was modelled using a P-T pseudosection taken from Wei *et al.* (2004; Fig. 8C). The prograde assemblage of this sample is interpreted to be staurolite-quartz-garnet-muscovite-biotite based on the presence of relict staurolite grains armoured within large quartz grains. The peak metamorphic assemblage is garnet-muscovite-kyanite-biotite-quartz. As with samples FRQ-1 and SH-9 the P-T path shows a significant increase in pressure with a modest temperature increase.

Sample FRQ-20 was modelled using a P-T pseudosection taken from White *et al.* (2001; Fig. 8D). The prograde mineral assemblage for this sample is defined by mineral inclusions in garnet giving an assemblage of garnet-kyanite-muscovite-biotite-plagioclase-quartz. The peak assemblage is interpreted to be kyanite-garnet-biotite-K-felspar-plagioclase-sillimanite-ilmenite-quartz. Kyanite is partially replaced by muscovite, while sillimanite is almost completely replaced by muscovite, this suggests the retrograde evolution crossed fields containing kyanite-muscovite bearing assemblages. Based on the textural relationship involving kyanite-muscovite, the retrograde assemblage is interpreted to be muscovite-kyanite-garnet-biotite-plagioclase-quartz. These three assemblages define a P-T path that has a dramatic prograde increase in temperature with comparatively little increase in pressure (this is defined by the growth of sillimanite). Following this the path shows an increase in both pressure and temperature, indicating burial. The retrograde P-T evolution is marked by the loss of sillimanite from the rock and the partial retention of kyanite.

Age constraints on metamorphism

EMPA

Monazite U-Th-Pb chemical dating was undertaken on a number of samples. The mean ages for each sample are summarized in Table 4 and Fig. 9, individual spot ages are given in Appendix 4 for each sample. Analysed monazites were typically subhedral grains up to 200 μm long (Fig. 10). Of the six samples that were analysed, monazites were in the matrix and as inclusions in garnet grains for samples SH-11, SH-9, SH-29, SH-31c. In sample SH-24 they were only present in the matrix while in SH-10 they were only present as inclusions in garnet. Samples SH-9, SH-31c and SH-24 give pooled metamorphic ages of ca. 460 Ma with SH-9 giving 458 ± 9 Ma (2σ, MSWD: 1.3), SH-31c giving 449 ± 7 Ma (2σ, MSWD: 1.2) and SH-24 giving 460 ± 21 Ma (2σ, MSWD: 0.61; Fig. 9). SH-29 shows two age populations giving 459 ± 9 Ma (2σ, MSWD: 1.01) and 923 ± 30 Ma (2σ, MSWD: 2.0; Fig. 9) SH-11 and SH-10 produce pooled metamorphic ages of 912 ± 7 Ma (2σ, MSWD: 1.09 and 896 ± 24 Ma (2σ, MSWD: 1.2) respectively (Fig. 9).

LA-ICPMS

Monazite from samples SH-9, SH-11 and SH-29 were also analysed by LA-ICPMS (Table 5). All of the samples were plotted as Terra-Wasserberg plots due to the presence of common lead in many of the analyses (Fig. 11). Ages given by the intercepts with the concordia line for each sample (Table 4) are 454 ± 4 Ma for SH-9 (MSWD= 0.82), 915 ± 15 Ma for SH-11 (MSWD=

0.38) and 455 ± 5 Ma for SH-29 (MSWD= 1.09). Analyses that were greater than 50% discordant were removed from the data along with analyses, which had an excessive amount of common lead.

Sm-Nd analysis

Four individual syn-tectonic euhedral garnet grains were analysed from this sample, these were from two separate rocks obtained from the same outcrop. The garnets were up to 1.5 cm in diameter. The results from the Sm-Nd analysis are given in Fig. 12 and Table 6. From Fig. 12 it is apparent that the results all plot close together as $^{147}Sm/^{144}Nd$ only varies between 0.12 and 0.16. This is not a wide enough range to produce a useful isochron. In order to explore why the analysed garnets had such a narrow range of isotopic compositions, the Sm-Nd compositions of garnet from one of the dated samples was analysed by LA-ICPMS (Table 7). The results showed that the garnet from SH-16 had exceptionally low Sm and Nd concentrations. As a result, the garnet separates would have been very susceptible to contamination by LREE-rich inclusions such as apatite and epidote.

Interpretation of Age Data

There has been considerable work done in recent years to understand the significance of monazite ages in metamorphic rocks. It is well recognised that monazite grows during prograde metamorphism (Smith & Barreiro 1990) and is generally present in metapelites from mid amphibolite-grade and above conditions (Rubatto *et al.* 2001). Several studies have shown monazite may grow over a considerable timing duration, apparently tracking the rate of prograde heating (Smith & Barreiro 1990; Rubatto *et al.* 2001). In these cases there are systematic age differences between monazite grains in different textural positions, with grains included in hosts such as garnet generally being younger that grains in the matrix of amphibolite-grade rocks. Additionally Fitzsimons *et al.* (2005) suggested that monazite may grow at different times in rocks of different bulk composition, making it difficult to easily interpret the significance of monazite ages in metamorphic rocks.

However in the samples analysed in this study, the insitu electron microprobe data revealed no systematic age differences between monazites in different textural locations. Additionally, aside from SH-10 and SH-11 which gave ages around 900 Ma, all samples gave ages within error, suggesting that the monazite age data from the Shetland samples probably equates to the timing

of peak or near peak metamorphism. The older ages obtained from SH-10 and SH-11 were also within error of each other suggesting they record a significant older metamorphic event.

Discussion

Caledonian metamorphism in the Shetland Islands

Monazite U-Pb LA-ICP MS and U-Th-Pb EPMA data (Fig. 13) from samples SH-9, SH-24, SH-29 and SH-31c suggest that peak Caledonian metamorphism in the Shetland Islands occurred at *c.* 460 Ma (Table 4). This is similar in timing to the Grampian Event recorded in the Scottish Highlands (Soper *et al.* 1999; Oliver *et al.* 2000; Strachan *et al.* 2002), and is also similar to the K-Ar ages obtained from hornblende in the metamorphic sole of the ophiolite (Spray, 1988). The age data also suggest that the effects of the Scandian Event are comparatively minor, at least in terms of high-T mineral growth, east of the Walls Boundary Fault.

Published P-T psuedosections applied to samples FRQ-1, FRQ-20, SH-9 and SH-24 (Fig. 8) all show P-T paths which indicate burial during heating. P-T conditions for samples FRQ-1, SH-13, SH-11, SH-14, SH-9, SH-24, SH-30a, SH-31, SH-31c and FRQ-20b give pressures of 8-9 kbar and temperatures of 550-850°C, increasing from Unst to Lunna Ness (Table 3). The average geothermal gradients obtained from all samples lies in the range 20 to 24°C/km. This relatively cool geothermal gradient is typically for terrains undergoing burial as a consequence of crustal thickening (Sandiford & Powell 1990; Sandiford & Powell 1991), and implies that the metamorphic record in the Shetlands reflects collision.

The samples examined in this study all come from structurally beneath the Shetland Ophiolite, and therefore the obduction of this sheet represents a plausible mechanism to drive the burial recorded by the metamorphic assemblages. The age of Shetland Ophiolite (Fig. 13) has been dated at 492 ± 3 Ma (U-Pb zircon age from a plagiogranite; Spray & Dunning 1991), and it was thought to have been obducted around *c.* 470 Ma (based on four K-Ar ages: 465 ± 6, 471 ± 3, 473 ± 6 and 479 ± 6 Ma from hornblende taken from the metamorphic sole of the ophiolite; Spray 1988). However, the significance of the K-Ar ages from the ophiolite sole is uncertain. Based on the available thermobarometry (Spray 1988; Flinn *et al.* 1991; Flinn 1994), the K-Ar ages will reflect cooling of the sole thrust rather than deformation, indicating that obduction would have occurred prior to *c.* 470 Ma. However, it is also possible that the K-Ar hornblende ages are too old due to the K-Ar method being unable to detect excess Ar (Baxter *et al.* 2001). Nevertheless, the ages are similar to the monazite ages obtained in this study from the

metapelitic assemblages beneath the ophiolite, suggesting that burial and heating of the Dalradian and Moine sequences occurred more or less around the time of obduction.

The ophiolite is thought to have been obducted in two sheets (Flinn 1985; Spray 1988; Spray & Dunning 1991; Flinn & Oglethorpe 2005) and its total thickness is estimated at 8-10 km (Spray 1988; Spray & Dunning 1991; Strachan 2000; Strachan *et al.* 2002). Thus even at its thickest, the ophiolite is not thick enough to produce the overburden to cause the metamorphism identified in this study. Conceivably the ophiolite was imbricated at higher structural levels to create a much larger structural thickness that has been subsequently removed by erosion. However the presently preserved ophiolite sheets are separated by the Funzie Conglomerate, which is a weakly metamorphosed sedimentary package (Flinn 1985). If the metamorphic overburden had been generated by imbrication of the ophiolite, the sequence between the ophiolite sheets would have to contain assemblages of similar metamorphic intensity (e.g. FRQ-1) to those observed beneath the basal ophiolite. For this reason, it seems likely that the peak metamorphism in the Shetland metasedimentary rocks must predate obduction in order to explain the contrast in metamorphism between the sequences immediately below the ophiolite and the metasedimentary packages between the sheets.

The magnitude of burial (*c.* 30 km) recorded by the metamorphic assemblages in northern and central Shetland requires a significant collisional event. A number of workers (Bluck 1983; Dewey & Ryan 1990; Phillips *et al.* 1999; Soper *et al.* 1999; Strachan, 2000; Dalziel & Soper 2001; Strachan et al. 2002) have suggested that the 470-460 Ma Grampian Event in the Scottish Highlands records the collision of Laurentia with an oceanic arc (Fig. 14). In Scotland, the Grampian event was associated with nappe development and Barrovian metamorphism, with peak pressures up to 10 kbar. The similarity in the timing and style of metamorphism between the Grampian Event in Scotland and the metamorphism recorded in the Shetlands suggests that they reflect the same collisional event. If the conclusion that peak metamorphism in the Shetlands predated ophiolite obduction is correct, the obduction event may reflect closure of a back-arc system and thrusting of the comparatively young (*c.* 25 Ma old) Shetland ophiolite crust onto the deformed orogenic margin (Fig. 14C). The subsequent Scandian Event (430-420 Ma) imbricated Moine rocks and basement, as well as Dalradian units west of the Walls Boundary Fault. The major expression of the Scandian Event was the westward transport of the Moine packages across the Caledonian Foreland (Strachan *et al.* 2002). The Scandian shortening is

interpreted to reflect terminal collision and oceanic closure between Baltica and Laurentia (Fig. 14D).

Neoproterozoic age rocks on Unst

Monazite U-Th-Pb EMPA and U-Pb LA-ICP MS geochronology (Fig. 13) for the two samples taken from Western Unst give peak metamorphic ages of *c.* 910 Ma. The samples, SH-10 and SH-11 were taken from a region interpreted to be Dalradian (Flinn 1985; Strachan *et al.* 2002). However the Neoproterozoic ages preclude this interpretation, and indicate that the metasedimentary rocks on western Unst belong to a previously unrecognised stratigraphic succession in the Shetland Islands.

Although the significance and origin of this sequence is unknown at this stage, there are two logical possibilities. The first possibility is that the sequence represents a piece of exotic crust accreted onto the Caledonian margin during convergence. The second possibility is that the sequence represents basement to the Dalradian succession on Unst. In the Grampian Terrain in the central Scottish Highlands, the Glen Banchor and Dava successions stratigraphically underlie the Dalradian and underwent metamorphism between 830-800 Ma (Highton 1999; Robertson & Smith 1999; Smith *et al.* 1999; Strachan *et al.* 2002). These metamorphic ages are similar to ages obtained for medium pressure Barrovian metamorphism in the Moine Supergroup in the Western Highlands Terrain (e.g. Vance *et al.* 1998), and suggest that the Glen Banchor and Dava successions are Moine equivalents. Additionally the Moine was intruded by the protolith of the West Highland Granite Gneiss at 873 ± 7 Ma (Millar 1999; Strachan *et al.* 2002). This has been interpreted to have been associated with extension, and potentially high geothermal gradient metamorphism (Millar 1999; Dalziel & Soper 2001; Strachan *et al.* 2002), and provides a minimum depositional age constraint for the Moine Supergroup in Scotland.

In the Shetlands, the *c.* 910 Ma EMPA monazite U-Th-Pb and LA-ICPMS U-Pb ages obtained from metamorphic rocks on western Unst are essentially identical to the timing of 920-930 Ma S-type granites that intrude the Krummedal Supracrustal sequence within the Caledonian Orogen in eastern Greenland (Kalsbeek *et al.* 2000; Watt *et al.* 2000; Watt & Thrane 2001; Gilloti & Elvevold 2002). The Krummedal Supracrustal sequence has been interpreted to be an equivalent on the Moine Supergroup (Kalsbeek *et al.* 2000; Watt & Thrane 2001). If this correlation is warranted, the timing of metamorphism in western Unst suggests the presence of a widespread *c.* 900 Ma tectonothermal event in the North Atlantic. Conceivably the 873 ± 7 Ma protoliths of

the West Highland Granite Gneiss represent part of this event, which has affected Moine correlatives. The style and evolution of this *c.* 900 Ma tectonothermal events is not clear at this stage. Sample SH-11 from western Unst contains a foliated sillimanite-garnet-biotite-bearing assemblage suggesting a relatively high geothermal gradient regime associated with deformation. An important outcome of this study is the recognition of Neoproterozoic (*c.* 900 Ma) metamorphism in the Shetland region, and future work should concentrate on both constraining the origin of the metamorphosed sequences, and examining the preserved structural and metamorphic record in order to understand the nature of this early tectonic event.

Conclusions

The are two major conclusions of this work.

1. The Shetlands experienced the Grampian Event of the Caledonian Orogeny with peak metamorphic temperatures in the central and northern Shetlands between 550°C (eastern Unst) and 800°C (Lunna Ness) and peak metamorphic pressures of ~8-10 kbar. Metamorphism was associated with Barrovian-style prograde metamorphic paths that reflect modest geothermal gradients, consistent with collisionally-driven metamorphism. Monazite EPMA and LA-ICPMS age constraints indicate prograde and peak metamorphism occurred at around 460 Ma. The driver for burial to depths around 30 km appears to have been crustal thickening prior to west-directed obduction of the Shetland Ophiolite which appears to have been too thin to have resulted in deep burial of its footwall. Instead the thickening event was probably caused by an arc terrane colliding with Laurentia.

2. Rocks on the western part of Unst, which were previously mapped as the Dalradian Supergroup give a pre-Dalradian peak metamorphic age of *c.* 910 Ma for upper amphibolite-grade mineral assemblages. These ages are similar to S-type granites in the Krummedal Supracrustal sequence (equivalent to the Moine Supergroup of Scotland) in eastern Greenland, and slightly older than protoliths to the West Highland Granite Gneiss, which intrudes the Moine Supergroup in Scotland. Conceivably these early mid-Neoproterozoic events represent part of an extensive tectonothermal event affecting early Neoproterozoic sequences in the North Atlantic region.

References

Baxter, E.F., DePaolo, D.J. & Renne, P.R. 2001. Spatially correlated anomalous 40Ar/39Ar "age" variations in biotites about a lithologic contact near Simplon Pass, Switzerland: A mechanistic explanation for excess Ar. *Geochimica et Cosmochimica Acta*, **66** (6), 1067-1083.

Bluck, B.J. 1983. Role of the Midland Valley of Scotland in the Caledonian orogeny. *Transactions of the Royal Society of Edinburgh: Earth Sciences*, **74**, 119-136.

Brasier, M.D. & Shields, G. 2000. Neoproterozoic chemostratigraphy and correlation of the Port Askaig glaciation, Dalradian Supergroup of Scotland. *Journal of the Geological Society, London*, **155**, 2-12.

Cawood, P.A., Nemchin, A.A., Strachan, R.A., Kinny, P.D. & Loewy, S. 2004. Laurentian provenance and an intracratonic tectonic setting for the Moine Supergroup, Scotland, constrained by detrital zircons from the Loch Eil and Glen Urquhart successions. *Journal of the Geological Society, London*, **161**, 861-874.

Condon, D.J. & Prave, A.R. 2000. Two from Donegal: Neoproterozoic glacial episodes on the northeast margin of Laurentia. *Geology*, **28**, 951-954.

Daly, J.S., Aitcheson, S.J., Cliff, R.A., Gayer, R.A. & Rice, A.H.N. 1991. Geochronological evidence from discordant plutons for a late Proterozoic orogen in the Caledonides of Finnmark, northern Norway. *Journal of the Geological Society, London,* **148**, 29-40.

Dalziel, I.W.D. & Soper, N.J. 2001. Neoproterozoic Extension on the Scottish Promontory of Laurentia: Palaeogeographical and Tectonic Implications. *The Journal of Geology*, **109**, 299-317.

Dewey, J.F. & Ryan, P.D. 1990. The Ordovician evolution of the South Mayo Trough, western Ireland. *Tectonics*, **9**, 887-903.

Fitzsimons, I.C.W., Kinny, P.D., Wetherley, S. & Hollingsworth, D.A. 2005. Bulk chemical control on metamorphic monazite growth in pelitic schists and implications for U/Pb age data. *Journal of Metamorphic Geology*, **23** (4), 261-277.

Flinn, D. 1985. The Caledonides of Shetland. *In*: Gee, D.G., Sturt, B.A. (eds). The Caledonide Orogen- Scandinavia and related areas. 1158-1171.

Flinn, D. 1988. The Moine rocks of Shetland. *In*: Winchester, J.A. (ed.) Later Proterozoic Stratigraphy of the Northern Atlantic Regions. Blackie, Glasgow, 74-85.

Flinn, D. 1994. Geology of Yell and some neighbouring islands in Shetland. *Memoir of the British Geological Survey*, Sheet 130 (Scotland).Gilotti, J.A. & Elvevold, S. 2002.

Extensional exhumation of a high-pressure granulite terrane in Payer Land, Greenland Caledonides: structural, petrologic, and geochronologic evidence from metapelites. *Canadian Journal of Earth Sciences*, **39**, 1169-1187.

Flinn, D., May, F. Roberts, J.L. & Treagus, J.E. 1972. A review of the stratigraphic succession of the East Mainland Succession of Shetland. *Scottish Journal of Geology*, **8**, 335-343.

Flinn, D., Pringle, I.R. 1976. Age of the migmatisation in the Dalradian of Shetland. *Nature*, **259**, 299-300.

Flinn, D., Frank, P. L., Brook, M. & Pringle, I. R. 1979. Basement-cover relations in Shetland. In The Caledonides of the British Isles, Harris, A., Holland, C. H. & Leake, B. E. (Eds.). London: Geological Society.

Flinn, D., Miller, J.A. & Roddom, D. 1991. The age of the Norwick hornblendic schists of Unst and Fetlar and the obduction of the Shetland ophiolite. *Scottish Journal of Geology*, **27** (1), 11-19.

Flinn, D., Key, R.M. & Khoo, T.T. 1996. Chloritoid schists of Shetland and their thermal metamorphism. *Scottish Journal of Geology*, **32**, 67-82.

Flinn, D. & Oglethorpe, R.J.D. 2005. A history of the Shetland Ophiolite Complex. *Scottish Journal of Geology*, **41**(2), 141-148.

Friend, C.R.L., Kinny, P.D., Rogers, G., Strachan, R.A. & Paterson, B.A. 1997. U-Pb zircon geochronological evidence for Neoproterozoic events in the Glenfinnan Group (Moine Supergroup): the formation of the Ardgour granite gneiss, north-west Scotland. *Contrib Mineral Petrol*, **128**, 101-113.

Friend, C.R.L., Strachan, R.A., Kinny, P.D. & Watt, G.R. 2003. Provenance of the Moine Supergroup of NW Scotland: evidence from geochronology of detrital and inherited zircons from (meta)sedimentary rocks, granites and migmatites. *Journal of the Geological Society, London*, **160**, 247-257.

Gilloti, J.A. & Elvevold, S. 2002. Extension exhumation of a high-pressure granulite terrane in Payer Land, Greenland Caledonides: structural, petrologic, and geochronologic evidence from metapelites. *Canadian Journal of Earth Science*, **39**, 1169-1187.

Gorokhov, I.M., Siedlecka, A., Roberts, D., Melnikov, N.N. & Turchenko, T.L. 2001. Rb-Sr dating of diagenetic illite in Neoproterozoic shales, Varanger Penisula, northern Norway. *Geological Magazine*, **138**, 541-562.

Guiraud, M., Powell, R. & Rebay, G. 2001. H2O in metamorphism and unexpected behaviour in the preservation of metamorphic mineral assemblages. *Journal of metamorphic Geology*, **19**, 445-454.

Highton, A.J., Hyslop, E.K. & Noble, S.R. 1999. U-Pb zircon geochronology of migmatization in the northern Central Highlands: evidence for pre-Caledonian (Neoproterozoic) tectonometamorphism in the Grampian block, Scotland. *Journal of the Geological Society, London*, **156**, 1195-1204

Holland, T.J.P. & Powell, R. 1998. An internally consistent thermodynamic data set for phases of petrological interest. *Journal of metamorphic Geology,* **13** (3), 309-343.

Kalsbeek, F., Thrane, K., Nutman, A.P. & Jepson H.F. 2000. Late Mesoproterozoic to early Neoproterozoic history of the East Greenland Caledonides: evidence for Grenvillian Orogenisis? *Journal of the Geological Society, London*, **157**, 1215-1225.

Kinny, P.D., Friend, C.R.L., Strachan, R.A., Watt, G.R. & Burns, I.M. 1999. U-Pb geochronology of regional migmatites in East Sutherland, Scotland: evidence of crustal melting during the Caledonian Orogeny. *Journal of the Geological Society, London*, **156**, 1143-1152.

Kinny, P.D., Strachan, R.A., Friend, C.R.L., Kocks, H., Rogers, G. & Paterson, B. 2003.U-Pb geochronology of deformed metagranites in central Sutherland, Scotland: evidence for widespread late Silurian metamorphism and ductile deformation of the Moine Supergroup during the Caledonian orogeny. *Journal of the Geological Society, London*, **160**, 259-269.

Kocks, H., Strachan, R.A. & Evans J.A. 2006. Heterogeneous reworking of Grampian metamorphic complexes during Scandian thrusting in the Scottish Caledonides: insights from the structural setting and U–Pb geochronology of the Strath Halladale Granite. *Journal of the Geological Society, London,* **163**, 525-538.

Ludwig, K.R. 2001. Users manual for Isoplot/Ex: a geochronological toolkit for Microsoft excel. *Berkely Geochronology Centre Special Publication No. 1a.*

Mawby, J. 2000. Metamorphic and geochronologic constraints on Palaeozoic tectonism in the eastern Arunta Inlier, *University of Adelaide PhD unpub*, 154.

McKerrow, W.S., Mac Niocaill, C. & Dewey, J.F. 2000. The Caledonian Orogeny redefined. *Journal of the Geological Society, London*, **157**, 1149-1154.

Millar, I.L. 1999. Neoproterozoic extensional basic magmatism associated with the West Highland granite gneiss in the Moine Supergroup of NW Scotland. *Journal of the Geological Society, London*, **156**, 1153-1162.

Miller, J.A. & Flinn, D. 1966. A survey of the age relations of the Shetland rocks. *Geol. J.* **5**, 95-116.

Montel, J.M., Foret, S., Veschambre, M., Nicollet, C. & Provost, A. 1996. Electron microprobe dating of monazite. *Chemical Geology*, **131**, 37-53.

Montel, J.M., Kornprobst, J. & Vielzeuf, D. 2000. Preservation of old U-Th-Pb ages in shielded monazite; example from the Benmi Bousera Hercynian kinzigites (Morocco). Journal of metamorphic Geology, 18 (3), 335-342.

Murphy, J.B., Fernandez-Suarez, J. & Jeffries, T.E. 2004. Lithogeochemical and Sm-Nd and U-Pb isotope data from the Silurian–Lower Devonian Arisaig Group clastic rocks, Avalon terrane, Nova Scotia:A record of terrane accretion in the Appalachian-Caledonide orogen. *GSA Bulletin*,**116** (9/10), 1183-1201.

Murphy J.B., Fernandez-Suarez, J., Keppie, J.D. & Jeffries, T.E. 2004. Contiguous rather than discrete Paleozoic histories for the Avalon and Meguma terranes based on detrital zircon data. *Geology*, **32** (7), 585-588.

Noble, S.R., Hyslop, E.K. & Highton, A.J. 1996. High-precision U-Pb monazite geochronology of the c. 806 Ma Grampian Shear Zone and the implications for the evolution of the Central Highlands of Scotland. *Journal of the Geological Society, London*, **153**, 511-514.

Oliver, G.J.H., Chen, F. Buchwald, R. & Heger, E. 2000 Fast tectonothermal metamorphism and exhumation in the type area of the Barrovian and Buchan zones. *Geology*, **28**, 459-462.

Parrish, R.R. 1990. U-Pb dating of monazite and its applications to geological problems. *Canadian Journal of Earth Sciences*, **27** (11), 72-75.

Payne, J.L., Barovich, K.M. & Hand, M. 2006. Provenance of metasedimentary rocks in the northern Gawler Craton, Australia: Implications for Palaeoproterozoic reconstructions. *Precambrian Research*, **148**, 275-291.

Payne, J.L., Wade, B.P., Hand, M., Barovich, K.M., Maidment, D. & Netting, A. Submitted. Optimisation, fractionation and accuracy of LA-ICP-MS for U-Pb monazite geochronology: Applications from the earliest Palaeoproterozoic to Palaeozoic. *Submitted to Chemical Geology*.

Phillips, E.R., Highton, A.J., Hyslop, E.K. & Smith, M. 1999a. The timing and P-T conditions of regional metamorphism in the Central Highlands, Scotland. *Journal of the Geological Society, London*, **156**, 1175-1193.

Powell, R. & Holland, T. 1988. An internally consistent thermodynamic dataset with uncertainties and corrections: 3 Applications to geobarometry, worked examples and a computer program. *Journal of Metamorphic Geology*, **6**, 173-204.

Powell, R. & Holland, T. 1994. Optimal geothermometry and geobarometry. *American Mineralogist*, **79** (1-2), 120-133.

Powell, R., Holland, T.B.J. & Worley, B. 1998. Calculating phase diagrams involving solid solutions via non-linear equations with examples using THERMOCALC. *Journal of Metamorphic Geology*, **16**, 257-271.

Prichard, H.M. 1985. The Shetland ophiolite. *In*: Gee, D.G. & Sturt, B.A. (eds). The Caledonide Orogen-Scandinavia and related areas. 1173-1184.

Pyle, J.M., Spear, F.S., Wark, D.A., Daniel, C.G. & Storm, L.C. 2005. Contributions to precision and accuracy of chemical ages of monazite. American Mineralogist, 90 (4), 547-577.

Ramsay, J.G. 1963. Structure and metamorphism of the Moine and Lewisian rocks of the North-West Caledonides. *In*: Johnson, M.R.W. & Stewart, F.H. (eds). The British Caledonides. Oliver & Boyd, Edinburgh, 143-170.

Ritchie, J.D., Hitchen, K. & Mitchell, J.G. 1987. The offshore continuation of the Moine Thrust north of Shetland as deduced from basement isotopic ages. *Scottish Journal of Geology*, **23** (2), 163-173.

Roberts, D. 2003. The Scandinavian Caledonides: event chronology, palaeogeographic settings and likely modern analogues. *Tectonophysics,* **365**, 283-299.

Robertson, S. & Smith, M. 1999. The significance of the Geal Charn-Ossian Steep Belt in basin development in the Central Scottish Highlands. *Journal of the Geological Society, London*, **156**, 1175-1182.

Rogers, G., Hyslop, E.K., Strachan, R.A., Paterson, B.A. & Holdsworth, R.E. 1998. The structural setting and U-Pb geochronology of Knoydartian pegmatites in W Inverness-shire: evidence for Neoproterozoic tectonothermal events in the Moine of NW Scotland. *Journal of the Geological Society, London*, **155**, 685-696.

Rubatto, D., Williams, I.S. & Buick, I.S. 2001. Zircon and monazite response to prograde metamorphism in the Reynolds Range, central Australia. *Contrib Mineral Petrol*, **140**, 458-468.

Sandiford, M. & Powell, R. 1990. Some isostatic consequences of the vertical strain geometry in convergent orogens. *Earth and Planetary Science Letters*, **98**, 154-165.

Sandiford, M. & Powell, R. 1991. Some remarks on high-temperature-low pressure metamorphism in convergent orogens. *Journal of metamorphic Geology*, **9**, 333-340.

Schwab, F.L., Nystuen, J.P. & Gunderson, L. 1988. Pre-Arenig evolution of the Appalachian-Caledonide orogen: sedimentation and stratigraphy. From Harris, A.L., Fettes, D.J. (eds), 1988. The Caledonian-Appalachian Orogen. Geological Society Special Publication No. 38, pp. 75-91.

Smith, H.A. & Barreiro, B. 1990. Monazite U-Pb dating of staurolite grade metamorphism in pelitic schists. *Contrib Mineral Petrol*, **105**, 602-615.

Smith, M., Robertson, S. & Rollin, K.E. 1999. Rift basin architecture and stratigraphical implications for basement-cover relationships in the Neoproterozoic Grampian Group of the Scottish Caledonides. *Journal of the Geological Society*, London, **156**, 1163-1173.

Soper, N.J., Ryan, P.D. & Dewey, J.F. 1999. Age of the Grampian orogeny in Scotland and Ireland. *Journal of the Geological Society, London*, **156**, 1231-1236.

Spear, F.S. 1993. Inverted metamorphism, P-T paths and tectonic history of west-central New Hampshire. *In*: Field trip guidebook for the northeastern United States. 28-33.

Spray, J.G. 1988. Thrust-related metamorphism beneath the Shetland Islands oceanic fragment, northeast Scotland. *Canadian Journal of Earth Sciences*, **25**, 1760-1776.

Spray, J.G. & Dunning, G. R. 1991. A U/Pb age for the Shetland Islands oceanic fragment, Scottish Caledonides: evidence from anatectic plagiogranites in 'layer 3' shear zones. *Geological Magazine*, **128** (6), 667-671.

Storey, C.D., Brewer, T.S. & Parrish, R.R. 2004. Late-Proterozoic tectonics in northwest Scotland: one contractional orogeny or several? *Precambrian Research*, **134**, 227-247.

Strachan, R.A. 2000. The Grampian Orogeny: Mid-Ordovician arc-continent collision along the Laurentian margin of Iapetus. In: Woodcock, N.H., Strachan, R.A. (eds) *Geological History of Britain and Ireland*. Blackwell Science Ltd, Oxford, 88-106.

Strachan, R.A., Harris, A.L., Fettes, D.J. & Smith, M., 2002. The Highland and Grampian terranes. In: Trewin, N.H. (eds). The Geology of Scotland. *The Geological Society, London*, 81-148.

Tanner, P.W.G. & Bluck, B.J., 1999. Current controversies in the Caledonides. Journal of the *Geological Society, London*, **156**, 1137-1141.

Tanner, P.W.G. & Evans, J.A. 2003. Late Precambrian U-Pb titanite ages for peak regional metamorphism and deformation (knoydartian orogeny) in the western Moine, Scotland. *Journal of the Geological Society, London*, **160**, 555-564.

Tinkham, D.K., Zuluaga, C.A. & Stowell, H.H., 2001. Metapelite phase equilibria modeling in MnNCKFMASH: The effect of variable Al2O3 and MgO/(MgO+FeO) on mineral stability. *Geological Materials Research*, **3** (1), 1-42.

Tinkham, D.K. & Ghent, E.D. 2005. Estimating P-T conditions of garnet growth with isochemical phase-diagram sections and the problem of effective bulk-composition. *The Canadian Mineralogist*, **43**, 35-50.

Vance, D., Strachan, R.A. & Jones, K.A. 1998. Extensional versus compressional setting for metamorphism: Garnet chronometry and pressure-temperature-time histories in the Moine Supergroup, northwest Scotland. *Geology*, **26** (10), 927-930.

Watt, G.R., Kinny, P.D., Friderichsen, J.D., 2000. U-Pb geochronology of Neoproterozoic and Caledonian tectonothermal events in the East Greenland Caledonides. *Journal of the Geological Society, London*, **157**, 1031-1048.

Watt, G.R. & Thrane, K., 2001. Early Neoproterozoic events in East Greenland. *Precambrian Research*, **110**, 165-184.

Wei, C.J., Powell, R. & Clarke, G.L., 2004. Calculated phase equilibria for low- and medium-pressure metapelites in the KFMASH and KMnFMASH systems. *Journal of Metamorphic Geology*, **22**, 495-508.

White, R.W., Powell, R. & Holland, T.J.B. 2001. Calculation of partial melting equilibria in the system Na2O-CaO-K2O-FeO-MgO-Al2O3-SiO2-H2O (NCKFMASH). *Journal of Metamorphic Geology*, **19**, 139-153.

White, R.W., Powell, R. & Phillips, G.N. 2003. A mineral equilibria study of hydrothermal alteration in mafic greenschist facies rocks at Kalgoorlie, Western Australia. *Journal of Metamorphic Geology*, **21**(5), 455-468.

Figure captions

Fig. 1. **A**. Map of the North Atlantic region with the extent of the Caledonian Orogeny marked on in black (Taken from Kocks *et al.* 2006). **B**. Map of Scotland taken from Tanner & Evans (2003).

Fig. 2. Map of the Shetland Islands. **A** Location of the Shetland Islands with respect to Great Britain. **B** Simplified geological map of the islands.

Fig. 3. **A**. Plot of pressure against XH_2O (mole fraction of H_2O in a H_2O-CO_2 fluid) at a temperature of 650°C Note that as the XH_2O decreases, the pressure increases. The calculated pressures are within 95% confidence when the fit value is below 1.54. **B**. Plot of temperature against XH_2O at a pressure of 10 kbar. Note that temperature decreases with decreasing XH_2O. The calculated temperatures are within 95% confidence when the fit value is below 1.54.

Fig. 4. Sample locations in the Shetlands. Southern mainland is omitted from this Figure for simplification.

Fig. 5. Field photographs of the Shetlands. **A.** Shetland ophiolite, which sits along the east coast of Unst and Fetlar. The ophiolite is comprised of 2 sheets of oceanic crust that have been obducted onto the continental crust of the islands (hammer is 40cm long; Photograph courtesy of Martin Hand). **B.** Low-grade rocks of Unst directly to the west of the obducted ophiolite, GR: 63123, 16449 (pencil is 15cm long). **C.** Higher-grade rocks on the western side of Unst, GR: 56933, 05872 (west of the Burra Firth Lineament, hammer is 40cm long; Photograph courtesy of Dave Kelsey). **D.** Schistose rocks of Yell, GR: 49991, 81530 (Photograph courtesy of Dave Kelsey). **E.** High-grade rocks of Lunna Ness, partial melt is visible and mafic rocks appear to make up about 20% of the outcrop, GR: 52301, 73112 (Photograph courtesy of Martin Hand). **F.** Shows the Moine rocks of Shetland from North Mainland, GR: 37174, 94000 (Photograph courtesy of Martin Hand).

Fig. 6. Photomicrographs of key petrological relationships. **A.** SH-13 showing a shattered garnet, partially altered to chlorite. Cl is chlorite, Gt is garnet, Ilm is ilmenite, Ms is muscovite, Pl is plagioclase and Qtz is quartz. **B.** Sample FRQ-1 showing the peak assemblage of the mineral. St is staurolite, Gt is garnet, Cl is chlorite, Ctd is Chloitoid, Ms is muscovite and Ilm is ilmenite. **C.** SH-10 showing the replacement of garnet by chlorite. Cl is chlorite, Gt is garnet, Ms is muscovite, Ilm is ilmenite, Bt is biotite, Pl is plagioclase and Qtz is quartz. **D.** Replacement of plagioclase by unfoliated muscovite in SH-10. Ms is muscovite, Bt is biotite, Pl is plagioclase and Qtz is quartz. **E.** Sillimanite inclusions in a garnet from sample SH-11. Gt is garnet, Sil is sillimanite, Ms is muscovite, Bt is biotite, Ilm is ilmenite and Qtz is quartz. **F.** Sample SH-14 giving the peak assemblage, a muscovite porphyroblast can be seen at the edge of the image. Gt is garnet, Ms is muscovite, Bt is biotite, Pl is plagioclase and Qtz is quartz. **G.** Peak assemblage for sample SH-9. Gt is garnet, Ms is muscovite, Bt is biotite, Ky is kyanite, St is staurolite, Pl is plagioclase and Qtz is quartz. **H.** Peak assemblage of SH-24. Gt is garnet, Ms is muscovite, Bt is biotite, Ky is kyanite, St is staurolite and Qtz is quartz. **I.** Peak assemblage in SH-30a. Gt is garnet, Hb is hornblende, Ti is titanite, Pl is plagioclase and Qtz is quartz. **J.** Distinct layers of hornblende and biotite in sample SH-31. Hb is hornblende, Bt is biotite, Gt is garnet, Ilm is ilmenite, Ti is titanite, Pl is plagioclase and Qtz is quartz. **K.** Sample SH-29, K-feldspar is being replaced by fine-grained muscovite. Gt is garnet, Ms is muscovite, Kfs is K-feldspar, Pl is plagioclase, Bt is biotite and Qtz is quartz. **L.** Garnet in SH-31c being replaced by biotite. Gt is

garnet, Bt is biotite, Pl is plagioclase, Ilm is ilmenite and Qtz is quartz. **M.** Peak mineral assemblage of sample FRQ-20B. Gt is garnet, Bt is biotite, Pl is plagioclase, Ky is kyanite, Sil is sillimanite, Kfs is K-feldspar and Qtz is quartz. **N.** Sample FRQ-20A showing inclusions of muscovite in a garnet, the replacement of sillimanite by muscovite is also apparent. Gt is garnet, Ms is muscovite, Bt is biotite, Ilm is ilmenite, Pl is plagioclase and Qtz is quartz. **O.** Kyanite, partially replaced by muscovite from Sample FRQ-20A. Gt is garnet, Ky is kyanite, Ms is muscovite, Bt is biotite and Qtz is quartz. **P.** Helitical inclusion trail in a garnet of SH-16, the yellow line highlights the trend of the inclusions. Gt is garnet, Cl is chlorite, Bt is biotite, Ms is muscovite and Qtz is quartz.

Fig. 7. **i)** Compositional maps of the garnet grains, **ii)** shows the zoning profiles of the mapped grains. **A** is sample SH-16a, **B** is sample SH-16b, **C** is sample FRQ-1, **D** is sample SH-31c, **E** is sample SH-9, **F** is sample SH-11 and **G** is sample SH-14. Note: samples SH-16a and SH-16b are two grains taken from the same sample.

Fig. 8. **A.** Phase diagram for sample SH-9 based on one from Tinkham *et al.* (2001). The diagram was calculated using rocks of a similar composition to those of SH-9. Based on mineralogy, the peak mineral assemblage of SH-9 is garnet-biotite-muscovite-plagioclase-kyanite-quartz. Relict staurolite grains armoured within large plagioclase grains give a prograde assemblage for the sample of staurolite-garnet-plagioclase-biotite-muscovite-quartz. Using both of these assemblages a, PT path can be defined (red arrow). The white ellipses represent calculated PT conditions with 1σ errors (c represents the core, r the rim; Table 3) that are plotting over the peak mineral assemblage. **1.** Shows the prograde assemblage in thin-section. **2.** Shows the peak mineral assemblage in thin-section.

Fig. 8 **B.** Phase diagram for sample FRQ-1, based on one from Tinkham & Ghent, (2005). The PT path here is defined by the mineralogy. The peak assemblage is given by the stable mineral assemblage of garnet-staurolite-muscovte-chlorite-chloritoid-ilmenite-quartz. The mineral inclusions present in the garnet represent the prograde assemblage of chloritoid-muscovite-chlorite-ilmentite-quartz. Staurolite is also present in the garnet which probably indicates that it grew at the same time. The foliation which wraps the staurolite and garnet gives the retrograde assemblage of muscovite-chlorite-chloritoid-ilmenite-quartz. The white ellipses give the calculated PT conditions with 1σ errors (c is for core, r for rim). The red arrow indicated the PT path of the sample. **1.** Shows the prograde assemblage in thin-section, present as garnet

inclusions. **2.** Shows the peak assemblage in thin-section. **3.** Shows the retrograde assemblage as the foliation surrounding the garnet and staurolite.

Fig. 8 **C**. Phase diagram for sample SH-24 based on one taken from Wei *et al.* (2004). The diagram is based on rocks of a similar composition to SH-24. The peak assemblage of this sample is garnet-muscovite-kyanite-biotite-quartz. This sample also contains relict staurolite grains (similar to SH-9), which are armoured inside quartz grain, some of which are included in garnet grains. This gives a prograde assemblage for this sample of staurolite-quartz-muscovite-biotite and indicates the growth of garnet subsequent to this. The PT path is represent by the red arrow. The white ellipse gives the calculated PT conditions for the sample with 1σ errors (rim only). **1.** Shows the staurolite inclusion within a garnet, which indicates the prograde assemblage. **2.** Shows the peak mineral assemblage in thin-section.

Fig. 8 **D**. Phase diagram for sample FRQ-20, based on a diagram from White *et al.* (2001). The P-T path is defined by the prograde, peak and retrograde assemblages. The peak mineral assemblage for this sample is kyanite-garnet-biotite-plagiocalse-k-felspar-sillimanite-ilmenite-quartz based on the stable mineral assemblage of the sample. Inclusions of muscovite, biotite and kyanite in garnet give a prograde assemblage of garnet-kyanite-muscovite-biotite-plagioclase-quartz. Kyanite is seen to be slightly replaced and sillimanite almost completely replaced by mica. This could indicate moving through a kyanite unstable field and moving out of the sillimanite stable field. Thus a retrograde assemblage for this sample is garnet-kyanite-muscovite-biotite-plagioclase-quartz. The P-T path is represented by the red arrow. The white ellipse shows the calculated pressure and temperature conditions with 1σ errors (c is core, r is rim) this plots over the peak assemblage. **1.** Shows the inclusions of kyanite and muscovite in the garnet grains (SH-20A). **2.** Shows the peak assemblage of SH-20B in thin-section. **3.** Shows the almost complete replacement of sillimanite by muscovite. **4.** Shows the slight replacement of kyanite by muscovite, indicating that the rock probably went through a field where kyanite is unstable, then re-entered a stable field.

Fig. 9. Monazite age data acquired from the electron microprobe in the form of histograms obtained using the isoplot add on to Microsoft excel. **A** is from sample SH-10, **B** is sample SH-11, **C** is sample SH-24, **D** is sample SH-29, **E** is sample SH-31c and **F** is sample SH-9.

Fig. 10. Monazite grains analysed on the electron microprobe where **A** is sample SH-9 from Yell with a GR: 54080 98765, **B** is sample SH-11 from Western Unst with a GR: 56886 05954, **C** is sample SH-24 from Yell with a GR: 54996 96973, **D** is SH-29 from Lunna Ness with a GR: 51620 74106 and **E** is SH-31c from Lunna Ness with a GR: 51851 74117. The blue spots represent places where the grain has been probed and the numbers indicate the analysis number for that sample.

Fig. 11. Concordia plots obtained from the LA-ICPMS. **A** is from sample SH-9, inset are some images taken on the laser of the grains analysed. **B** is from sample SH-11, inset are images of some of the grains analysed taken on the laser. **C** is from sample SH-29. All figures are given as Terra-Wasserberg plots due to excess common lead in the samples.

Fig. 12. Isochron obtained from the Sm-Nd isotopic data. An age cannot be acquired from this plot as all the points plot too close together to define an accurate isochron.

Fig. 13. Simplified geological map of the Shetlands (omitting southern mainland) including all data collected during this project and all data collected previously. Pressure and temperature information is given in rectangles with all black data collected during this project, asterixed data represents PT calculations using minerals cores while the rest are done using mineral rims. Red pressure and temperature data has been taken from Flinn (1994). Geochronological data is given in ovals with the black once again representing data gathered from this project where the asterix mark the LAICPMS data, while the rest of the geochronology is from the EMPA data. Blue represents data taken from papers.**1**. U/Pb zircon age of a plagiogranite from the Shetland Ophiolite, taken from Spray & Dunning (1991). **2**. Ar/Ar isochron of a hornblende grain from the Norwick hornblendic schist, Flinn *et al.* (1991). **3**. Temperature data acquired using the hornblende-garnet geothermometer of Powell (1985), Pressure data acquired using the garnet-amphibolite geobarometer of Kohn & Spear (1990), Flinn *et al.* 1991. **4-7**. K-Ar ages of hornblende grains taken from beneath the Shetland Ophiolite, Spray (1988). This shows a metamorphic pattern with rocks directly to the west of the ophiolite (e.g. FRQ-1) being low grade, rocks to the west of the Burra Firth lineament (e.g. SH-14) being a higher grade. The rocks on Yell are mid-amphibolite grade, and the rocks of Lunna Ness are upper amphibolite transitional granulite.

Fig. 14. This Fig. shows a cross-section of the Caledonian collision, which caused the ophiolite obduction and thrusting throughout Shetland (adapted from Strachan *et al.* 2002; Strachan 2000). **A.** Shows the onset of the closure of the Iapetus ocean, with subduction beneath a mid-ocean arc, interpreted to be the Midland Valley terrane of Scotland. Arrows represent plate movement at this time. **B.** Shows the onset of Grampian orogenesis with the collision of Laurentia with the mid-ocean arc, this is interpreted to have caused the ca. 460 Ma metamorphism found in the Shetland Islands. Arrows represent plate movement at this time. **C.** This shows the late phase of the Grampian Event where continued pressure from the east caused the obduction of the Shetland Ophiolite. This pressure has also caused further subduction beneath the Laurentia-arc plate. **D.** Illustrates the Scandian event caused by the complete closure of the Iapetus Ocean with the collision between Laurentia and Baltica.

Fig. 1.A

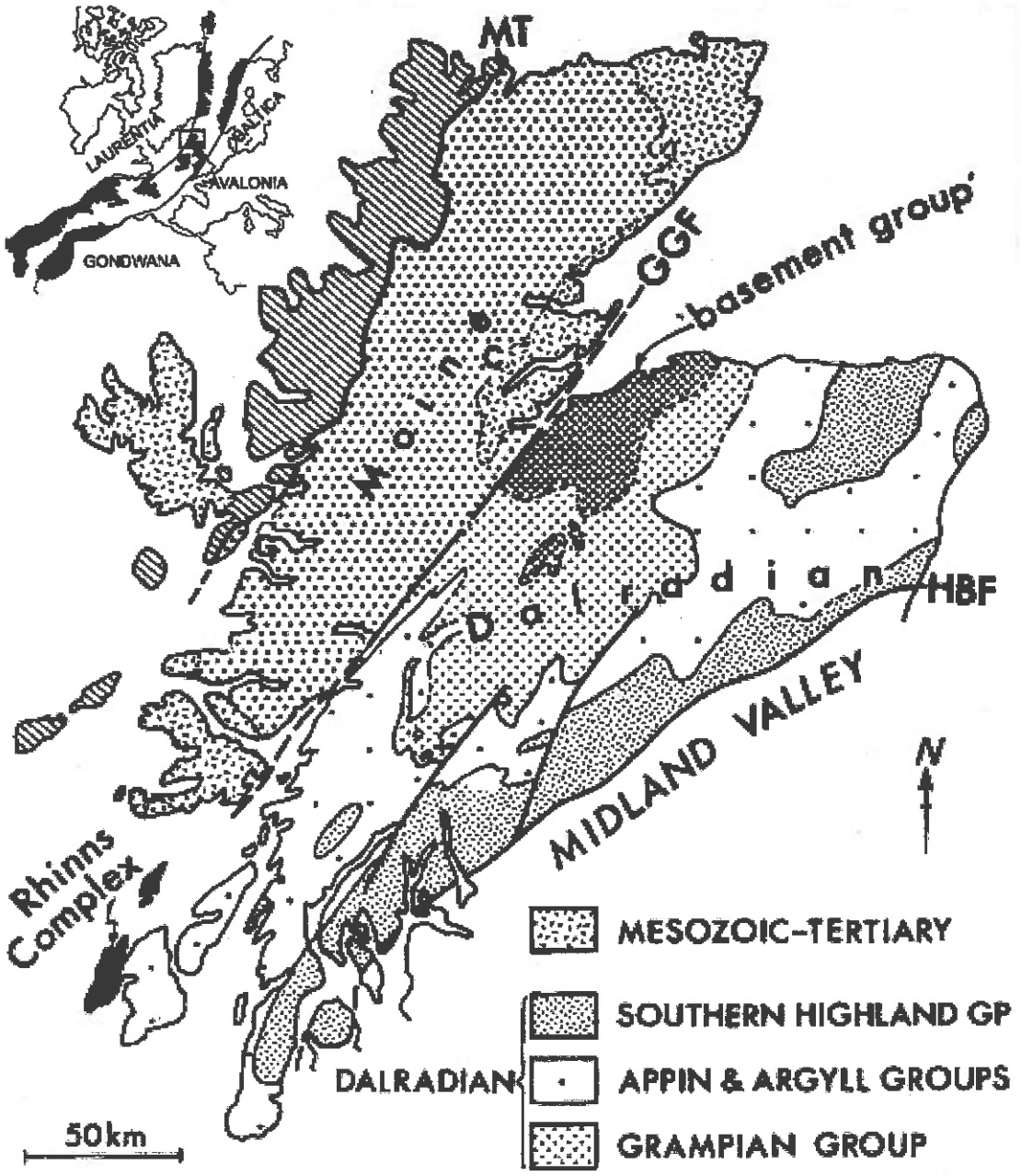

Fig. 1.B

Figure 1.

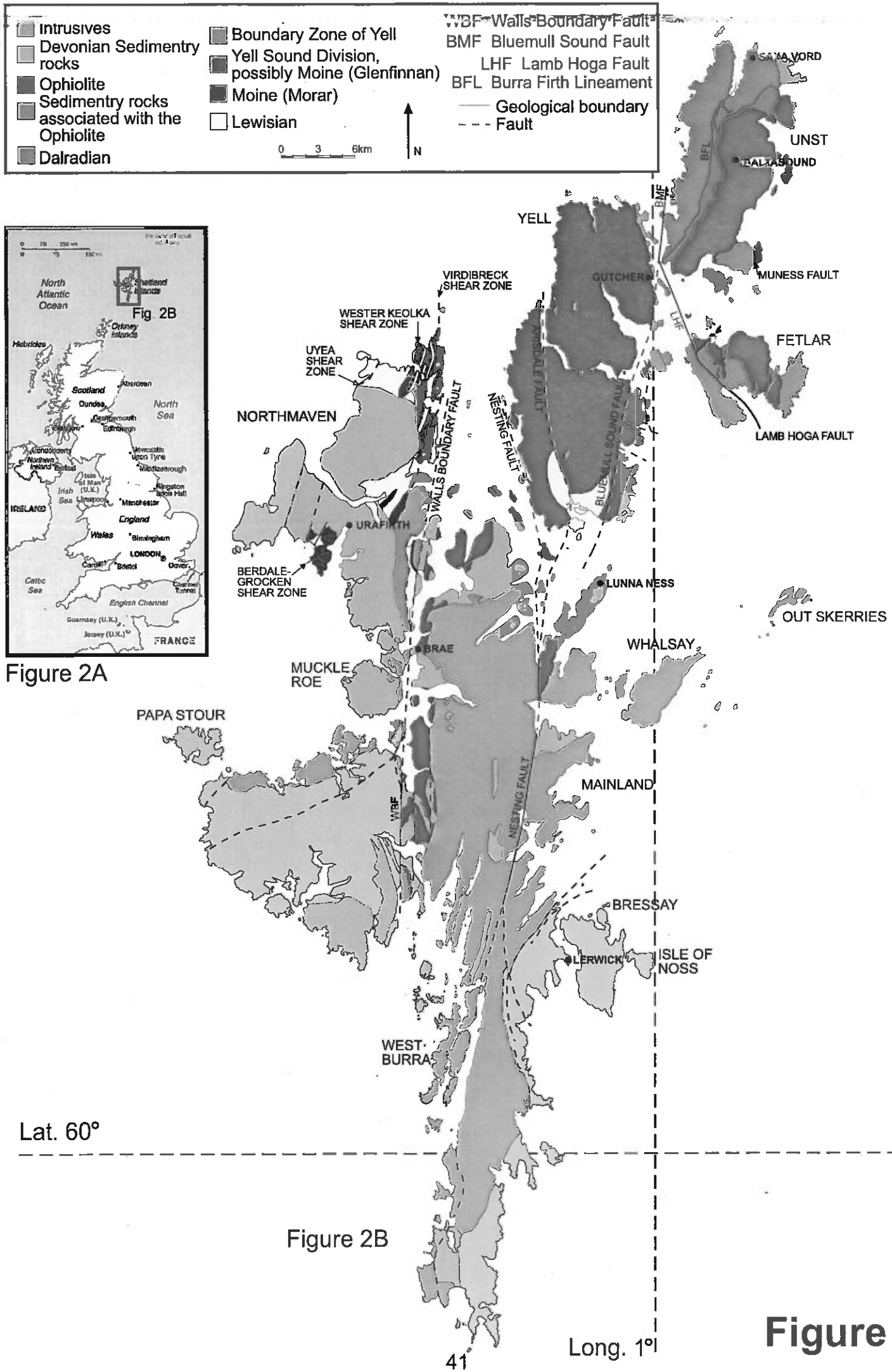
Intrusives
Devonian Sedimentry rocks
Ophiolite
Sedimentry rocks associated with the Ophiolite
Dalradian
Boundary Zone of Yell
Yell Sound Division, possibly Moine (Glenfinnan)
Moine (Morar)
Lewisian
0 3 6km
N
WBF Walls Boundary Fault
BMF Bluemull Sound Fault
LHF Lamb Hoga Fault
BFL Burra Firth Lineament
Geological boundary
Fault
North Atlantic Ocean
Fig. 2B
Orkney Islands
Hebrides
Scotland
Aberdeen
Dundee
North Sea
Edinburgh
Glasgow
Londonderry
Northern Ireland
Belfast
Irish Sea
Isle of Man (U.K.)
Liverpool
Manchester
IRELAND
England
Wales
Birmingham
LONDON
Cardiff
Bristol
Dover
Celtic Sea
English Channel
Guernsey (U.K.)
Jersey (U.K.)
FRANCE
Figure 2A
SAXA VORD
UNST
BALTASOUND
BFL
BMF
YELL
GUTCHER
MUNESS FAULT
VIRDIBRECK SHEAR ZONE
WESTER KEOLKA SHEAR ZONE
UYEA SHEAR ZONE
LHF
FETLAR
NORTHMAVEN
WALLS BOUNDARY FAULT
NESTING FAULT
BLUEMULL SOUND FAULT
LAMB HOGA FAULT
URAFIRTH
BERDALE-GROCKEN SHEAR ZONE
LUNNA NESS
OUT SKERRIES
WHALSAY
BRAE
MUCKLE ROE
PAPA STOUR
MAINLAND
WBF
NESTING FAULT
BRESSAY
LERWICK
ISLE OF NOSS
WEST BURRA
Lat. 60°
Long. 1°
Figure 2B

Figure 2.

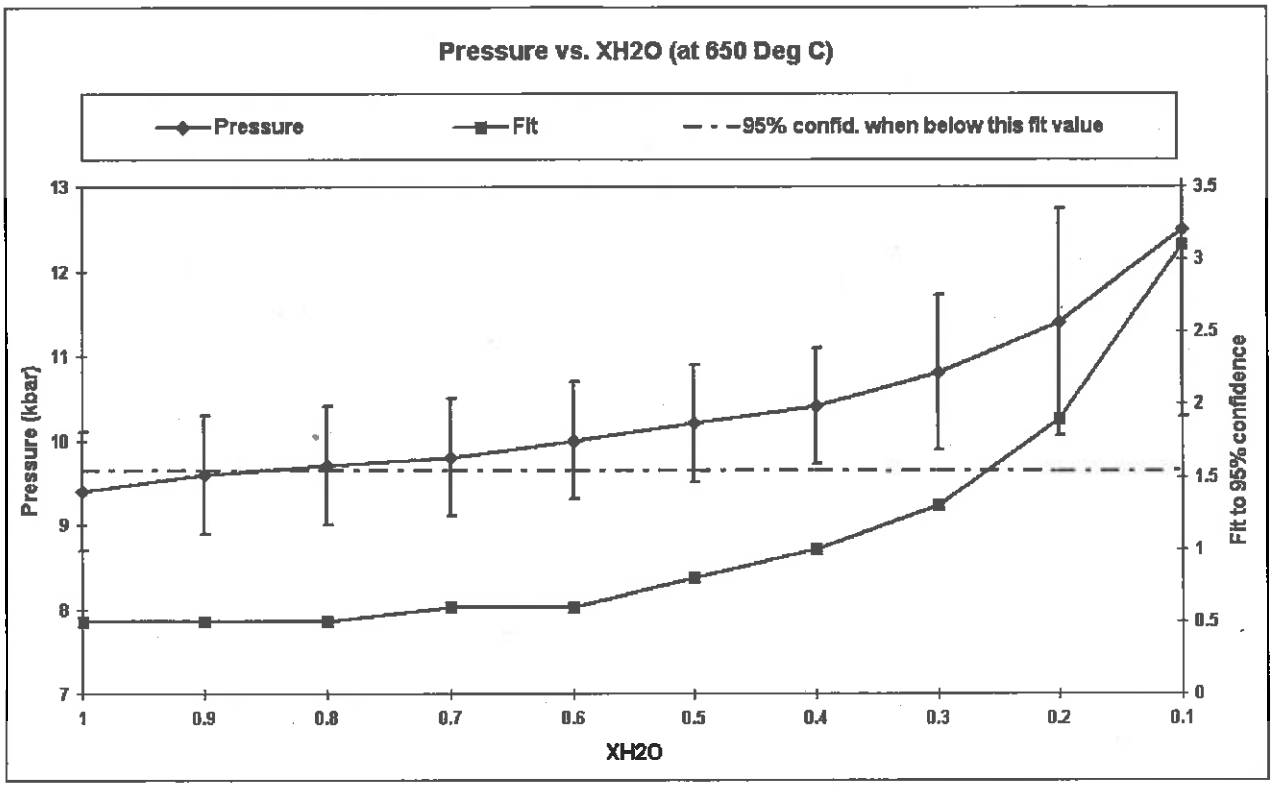

Figure 3A

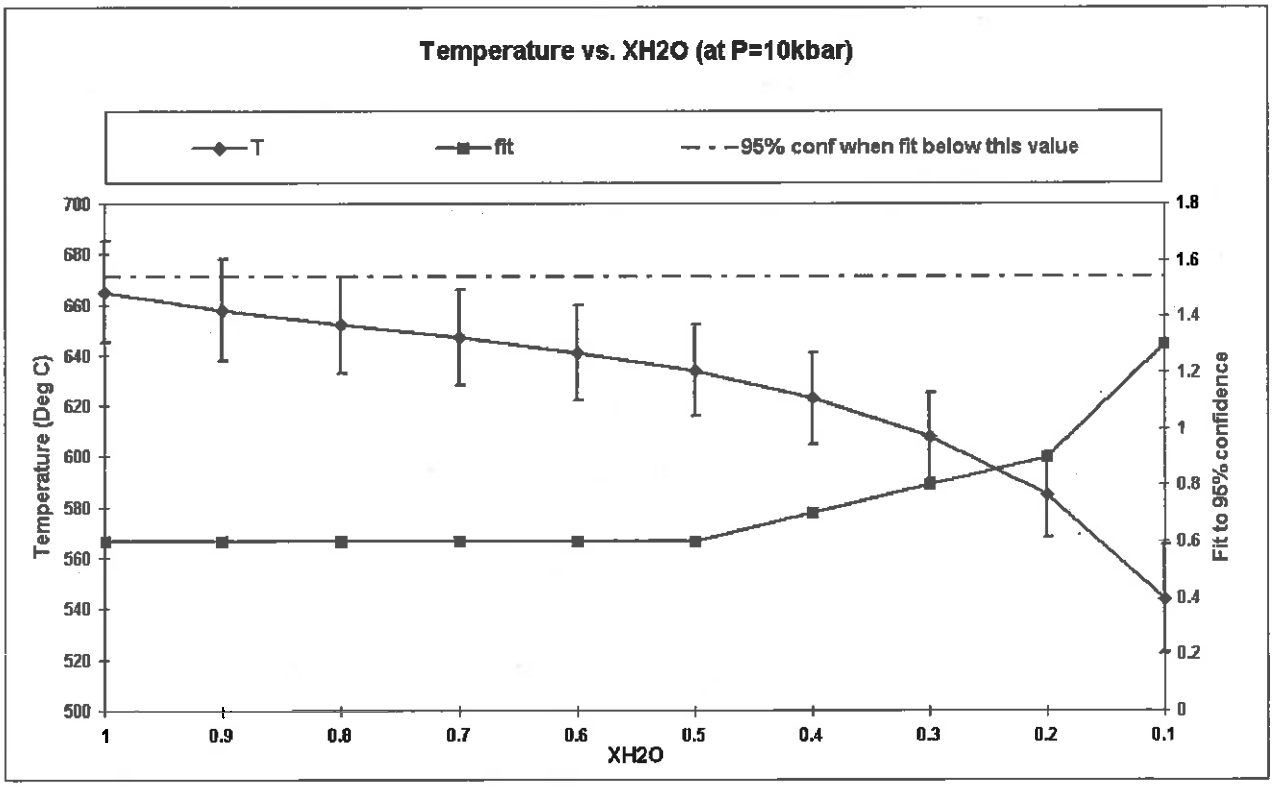

Figure 3B

Figure 3.

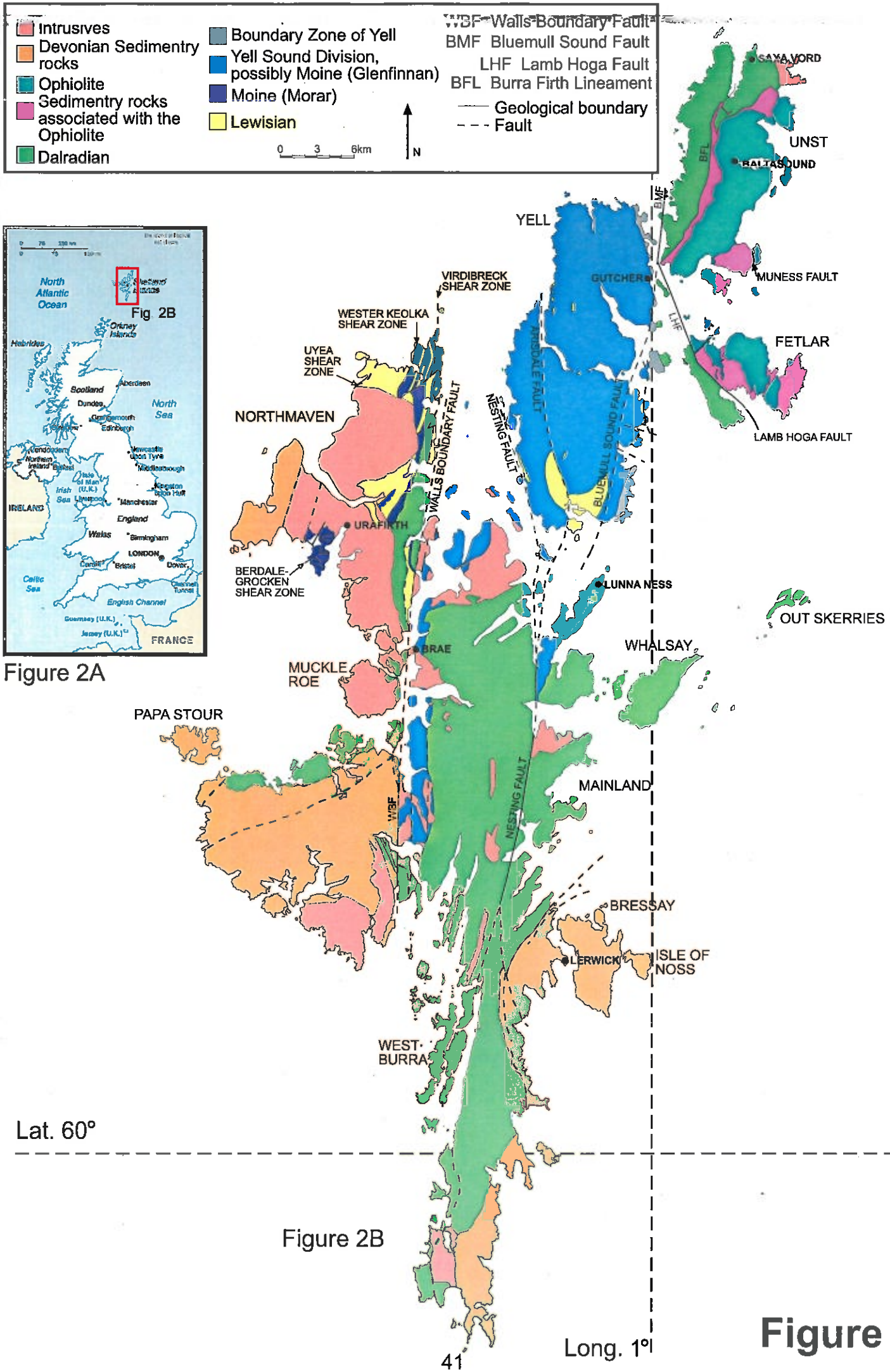

Figure 2A

Figure 2B

Figure 2.

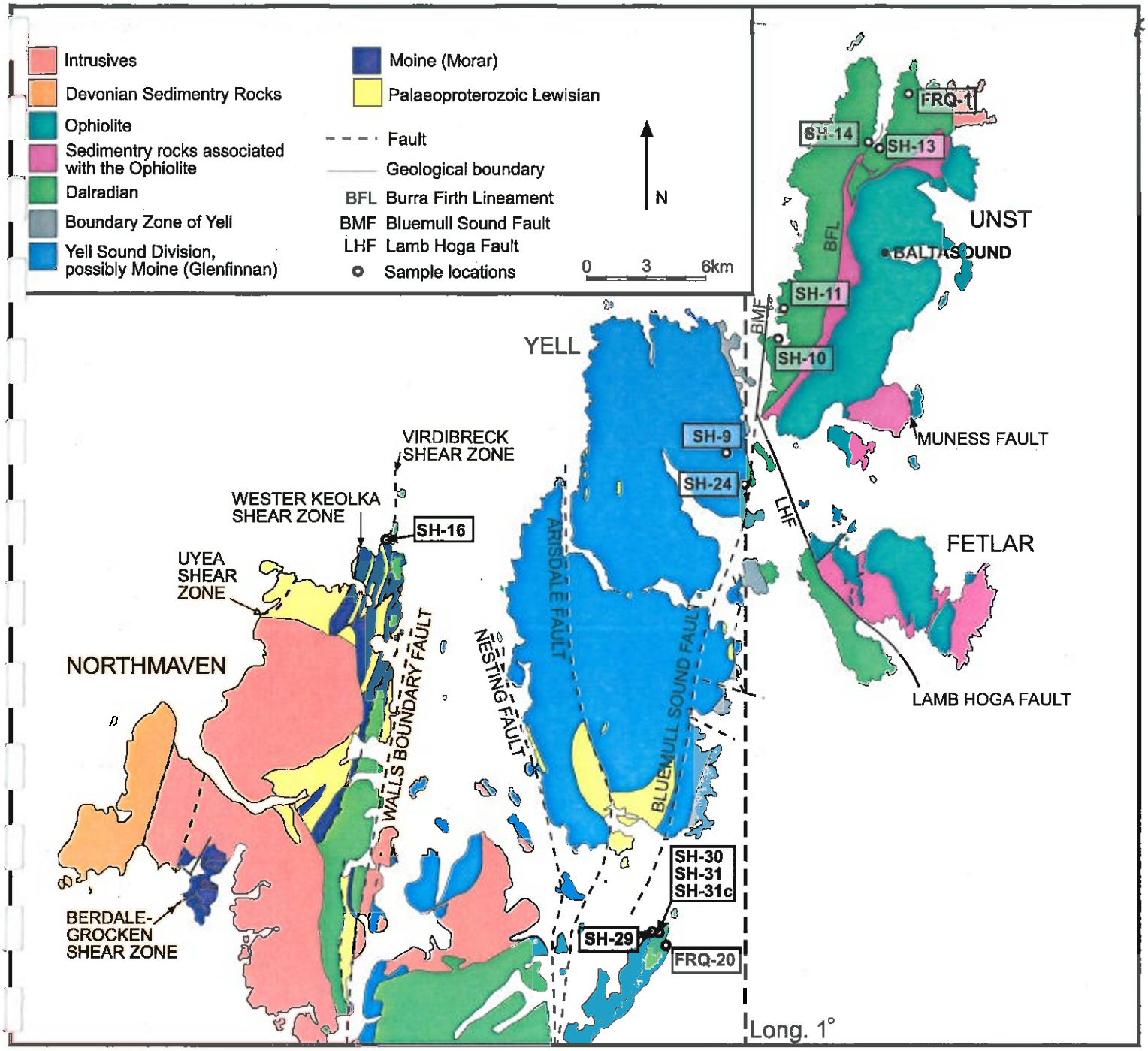
Intrusives
Devonian Sedimentry Rocks
Ophiolite
Sedimentry rocks associated with the Ophiolite
Dalradian
Boundary Zone of Yell
Yell Sound Division, possibly Moine (Glenfinnan)
Moine (Morar)
Palaeoproterozoic Lewisian
Fault
Geological boundary
BFL Burra Firth Lineament
BMF Bluemull Sound Fault
LHF Lamb Hoga Fault
Sample locations
N
0 3 6km
FRQ-1
SH-14
SH-13
UNST
BALTASOUND
BFL
SH-11
SH-10
BMF
MUNESS FAULT
YELL
SH-9
SH-24
LHF
FETLAR
LAMB HOGA FAULT
VIRDIBRECK SHEAR ZONE
WESTER KEOLKA SHEAR ZONE
SH-16
UYEA SHEAR ZONE
NORTHMAVEN
ARISDALE FAULT
NESTING FAULT
BLUEMULL SOUND FAULT
WALLS BOUNDARY FAULT
SH-30
SH-31
SH-31c
SH-29
FRQ-20
BERDALE-GROCKEN SHEAR ZONE
Long. 1°

Figure 4.

A.

B.

C.

D.

E.

F.

Figure 5.

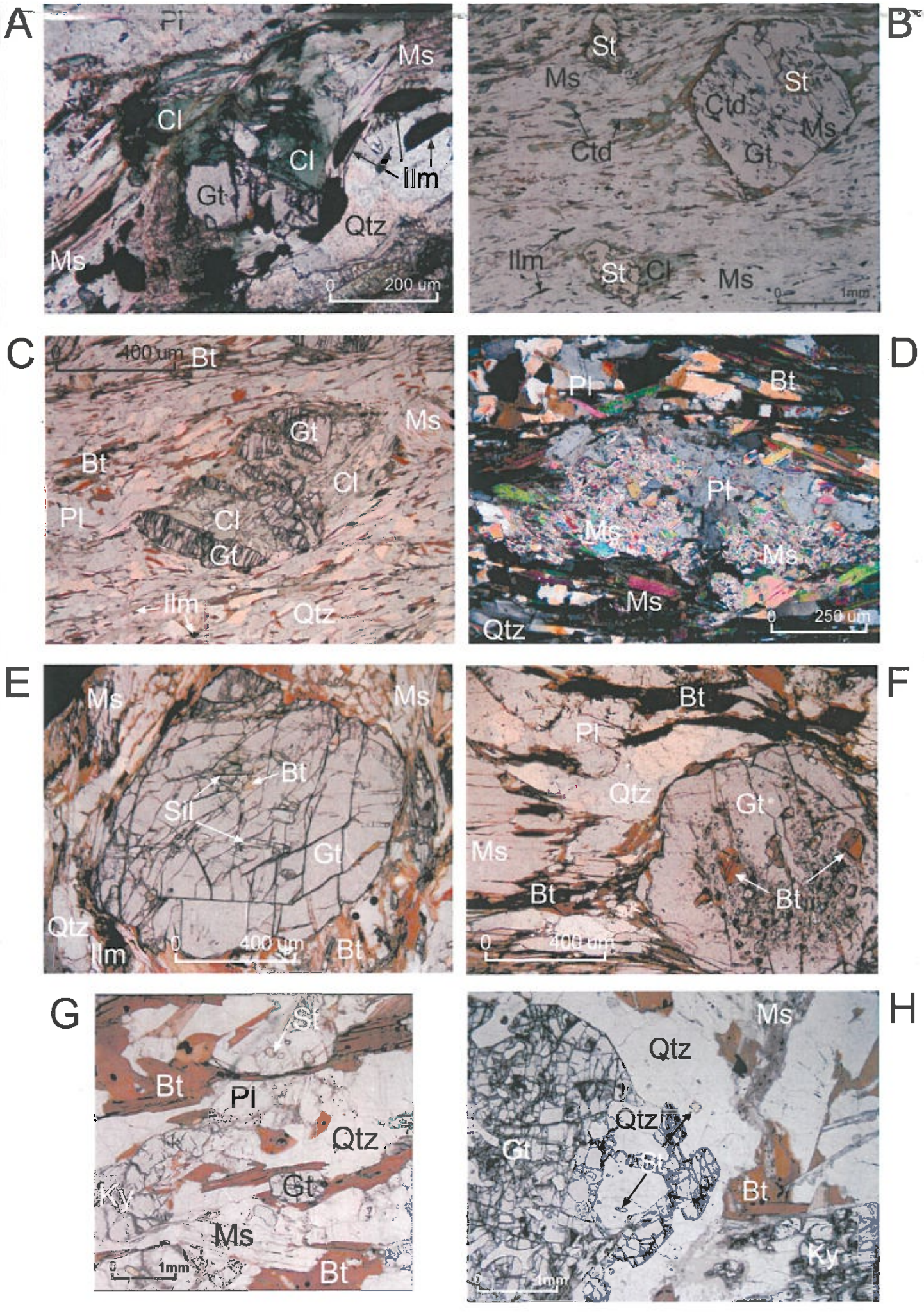
A
Pl
Ms
Cl
Cl
Gt
Ilm
Qtz
Ms
0
200 um
B
St
Ms
St
Ctd
Ms
Ctd
Gt
Ilm
St
Cl
Ms
0
1mm
C
0
400 um
Bt
Gt
Ms
Bt
Cl
Pl
Cl
Gt
Ilm
Qtz
D
Pl
Bt
Pl
Ms
Ms
Ms
Qtz
0
250 um
E
Ms
Ms
Bt
Sil
Gt
Qtz
Ilm
0
400 um
Bt
F
Bt
Pl
Qtz
Gt
Ms
Bt
Bt
0
400 um
G
St
Bt
Pl
Qtz
Gt
Ky
Ms
0
1mm
Bt
H
Ms
Qtz
Qtz
Gt
Bt
Bt
Ky
0
1mm

Figure 6

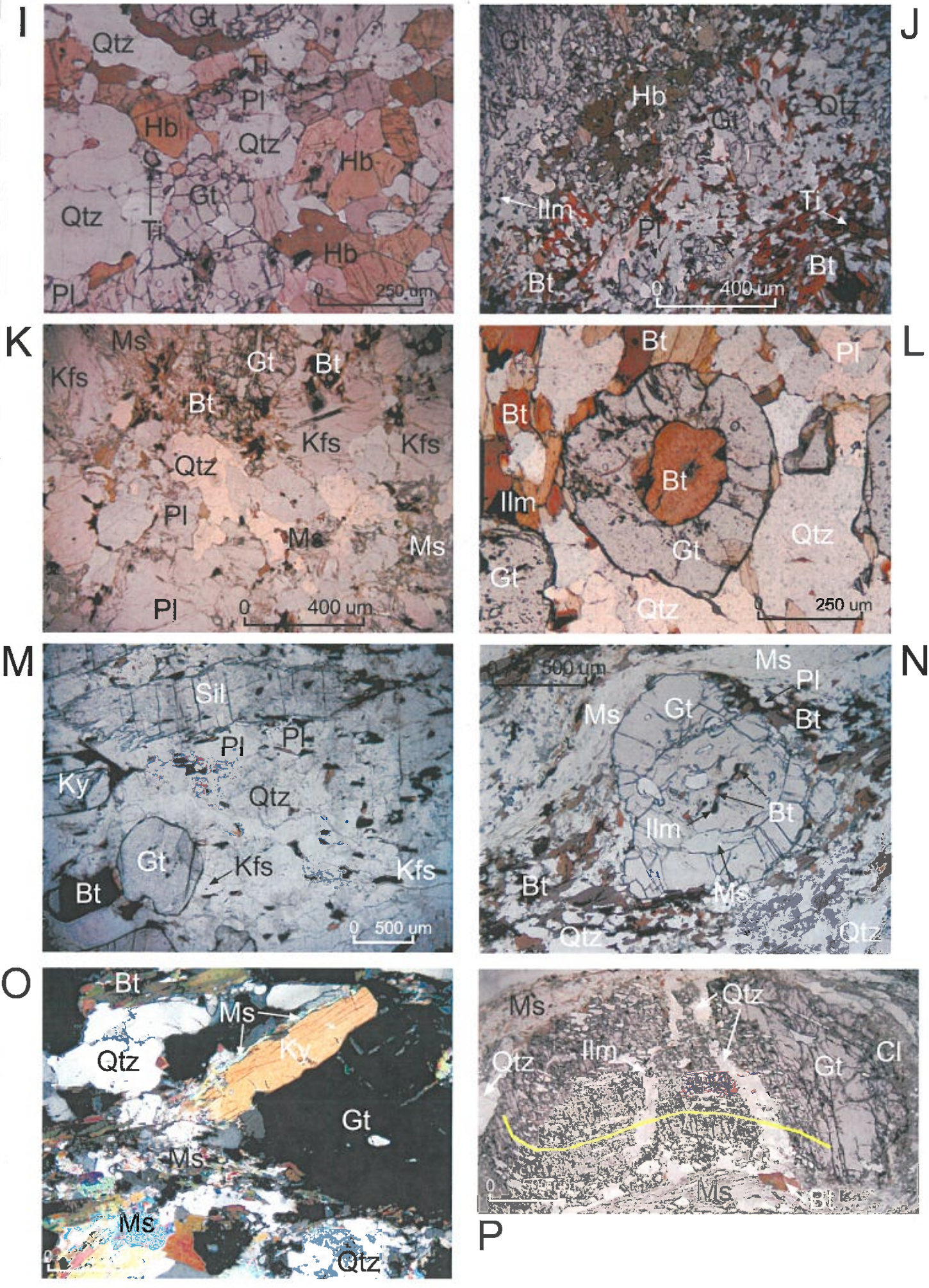

Figure 6 cont.

7i)

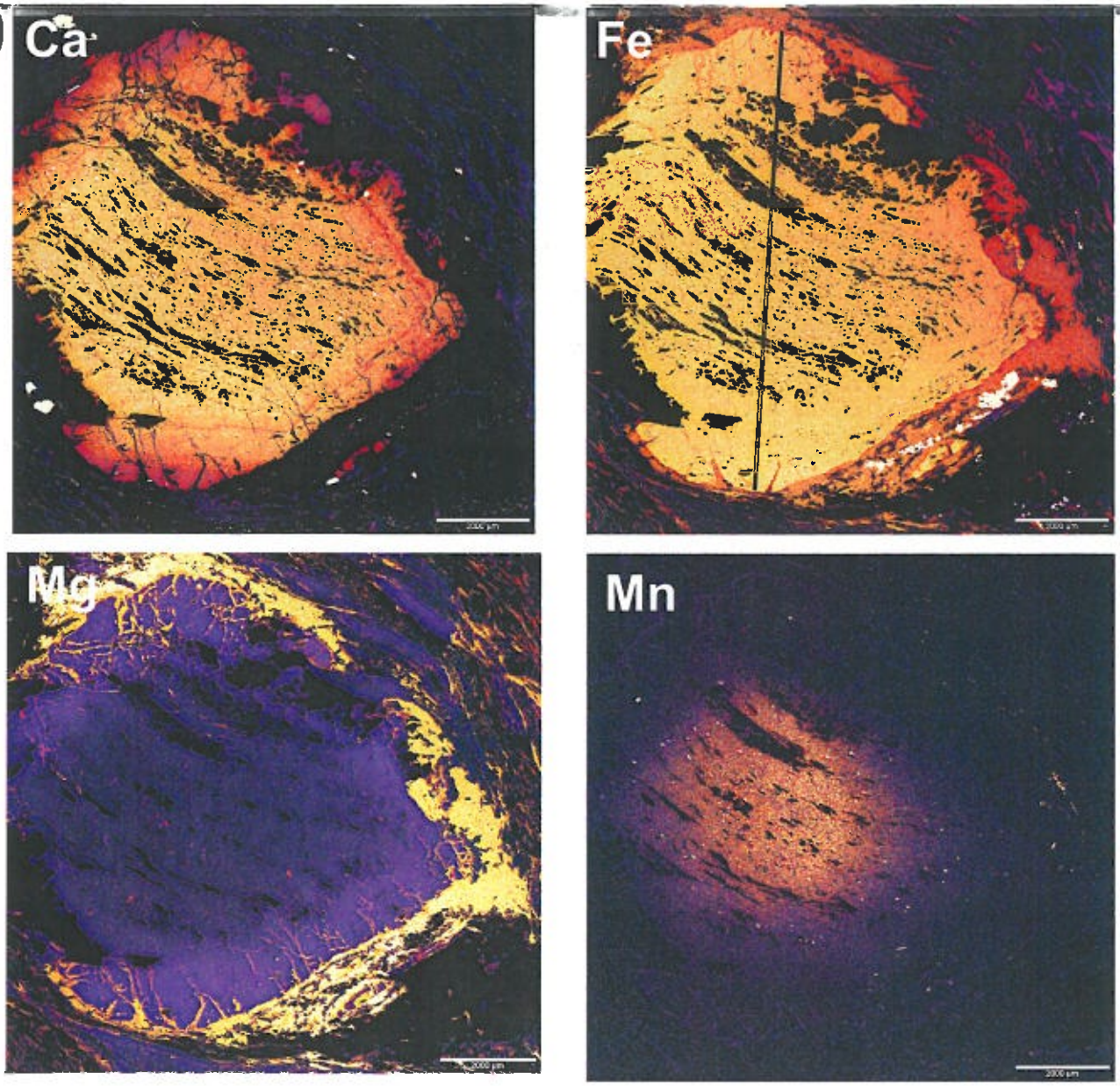

7ii)

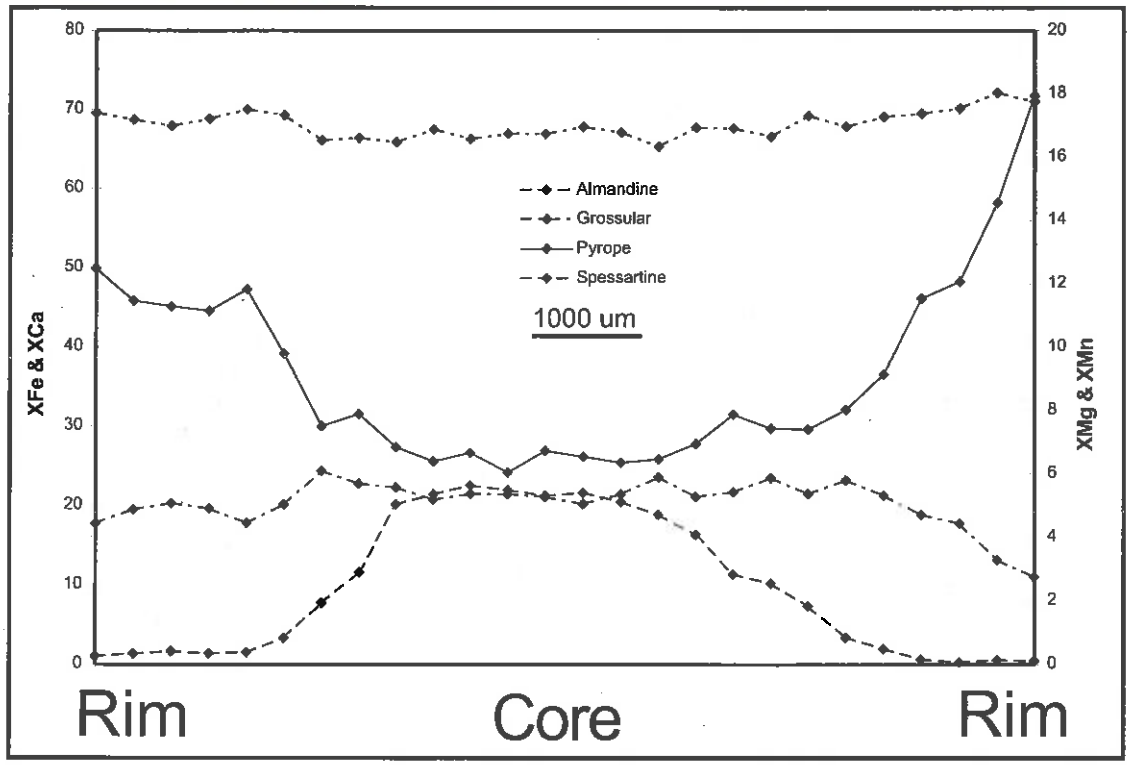

SH-16a

Figure 7A

7i)

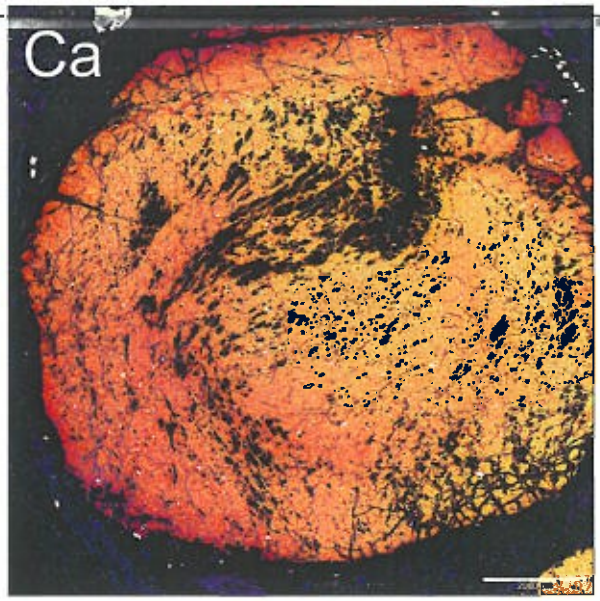

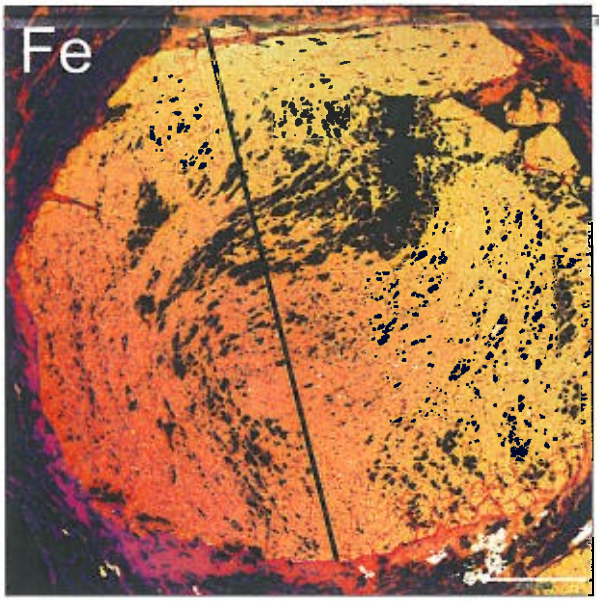

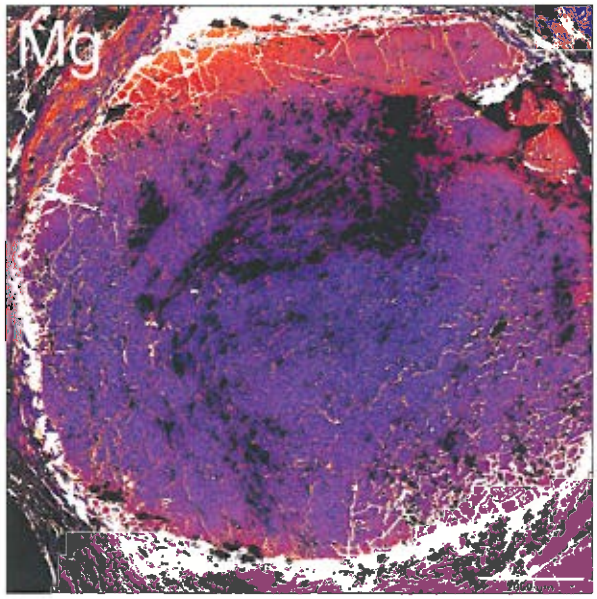

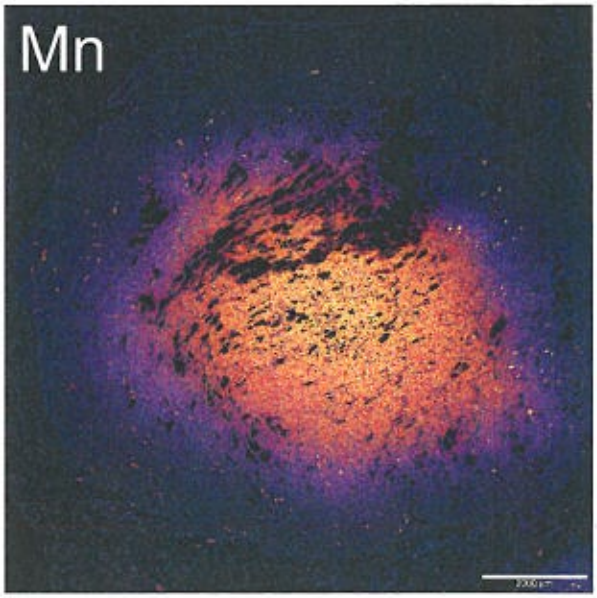

7ii)

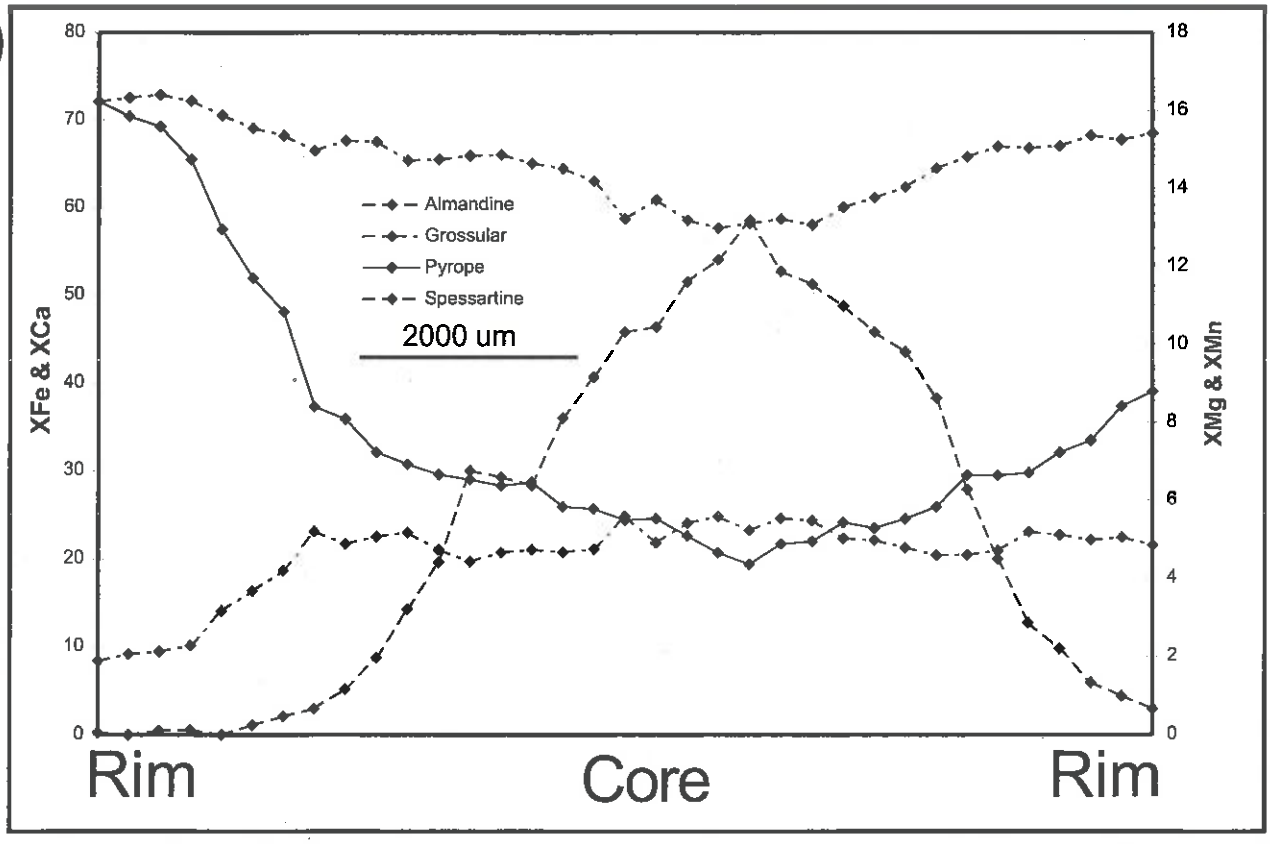

SH-16b

Figure 7B

7i)

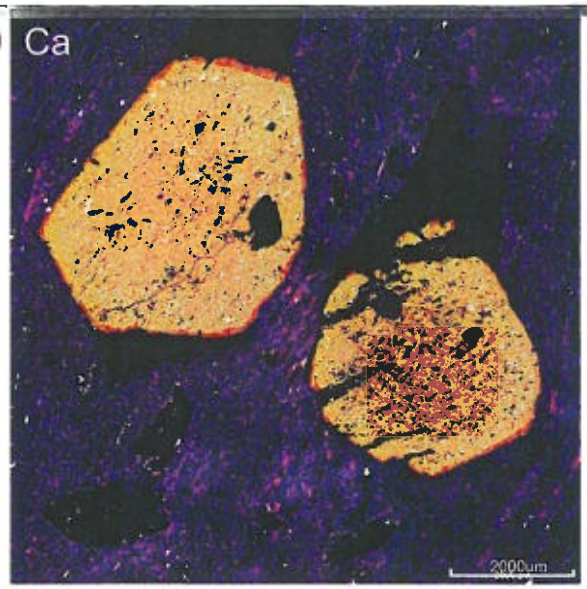

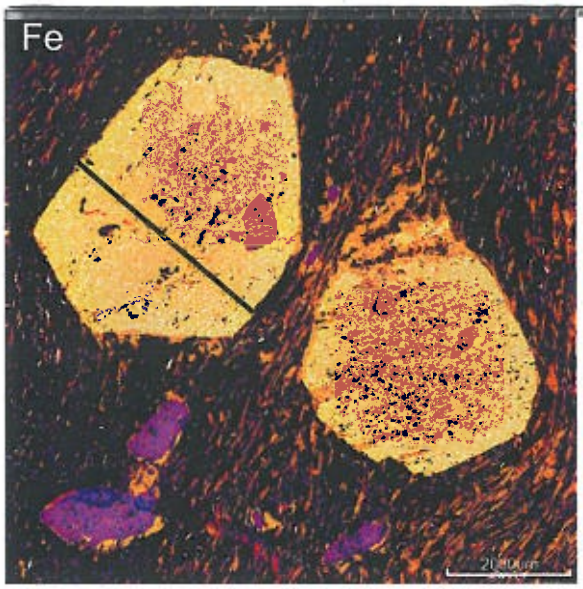

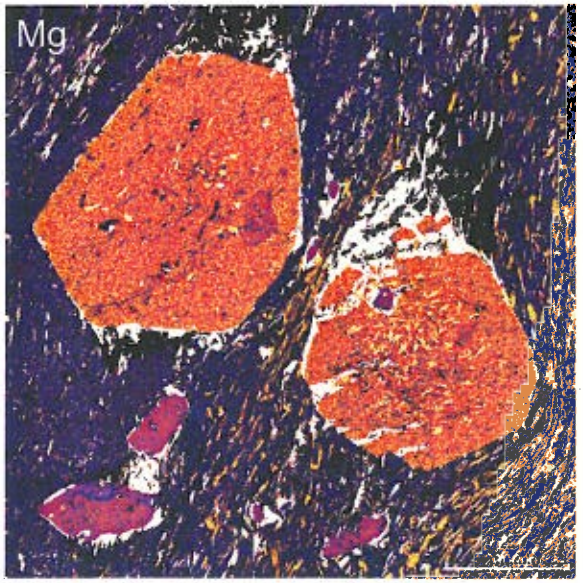

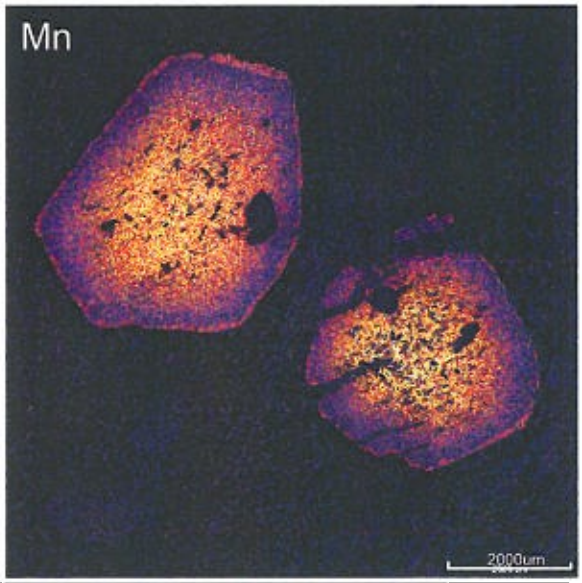

7ii)

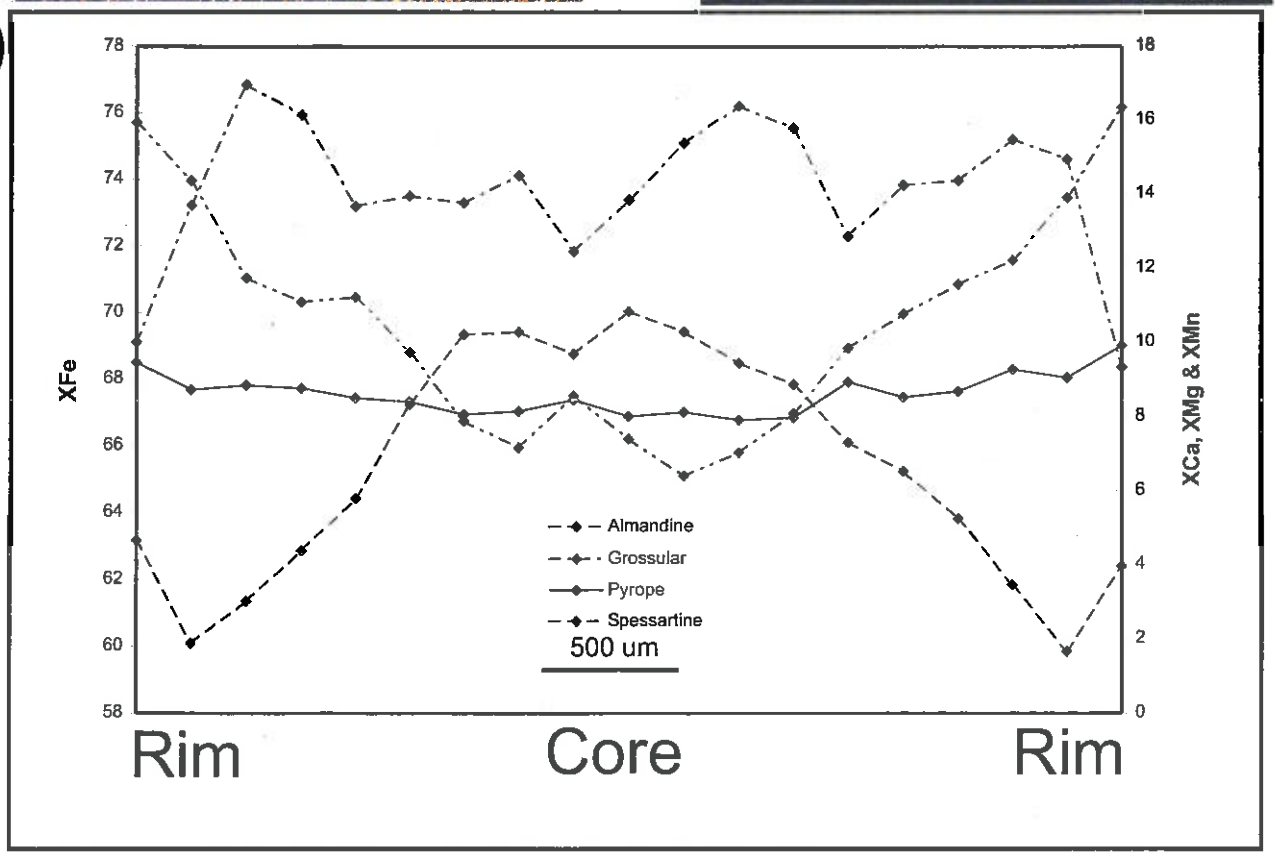

FRQ-1

Figure 7C

7i)

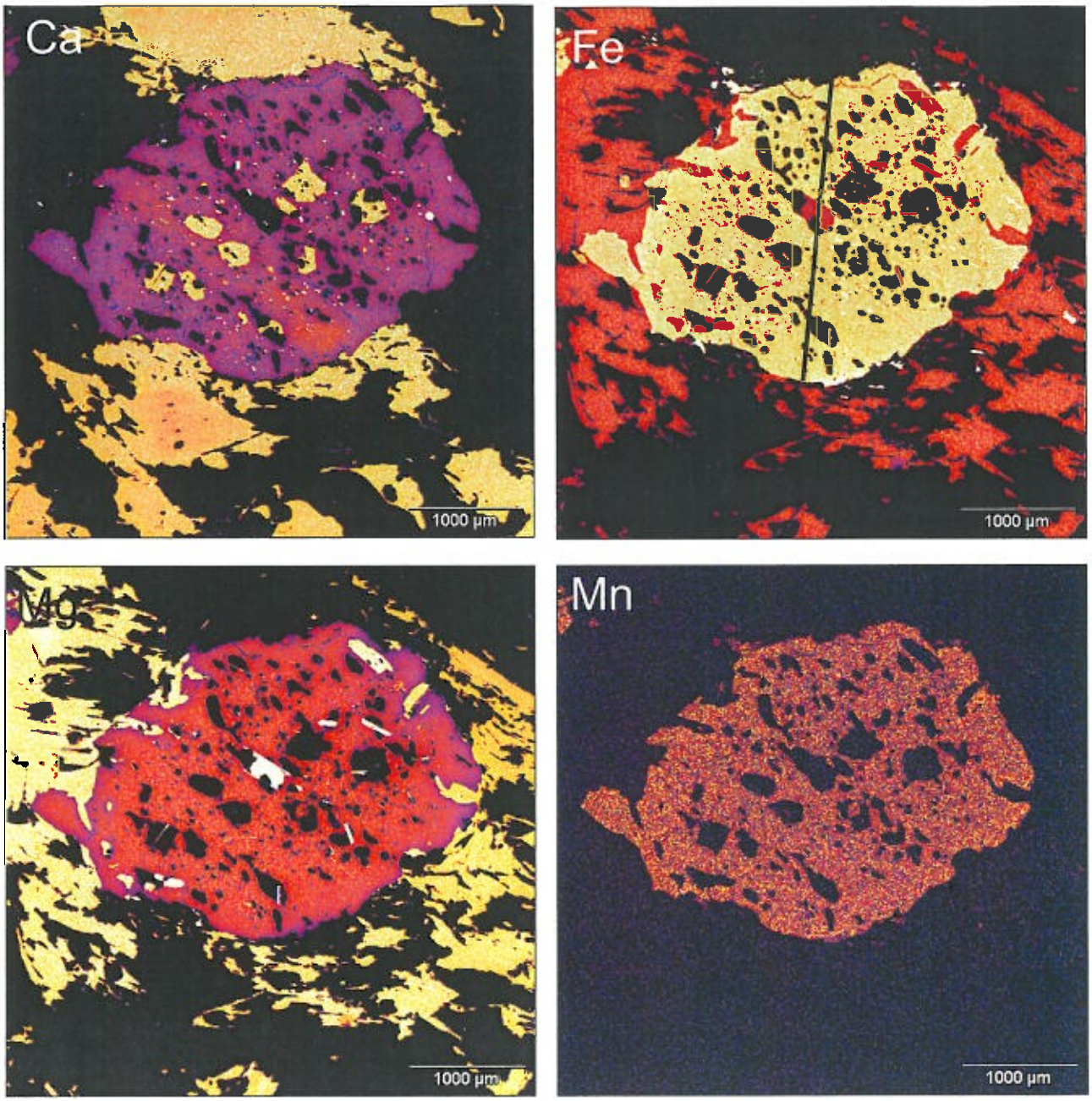

7ii)

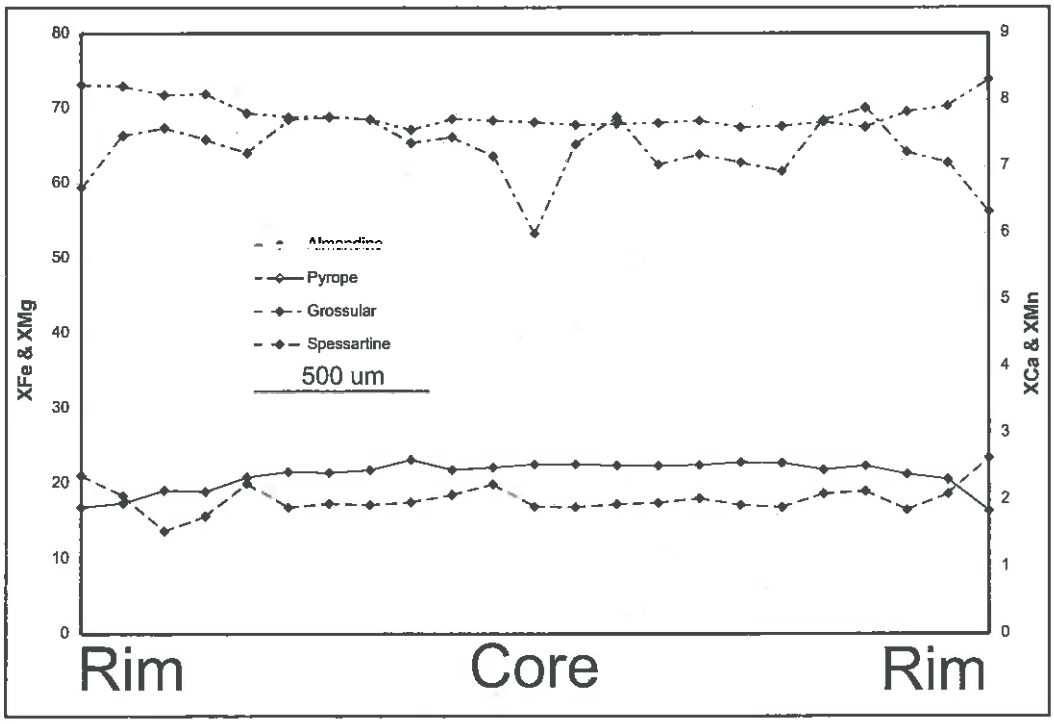

SH-31c

Figure 7D

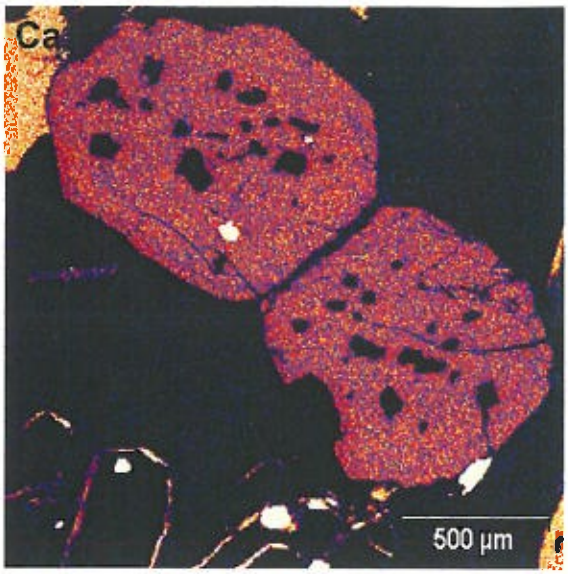

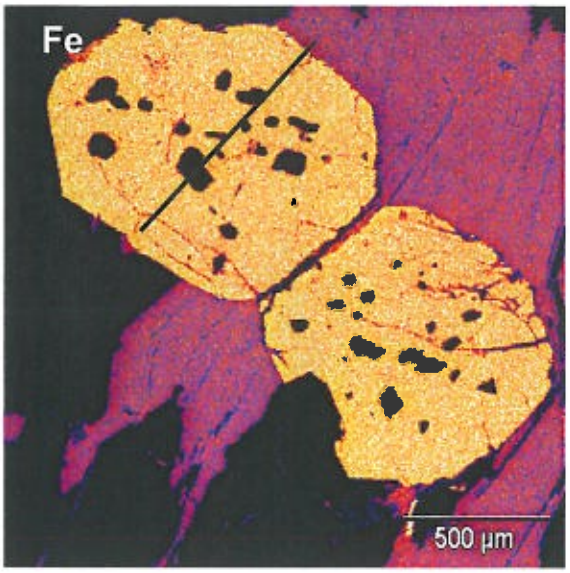

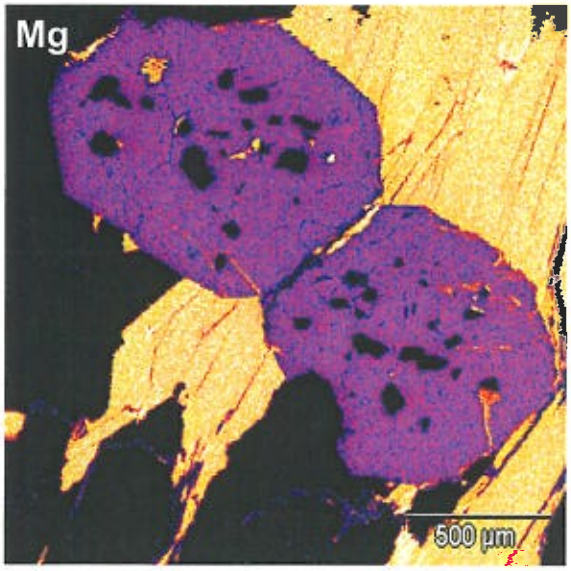

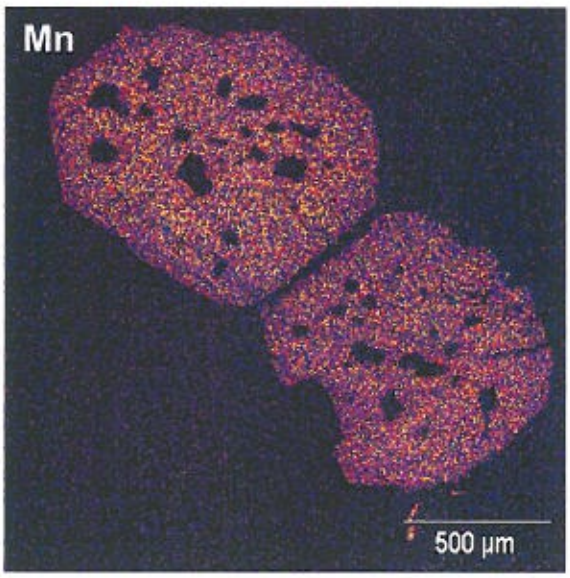

7i)

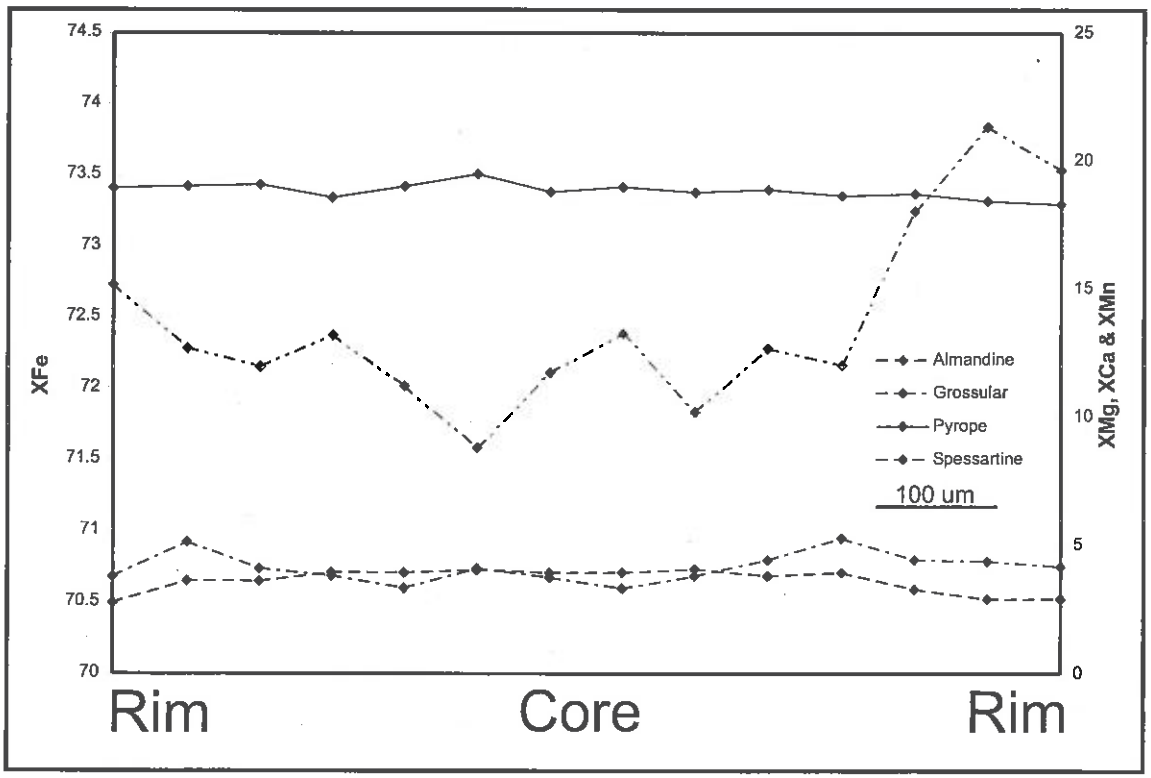

7ii)

SH-9

Figure 7E

7 i)

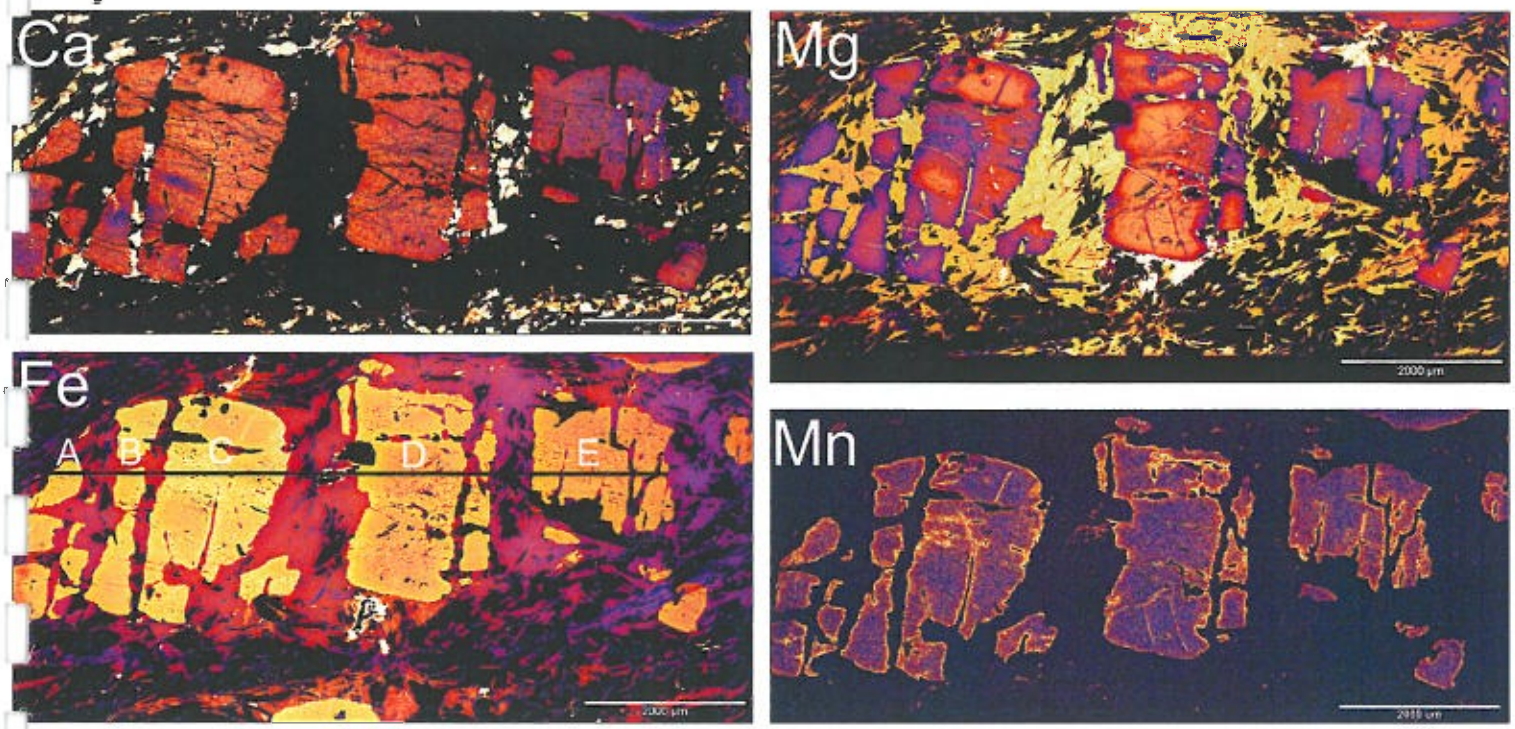

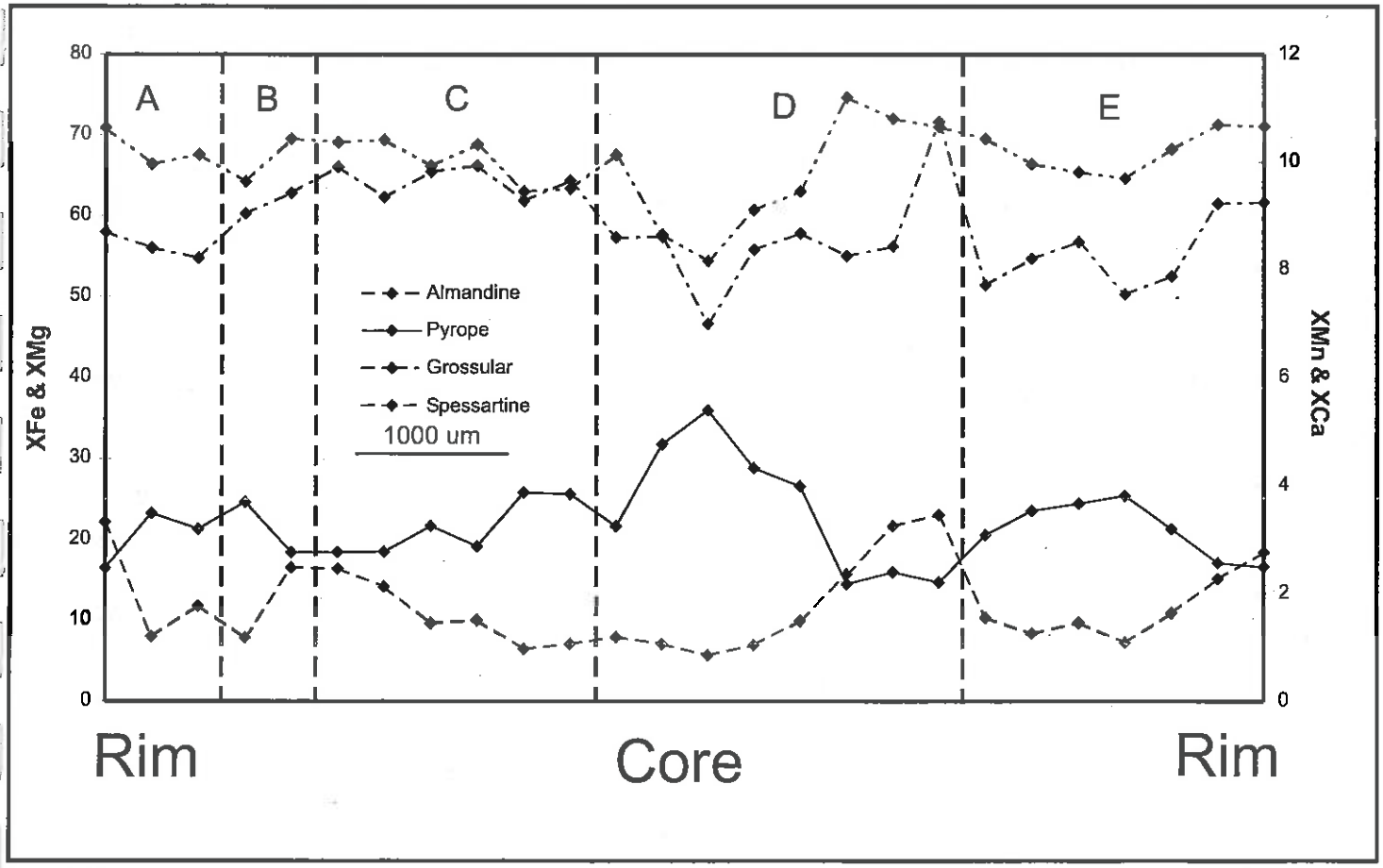

7 ii)

SH-11

Figure 7F

7i)

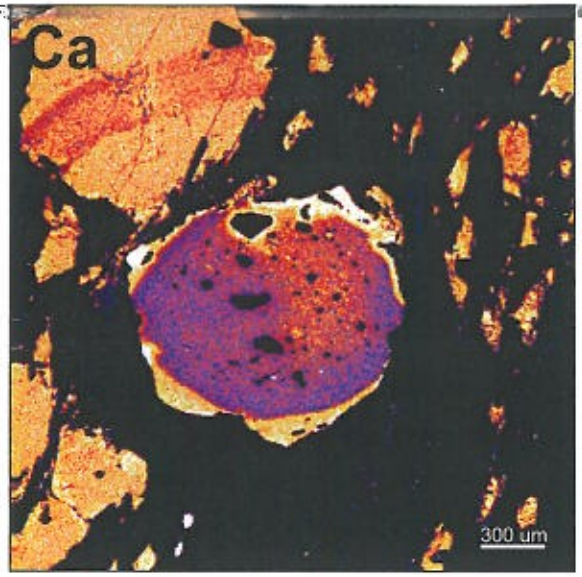

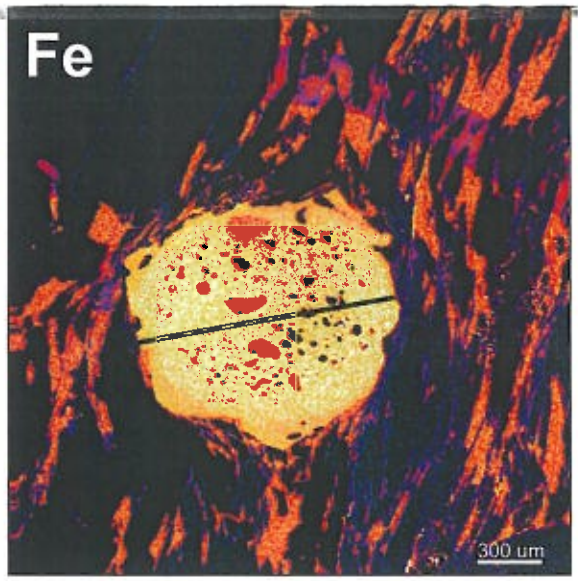

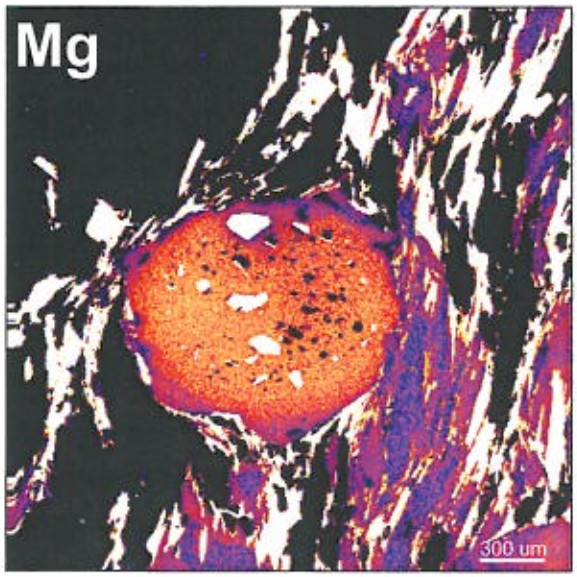

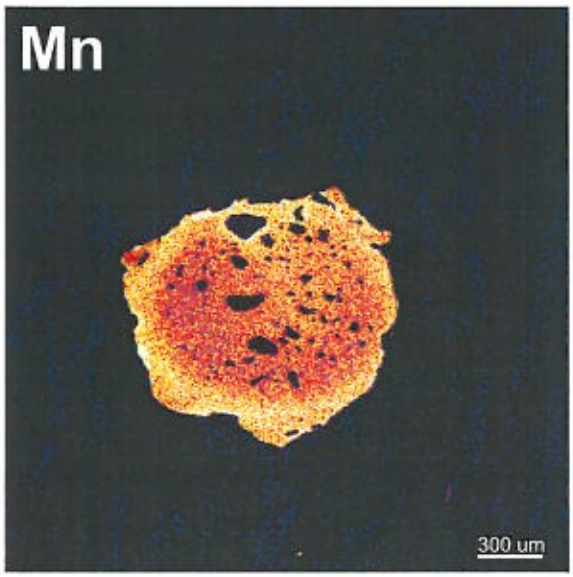

7ii)

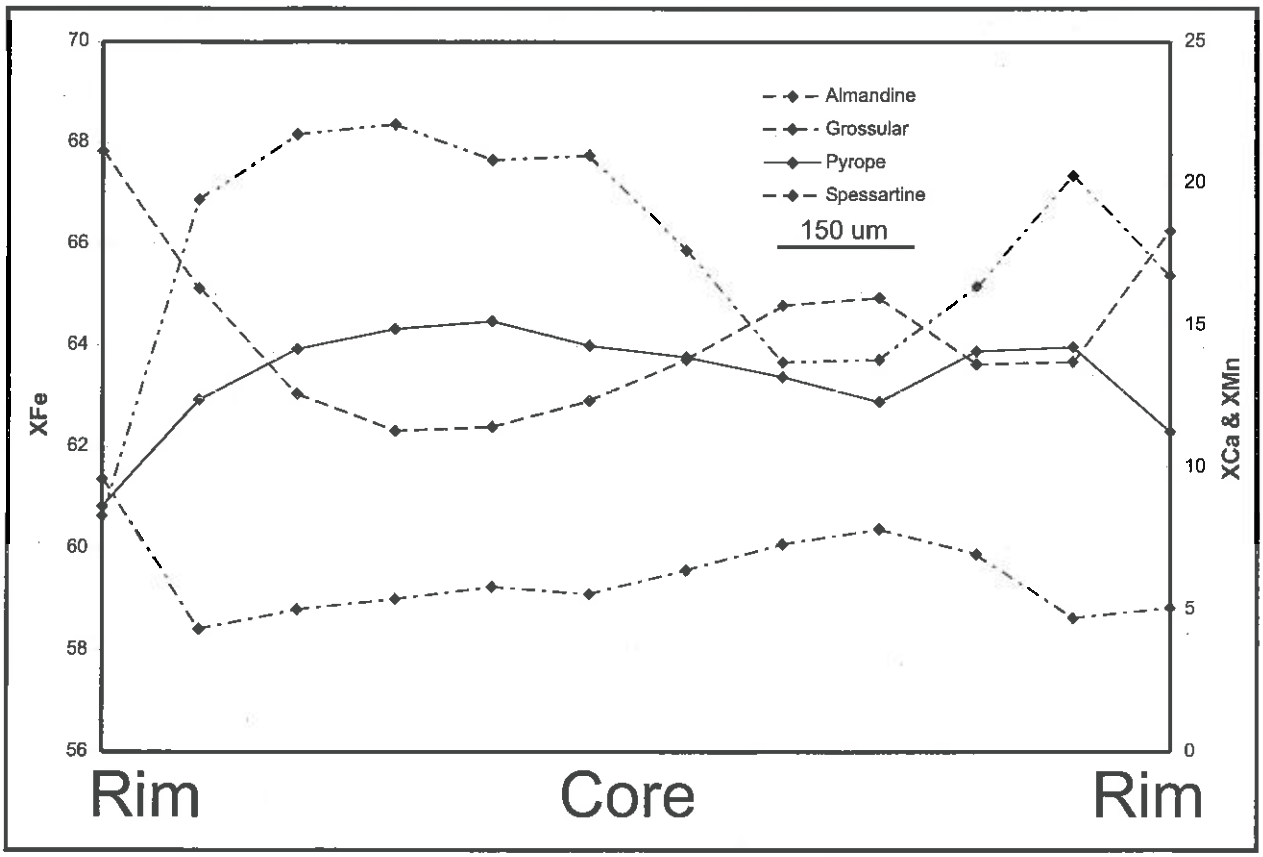

SH-14

Figure 7G

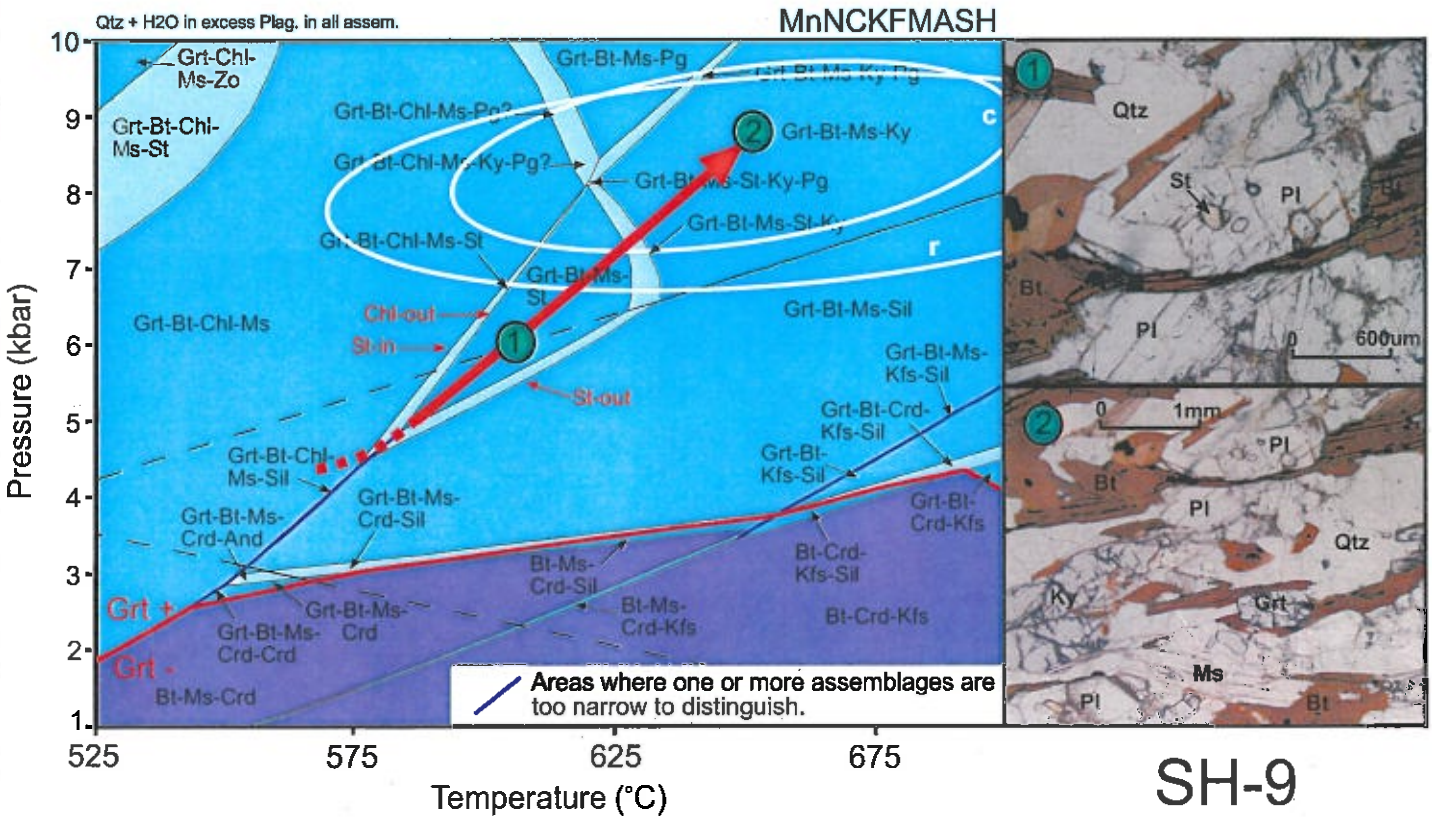
Qtz + H2O in excess Plag. in all assem.
MnNCKFMASH
Pressure (kbar)
Temperature (°C)
Grt-Chl-Ms-Zo
Grt-Bt-Chl-Ms-St
Grt-Bt-Ms-Pg
Grt-Bt-Chl-Ms-Pg?
Grt-Bt-Ms-Ky
Grt-Bt-Ms-St-Ky-Pg
Grt-Bt-Chl-Ms-St
Grt-Bt-Ms-St
Grt-Bt-Chl-Ms
Chl-out
St-in
St-out
Grt-Bt-Ms-Sil
Grt-Bt-Ms-Kfs-Sil
Grt-Bt-Crd-Kfs-Sil
Grt-Bt-Kfs-Sil
Grt-Bt-Chl-Ms-Sil
Grt-Bt-Ms-Crd-Sil
Grt-Bt-Ms-Crd-And
Grt-Bt-Crd-Kfs
Bt-Crd-Kfs-Sil
Bt-Ms-Crd-Sil
Bt-Ms-Crd-Kfs
Bt-Crd-Kfs
Grt-Bt-Ms-Crd
Grt-Bt-Ms-Crd-Crd
Grt +
Grt -
Bt-Ms-Crd
Areas where one or more assemblages are too narrow to distinguish.
Qtz
St
Pl
Bt
600um
1mm
Ky
Grt
Ms
SH-9

Figure 8A.

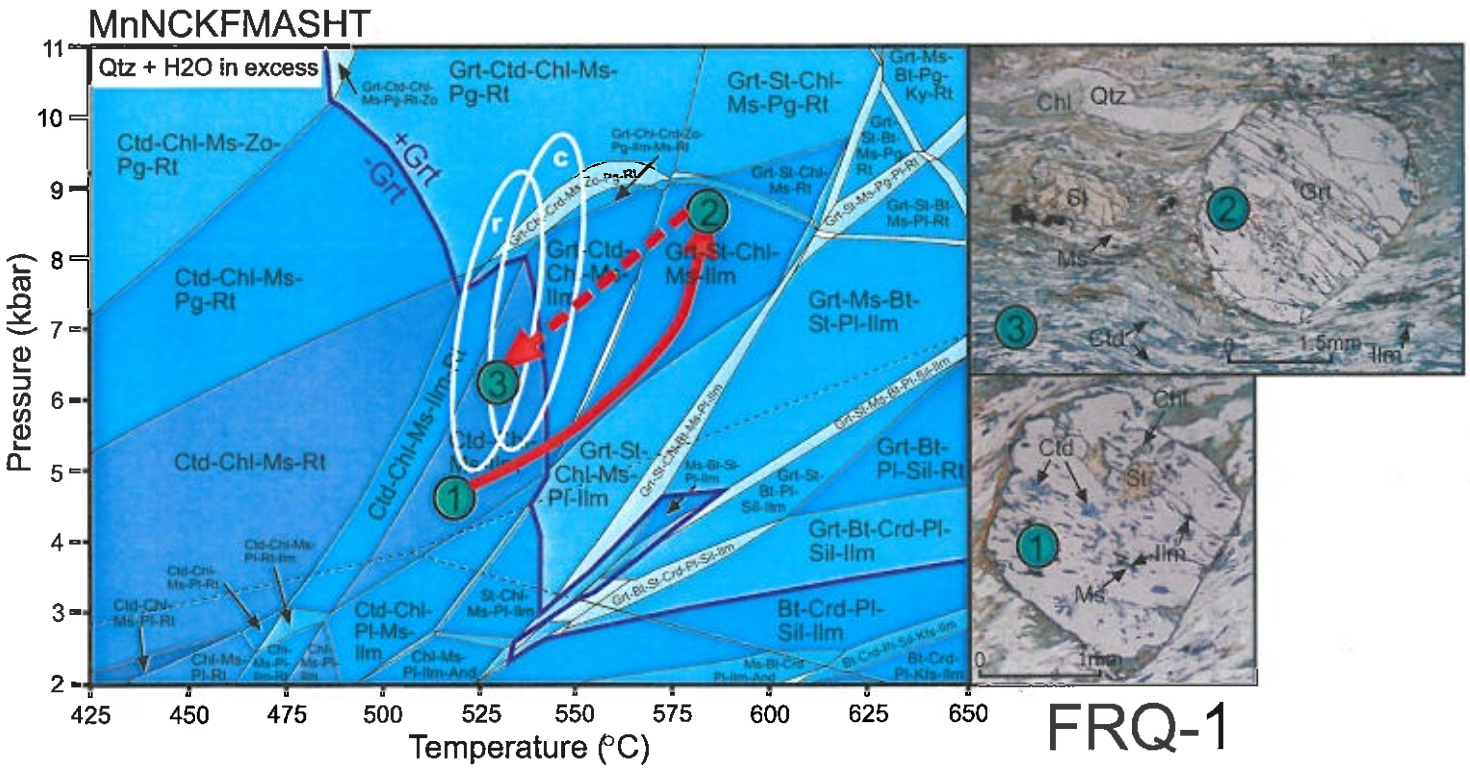
MnNCKFMASHT
Qtz + H2O in excess
Grt-Ctd-Chl-Ms-Pg-Rt
Grt-St-Chl-Ms-Pg-Rt
Ctd-Chl-Ms-Zo-Pg-Rt
+Grt
-Grt
Ctd-Chl-Ms-Pg-Rt
Grt-St-Chl-Ms-Ilm
Grt-Ms-Bt-St-Pl-Ilm
Ctd-Chl-Ms-Rt
Grt-Bt-Pl-Sil-Rt
Grt-Bt-Crd-Pl-Sil-Ilm
Ctd-Chl-Pl-Ms-Ilm
Bt-Crd-Pl-Sil-Ilm
Pressure (kbar)
Temperature (°C)
Chl
Qtz
Grt
Ms
Ctd
St
Ilm
1.5mm
1mm
FRQ-1

Figure 8B.

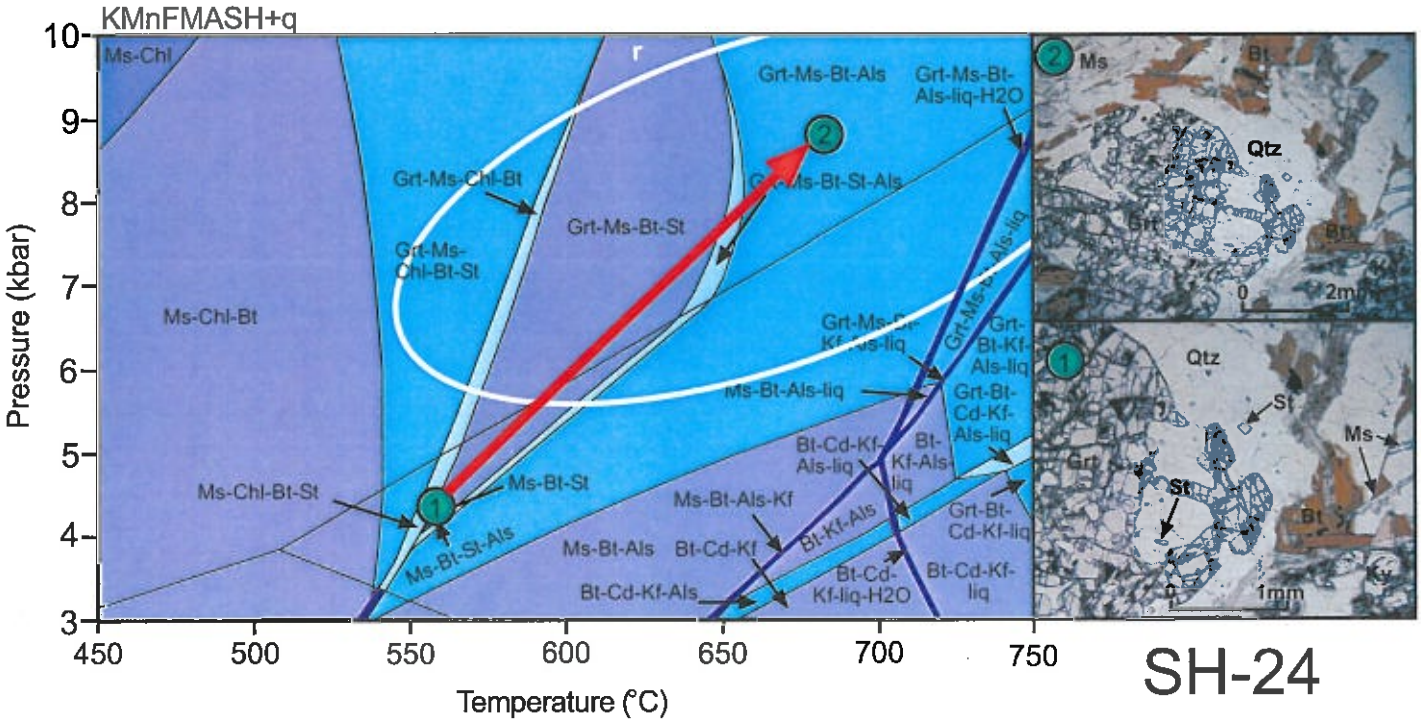
KMnFMASH+q
Pressure (kbar)
Temperature (°C)
10
9
8
7
6
5
4
3
450
500
550
600
650
700
750
Ms-Chl
Ms-Chl-Bt
Ms-Chl-Bt-St
Grt-Ms-Chl-Bt
Grt-Ms-Chl-Bt-St
Grt-Ms-Bt-St
Grt-Ms-Bt-St-Als
Grt-Ms-Bt-Als
Grt-Ms-Bt-Als-liq-H2O
Ms-Bt-St
Ms-Bt-St-Als
Ms-Bt-Als
Ms-Bt-Als-Kf
Bt-Cd-Kf
Bt-Cd-Kf-Als
Bt-Kf-Als
Bt-Cd-Kf-Als-liq
Bt-Kf-Als-liq
Ms-Bt-Als-liq
Grt-Bt-Kf-Als-liq
Grt-Bt-Cd-Kf-Als-liq
Grt-Bt-Cd-Kf-liq
Bt-Cd-Kf-liq-H2O
Bt-Cd-Kf-liq
r
Ms
Bt
Qtz
Grt
0
2mm
St
1mm
SH-24

Figure 8C.

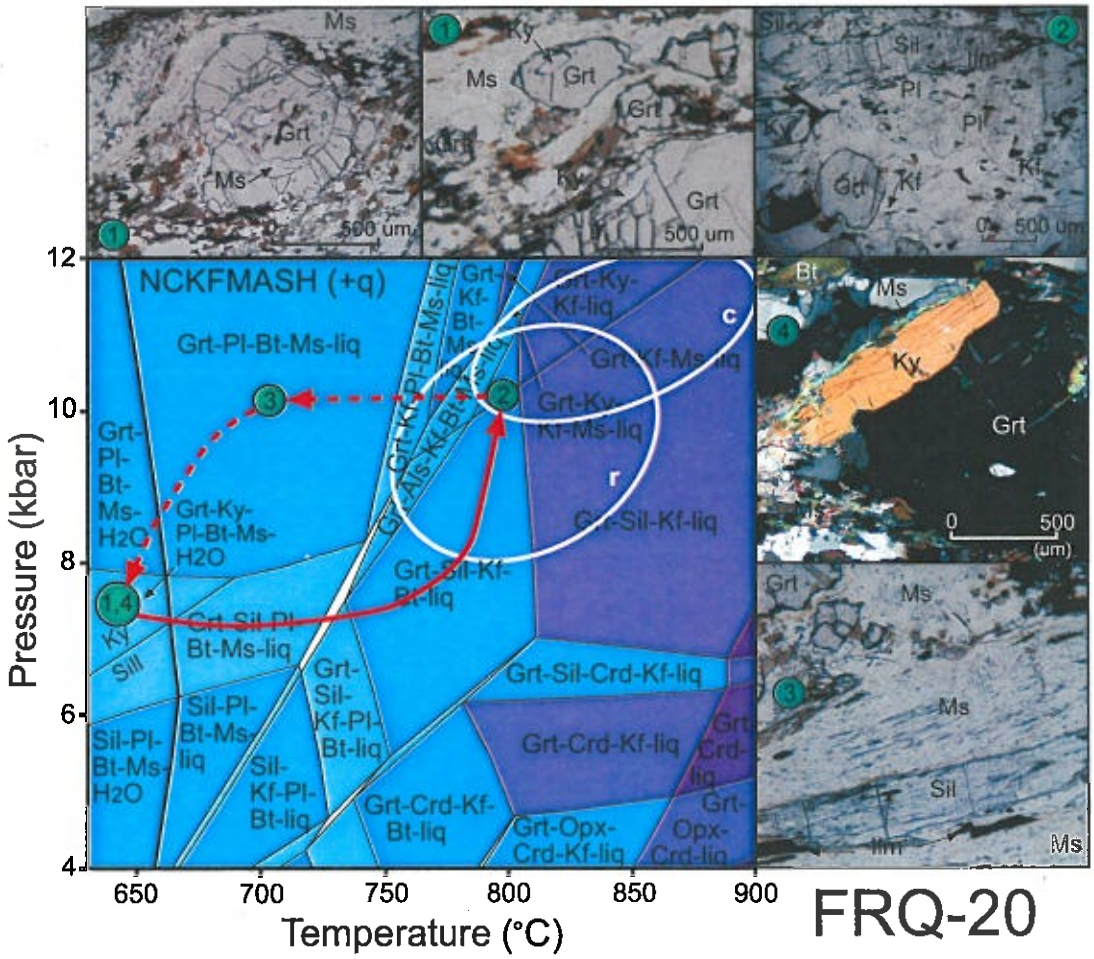
NCKFMASH (+q)
Grt-Pl-Bt-Ms-liq
Grt-Pl-Bt-Ms-H2O
Grt-Ky-Pl-Bt-Ms-H2O
Grt-Sil-Pl-Bt-Ms-liq
Grt-Sil-Kf-Bt-liq
Grt-Sil-Kf-Pl-Bt-liq
Grt-Sil-Crd-Kf-liq
Grt-Crd-Kf-liq
Grt-Crd-Kf-Bt-liq
Grt-Opx-Crd-Kf-liq
Grt-Ky-Kf-liq
Grt-Ky-Kf-Ms-liq
Grt-Sil-Kf-liq
Sil-Pl-Bt-Ms-liq
Sil-Pl-Bt-Ms-H2O
Sil-Kf-Pl-Bt-liq
Grt-Opx-Crd-liq
Pressure (kbar)
Temperature (°C)
FRQ-20

Figure 8D.

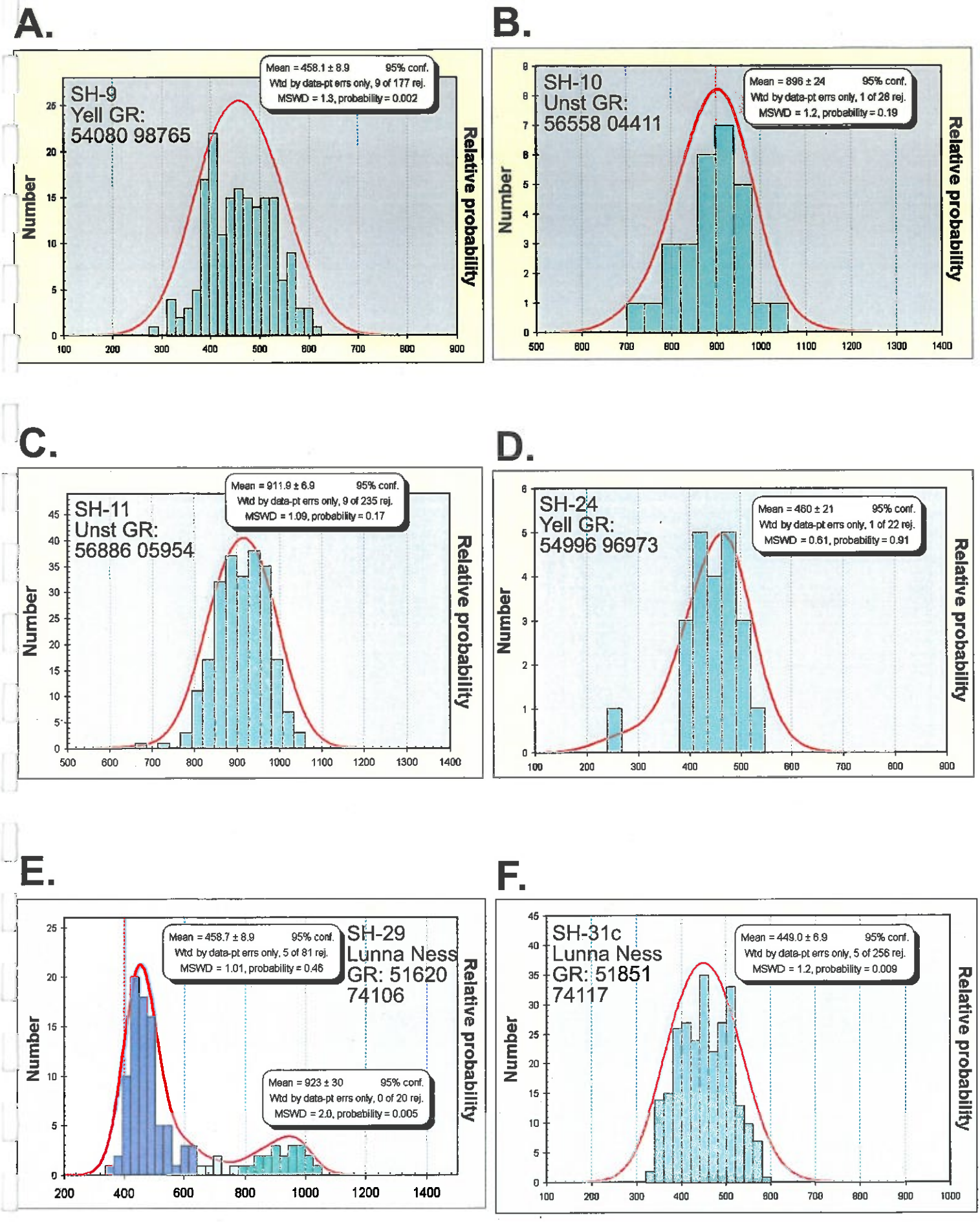
A.
SH-9
Yell GR:
54080 98765
Mean = 458.1 ± 8.9 95% conf.
Wtd by data-pt errs only, 9 of 177 rej.
MSWD = 1.3, probability = 0.002
Number
Relative probability
B.
SH-10
Unst GR:
56558 04411
Mean = 896 ± 24 95% conf.
Wtd by data-pt errs only, 1 of 28 rej.
MSWD = 1.2, probability = 0.19
Number
Relative probability
C.
SH-11
Unst GR:
56886 05954
Mean = 911.9 ± 6.9 95% conf.
Wtd by data-pt errs only, 9 of 235 rej.
MSWD = 1.09, probability = 0.17
Number
Relative probability
D.
SH-24
Yell GR:
54996 96973
Mean = 460 ± 21 95% conf.
Wtd by data-pt errs only, 1 of 22 rej.
MSWD = 0.61, probability = 0.91
Number
Relative probability
E.
SH-29
Lunna Ness
GR: 51620
74106
Mean = 458.7 ± 8.9 95% conf.
Wtd by data-pt errs only, 5 of 81 rej.
MSWD = 1.01, probability = 0.46
Mean = 923 ± 30 95% conf.
Wtd by data-pt errs only, 0 of 20 rej.
MSWD = 2.0, probability = 0.005
Number
Relative probability
F.
SH-31c
Lunna Ness
GR: 51851
74117
Mean = 449.0 ± 6.9 95% conf.
Wtd by data-pt errs only, 5 of 256 rej.
MSWD = 1.2, probability = 0.009
Number
Relative probability

Figure 9.

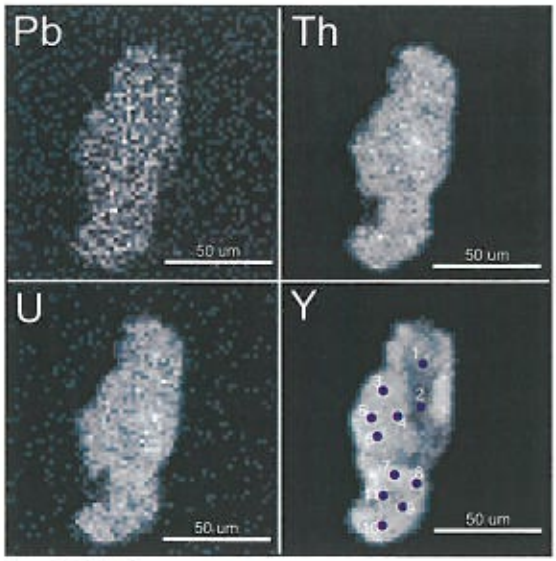

A. SH-9

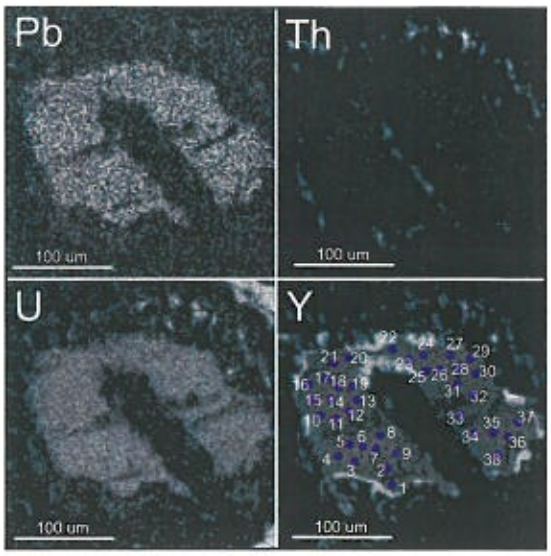

B. SH-11

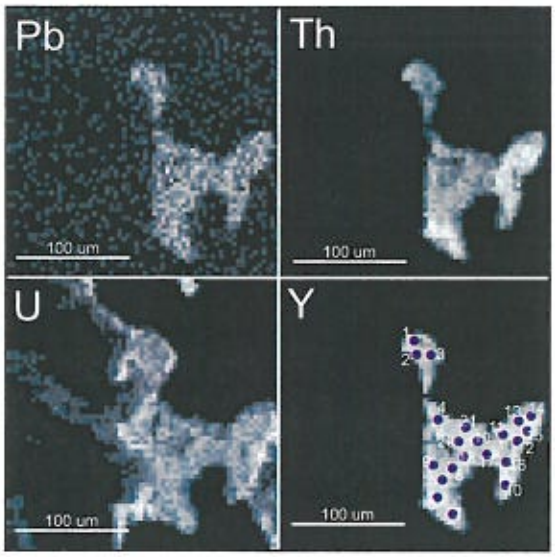

C. SH-24

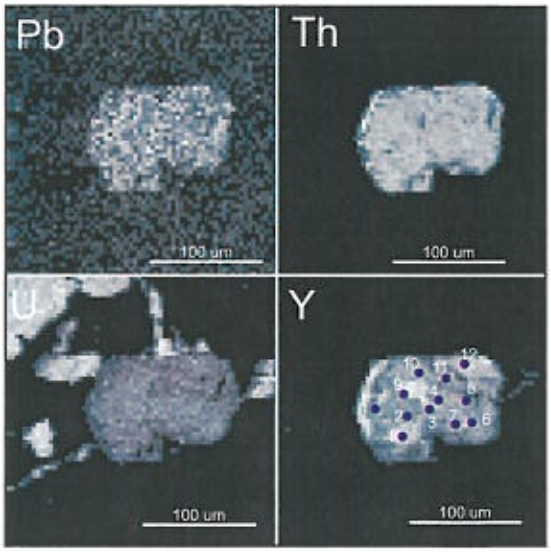

D. SH-29

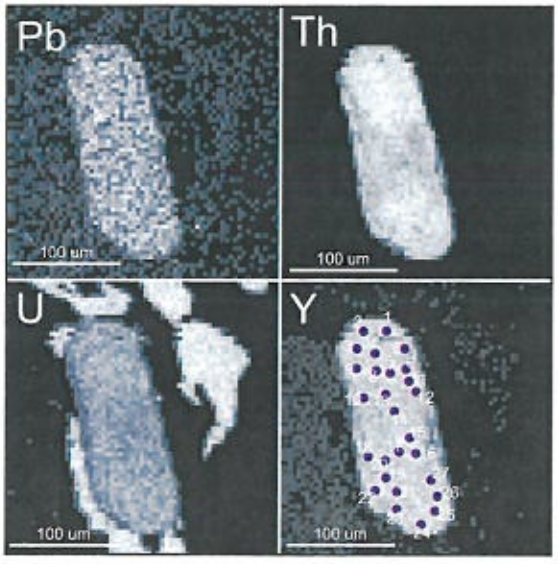

E. SH-31c

Figure 10.

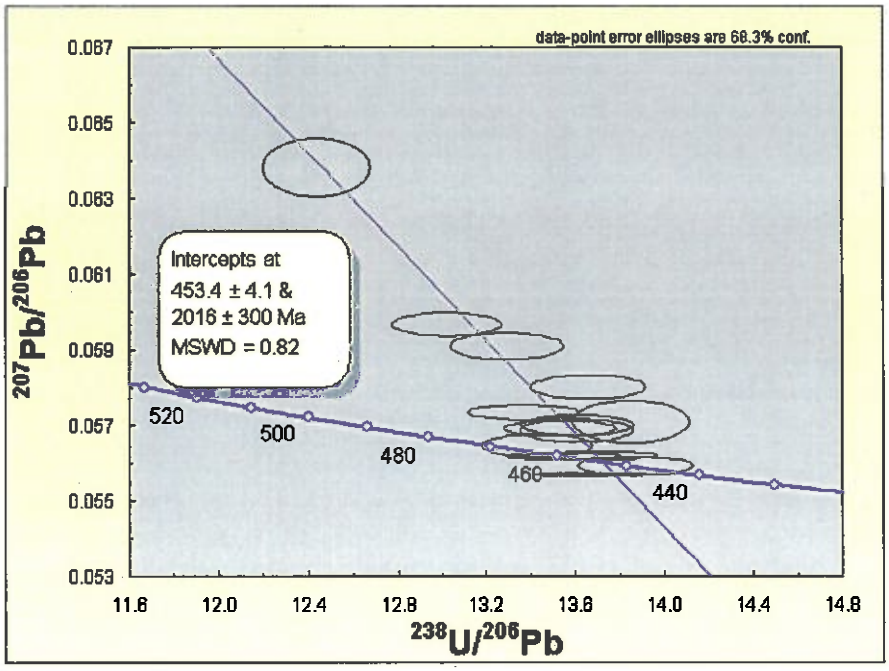

A. SH-9
Yell GR:
54080 98765

B. SH-11
Unst GR:
56886 05954

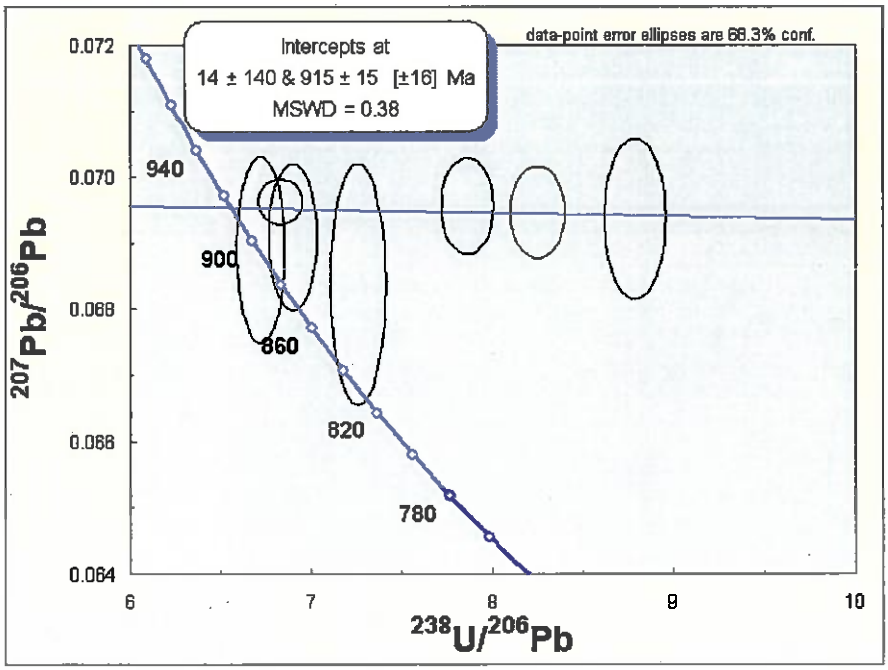

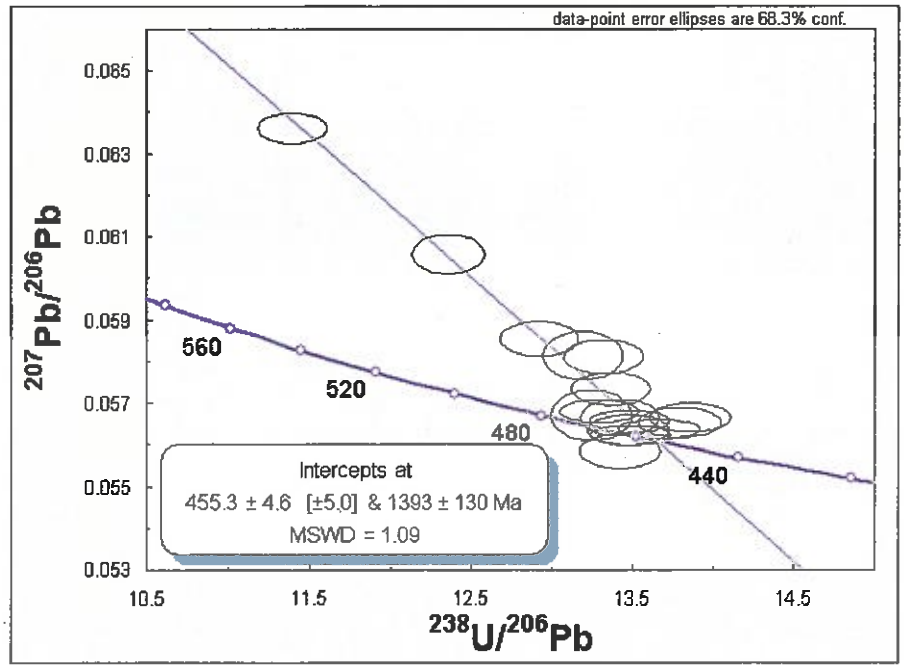

C. SH-29
Lunna Ness GR:
51620 74106

Figure 11.

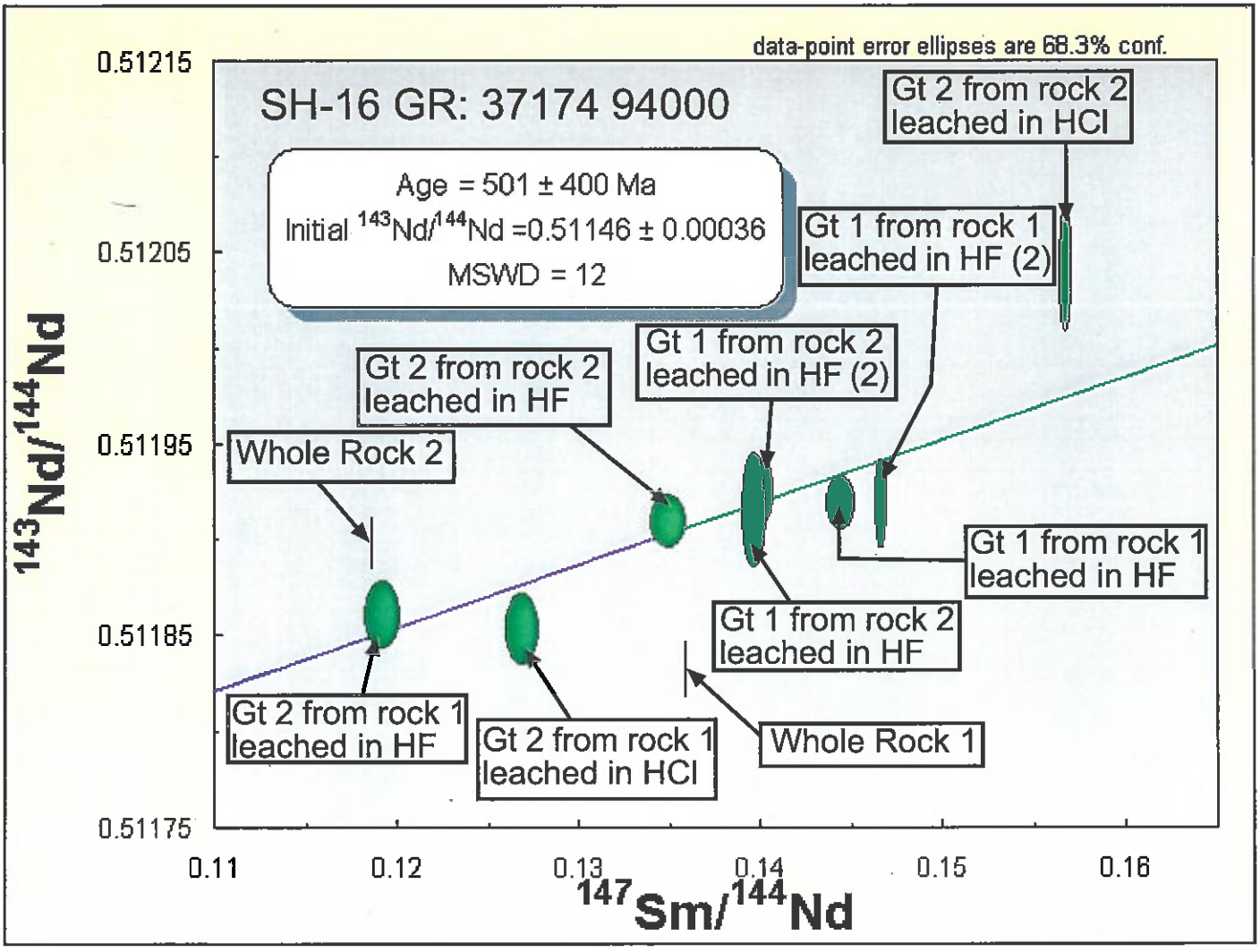
data-point error ellipses are 68.3% conf.
SH-16 GR: 37174 94000
Age = 501 ± 400 Ma
Initial $^{143}Nd/^{144}Nd$ =0.51146 ± 0.00036
MSWD = 12
Gt 2 from rock 2 leached in HCl
Gt 1 from rock 1 leached in HF (2)
Gt 1 from rock 2 leached in HF (2)
Gt 2 from rock 2 leached in HF
Whole Rock 2
Gt 1 from rock 1 leached in HF
Gt 1 from rock 2 leached in HF
Gt 2 from rock 1 leached in HF
Gt 2 from rock 1 leached in HCl
Whole Rock 1
0.51215
0.51205
0.51195
0.51185
0.51175
0.11
0.12
0.13
0.14
0.15
0.16
$^{143}Nd/^{144}Nd$
$^{147}Sm/^{144}Nd$

Figure 12.

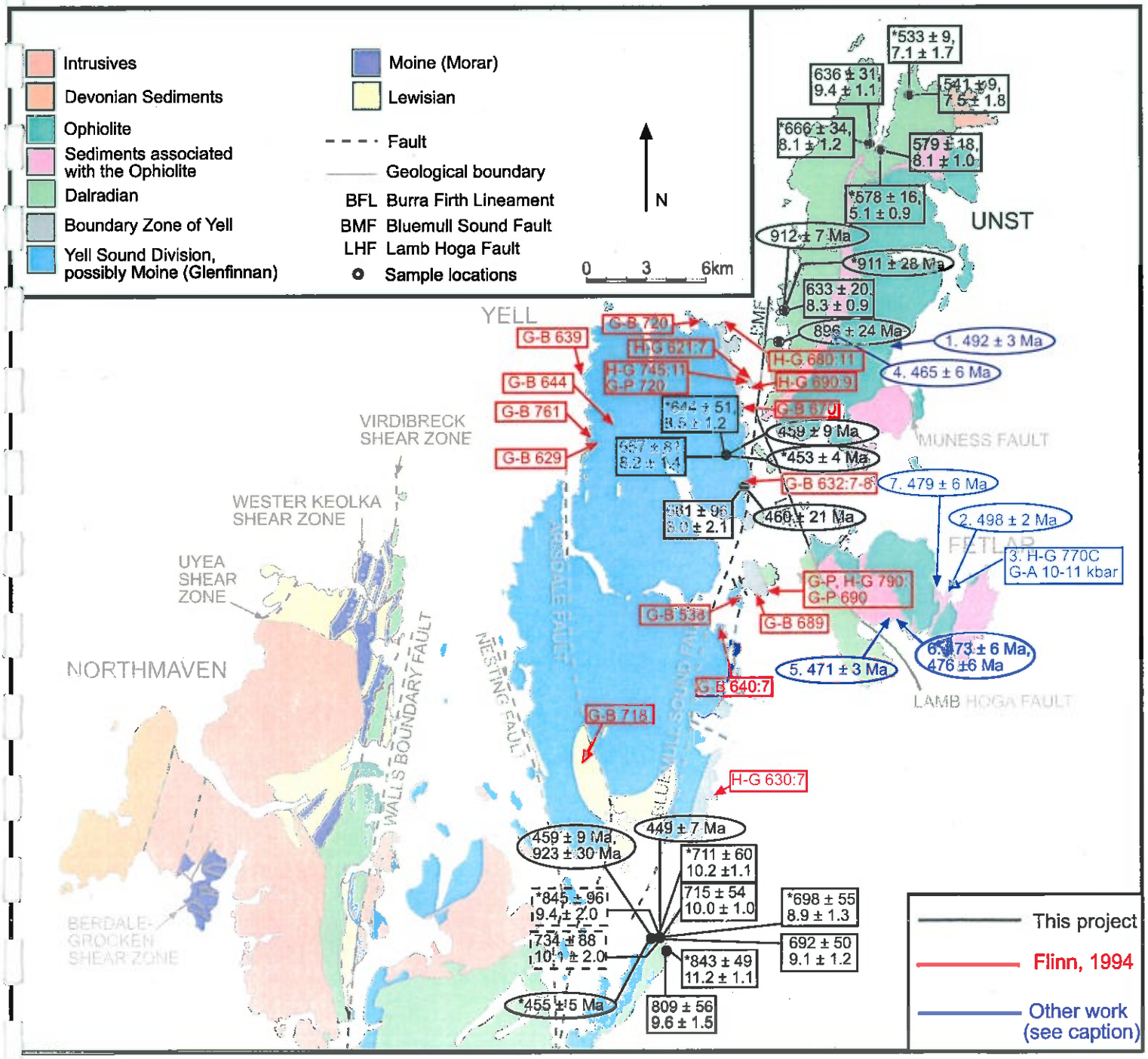
Intrusives
Devonian Sediments
Ophiolite
Sediments associated with the Ophiolite
Dalradian
Boundary Zone of Yell
Yell Sound Division, possibly Moine (Glenfinnan)
Moine (Morar)
Lewisian
Fault
Geological boundary
BFL Burra Firth Lineament
BMF Bluemull Sound Fault
LHF Lamb Hoga Fault
Sample locations
N
0 3 6km
YELL
UNST
FETLAR
NORTHMAVEN
VIRDIBRECK SHEAR ZONE
WESTER KEOLKA SHEAR ZONE
UYEA SHEAR ZONE
BERDALE-GROCKEN SHEAR ZONE
WALLS BOUNDARY FAULT
NESTING FAULT
ARDALE FAULT
BLUEMULL SOUND FAULT
MUNESS FAULT
LAMB HOGA FAULT
*533 ± 9, 7.1 ± 1.7
636 ± 31, 9.4 ± 1.1
541 ± 9, 7.5 ± 1.8
*666 ± 34, 8.1 ± 1.2
579 ± 18, 8.1 ± 1.0
*578 ± 16, 5.1 ± 0.9
912 ± 7 Ma
911 ± 28 Ma
633 ± 20, 8.3 ± 0.9
896 ± 24 Ma
1. 492 ± 3 Ma
4. 465 ± 6 Ma
G-B 720
G-B 639
H-G 621:7
H-G 745:11
G-P 720
G-B 644
G-B 761
G-B 629
H-G 680:11
H-G 690:9
*642 ± 51, 8.5 ± 1.2
G-B 670
459 ± 9 Ma
*453 ± 4 Ma
557 ± 81, 8.2 ± 1.4
G-B 632:7-8
7. 479 ± 6 Ma
581 ± 96, 8.0 ± 2.1
460 ± 21 Ma
2. 498 ± 2 Ma
3. H-G 770C G-A 10-11 kbar
G-P, H-G 790: G-P 690
G-B 538
G-B 689
5. 471 ± 3 Ma
6. 473 ± 6 Ma, 476 ± 6 Ma
G-B 640:7
G-B 718
H-G 630:7
449 ± 7 Ma
459 ± 9 Ma, 923 ± 30 Ma
*711 ± 60, 10.2 ±1.1
715 ± 54, 10.0 ± 1.0
*698 ± 55, 8.9 ± 1.3
*845 ± 96, 9.4 ± 2.0
734 ± 88, 10.1 ± 2.0
692 ± 50, 9.1 ± 1.2
*843 ± 49, 11.2 ± 1.1
*455 ± 5 Ma
809 ± 56, 9.6 ± 1.5
This project
Flinn, 1994
Other work (see caption)

Figure 13.

A. ~500 Ma, early closure of the Iapetus Ocean

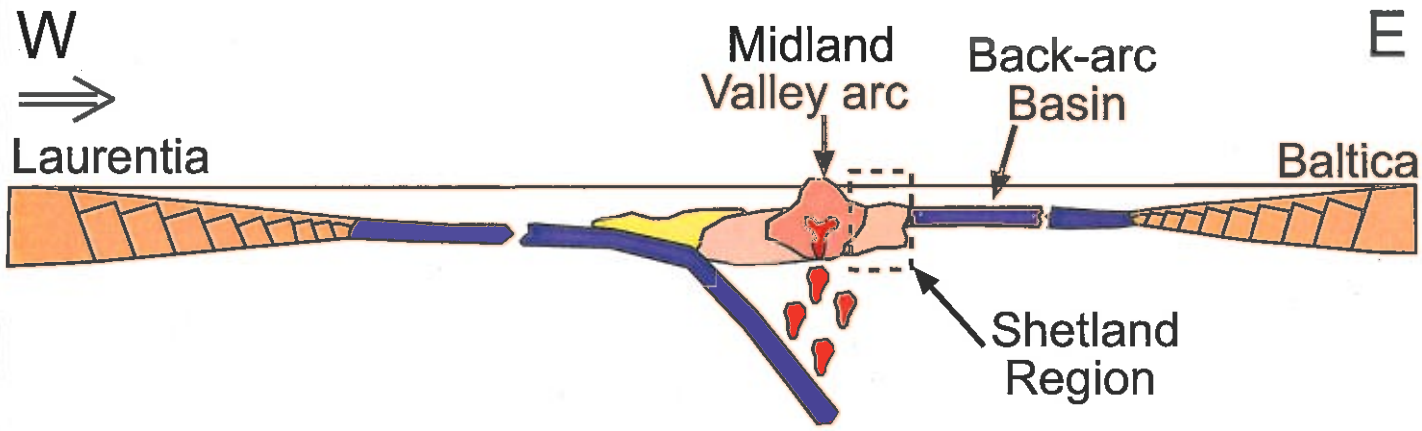

B. ~470-460 Ma, early phase Grampian

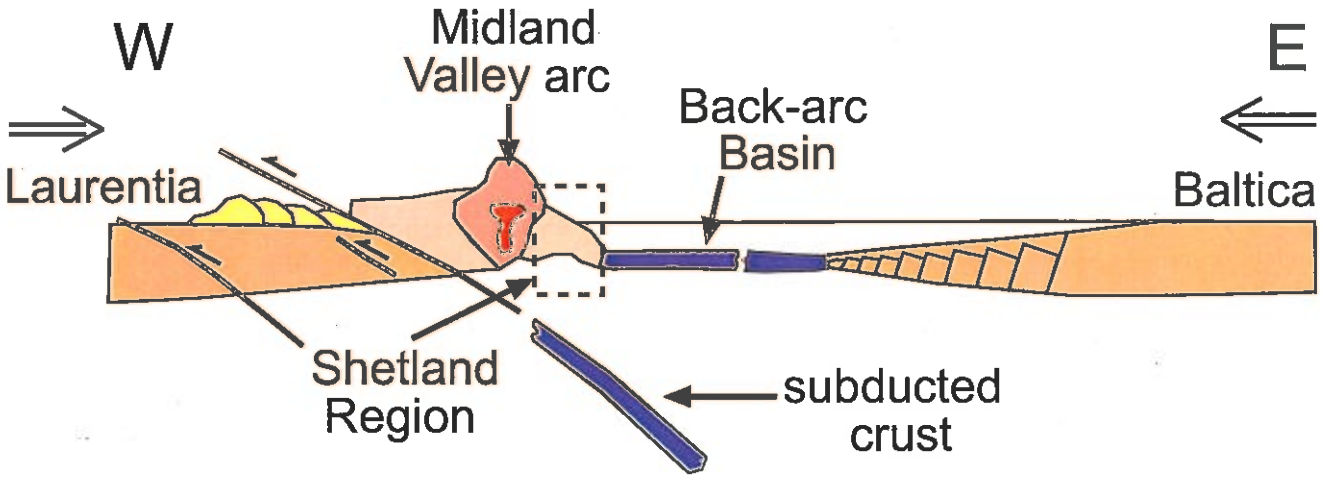

C. ~460 Ma, late phase Grampian Orogeny

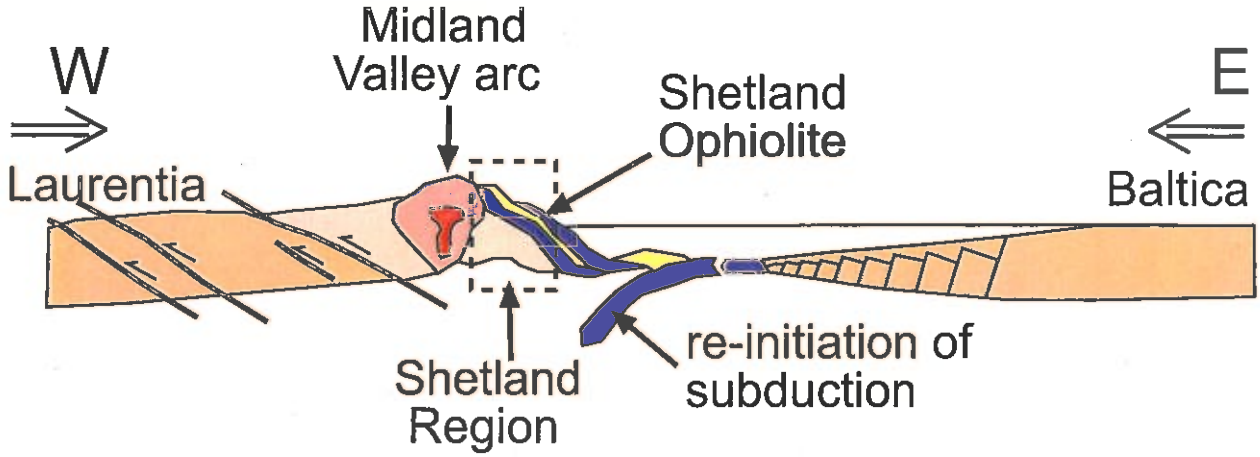

Figure 14.

D. ~410 Ma, Scandian Orogeny

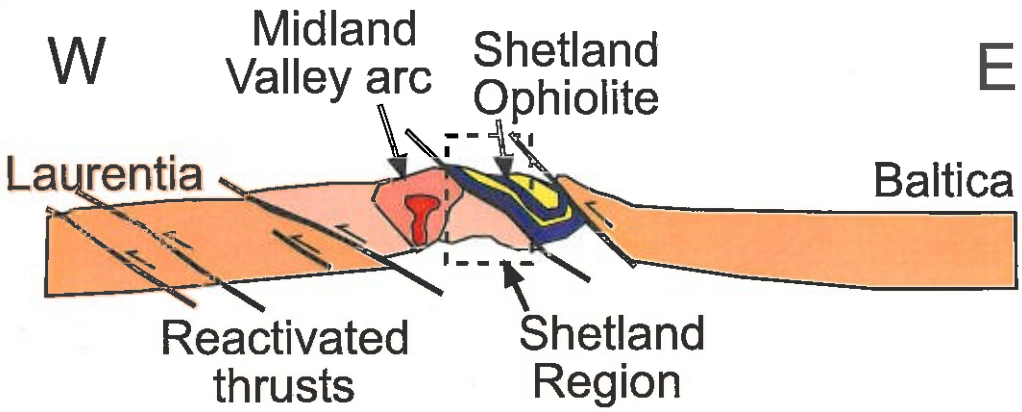

Figure 14 cont.

Table 1: Representative monazite compositions

Label	SH11-M1-4	SH11-M1-6	SH11-M1-9	SH11-M1-10	SH24-M4-1	SH24-M4-4	SH24-M3-1	SH29-M1-2	SH29-M1-6	SH29-M1-14	Standard
W%(O)	27.2442	26.9833	26.8314	27.1639	27.5127	27.6012	27.2904	28.5986	27.4739	27.4045	26.7587
W%(Al)	0.0202	0.0022	0.0092	0.0138	0.0991	0.0324	0.0495	0.0322	0.0079	0.0037	0.0003
W%(Si)	0.2645	0.2559	0.2855	0.2867	0.2487	0.203	0.4472	0.2704	0.1914	0.1745	0.7271
W%(P)	13.1003	12.894	12.7537	12.9435	13.0663	13.1301	13.0656	13.9066	13.0571	13.0211	12.2515
W%(Ca)	0.5531	0.5393	0.5493	0.5435	0.3845	0.4647	0.6397	2.0277	0.9207	0.9619	0.2851
W%(Y)	0.1055	0.0573	0.3666	0.0617	1.4169	2.9073	1.7379	0.7419	1.0717	1.0812	0.6284
W%(La)	12.7892	12.8882	12.6137	13.0269	11.207	10.3046	10.1494	10.5322	10.9727	10.5948	11.907
W%(Ce)	25.8394	26.2831	25.282	26.2869	26.4	24.7806	23.4819	22.9895	24.3716	24.0443	25.1365
W%(Pr)	2.8394	2.742	2.6913	2.7428	2.799	2.6378	2.4875	2.5104	2.6093	2.6584	2.7823
W%(Nd)	10.5146	10.4801	10.2819	10.5046	10.5535	10.3948	9.6161	10.4592	10.6314	10.8531	9.4
W%(Sm)	1.0738	1.0995	1.2099	1.055	2.0405	2.1646	1.8864	1.9809	1.9293	2.094	1.7639
W%(Gd)	0.2977	0.2674	0.5742	0.2884	1.6441	1.9137	1.5787	1.4059	1.5209	1.6541	0.8144
W%(Dy)	0.0504	0.0423	0.1944	0.0266	0.7826	1.1105	0.7883	0.4321	0.5531	0.5053	0.2335
W%(Er)	0.0109	0.0423	0.0606	0.0422	0.0514	0.1676	0.0662	0.1234	0.0893	0.1203	0.1208
W%(Pb)	0.2076	0.1961	0.1774	0.2042	0.0797	0.0941	0.1296	0.1778	0.1582	0.1803	0.1987
W%(Th)	4.4776	4.2743	4.8525	4.6441	2.1738	2.3027	4.4136	4.9155	5.1033	5.0829	6.7116
W%(U)	0.2349	0.2736	0.2327	0.2303	0.2726	0.4616	0.4104	0.4886	0.7241	0.8312	0.2027
Totals	99.6233	99.3209	98.9663	100.0651	100.7324	100.6713	98.2384	101.5929	101.3859	101.2656	99.9225

Table 2. End member compositions of garnet grains.

sample	Almandine		Grossular		Pyrope		Spessartine	
	core	rim	core	rim	core	rim	core	rim
SH-9	0.715	0.73	0.03	0.04	0.18	0.18	0.04	0.03
SH-11	0.55	0.7	0.08	0.09	0.3	0.17	0.01	0.03
SH-13	0.65	0.65	0.03	0.1	0.165	0.16	0.09	0.15
SH-14	0.68	0.62	0.08	0.05	0.15	0.1	0.11	0.2
SH-16a	0.66	0.7	0.22	0.16	0.06	0.15	0.06	0.001
SH-16b	0.58	0.7	0.24	0.9	0.04	0.16	0.13	0.0005
SH-24	0.63	0.69	0.08	0.06	0.19	0.18	0.12	0.07
SH-30a	0.54	0.55	0.25	0.22	0.11	0.20	0.08	0.03
SH-31	0.55	0.62	0.26	0.15	0.09	0.2	0.1	0.02
SH-31c	0.68	0.74	0.08	0.07	0.23	0.17	0.02	0.03
FRQ-1	0.65	0.76	0.16	0.10	0.08	0.1	0.1	0.04
FRQ-20B	0.64	0.68	0.08	0.06	0.23	0.23	0.02	0.02

Table 3: PT conditions calculated using THERMOCALC v3.21

Sample	Grid Reference (OSGB)	Average T (°C)	Average P (kbar)	Average PT (°C, kbar)	
Unst					
East of BFL		(Reference=8kbar)	(Reference=550°C)		
FRQ-1 cores†	63123, 16449	535.1 ± 8	8.9 ± 1.5	533 ± 9	7.1 ± 1.7
FRQ-1 rims†	63123, 16449	542.4 ± 8	8.3 ± 1.5	541 ± 9	7.5 ± 1.8
SH13 cores	61355, 14036	581 ± 13 (5.5kbar)	5.5 ± 0.9 (600°C)	578 ± 16	5.1 ± 0.9
SH13 rims	61355, 14036	577 ± 14	8.7 ± 0.9 (600°C)	579 ± 18	8.1 ± 1.0
West of BFL		(Reference=8kbar)	(Reference=650°C)		
SH14 cores	61064, 14234	662 ± 23	7.6 ± 0.8	666 ± 34	8.1 ± 1.2
SH14 rims	61064, 14234	650 ± 21 (10kbar)	9.8 ± 0.7	636 ± 31	9.4 ± 1.1
SH11 rims	56886, 05954	627 ± 13	8.7 ± 0.7	633 ± 20	8.3 ± 0.9
Yell		(Reference=8kbar)	(Reference=650°C)		
SH-9 cores†	54080, 98765	631.5 ± 40	8.6 ± 1.0	644 ± 51	8.5 ± 1.2
SH-9 rims†	54080, 98765	644 ± 54	8.1 ± 1.0	657 ± 81	8.2 ± 1.4
SH-24 rims†	54996, 96973	661.1 ± 99	8.0 ± 2.0	661 ± 96	8.0 ± 2.1
Lunna Ness		(Reference=10kbar)	(Reference=800°C)		
FRQ-20B cores†	52301, 73112	790 ± 5	10.2 ± 0.1	843 ± 49	11.2 ± 1.1
FRQ-20B rims†	52301, 73112	807 ± 50	9.5 ± 1.4	809 ± 56	9.6 ± 1.5
SH31c cores	51851, 74117	845 ± 96	9.4 ± 2.0	*	
SH31c rims	51851, 74117	734 ± 88	10.1 ± 2.0	*	
SH31 cores	51851, 74117	717 ± 45	8.9 ± 1.0 (700°C)	698 ± 55	8.9 ± 1.3
SH31 rims	51851, 74117	708 ± 43	9.2 ± 1.0 (700°C)	692 ± 50	9.1 ± 1.2
SH30a rims^	51851, 74117	694 ± 50	10 ± 0.9 (700°C)	711 ± 60	10.2 ±1.1
SH30a cores^	51851, 74117	707 ± 49	9.8 ± 0.8 (700°C)	715 ± 54	10.0 ± 1.0

NB XH_2O=0.75 for Yell and Unst samples, aH_2O=0.75 for Lunna Ness samples.

* Insufficient independent reactions to define an average PT.

^ aH2O=0.5 for this sample.

BFL is the Burra Firth Lineament (Figure 2)

† These samples have had a PT diagram made.

Table 4: Monazite EPMA and LA ICP MS ages

Sample	Monazite EPMA age (Ma)	Monazite LAICPMS age (Ma)
SH-9	459 ± 9 (n=177)	453 ± 4 (n=14)
SH-10	896 ± 24 (n=28)	-
SH-11	912 ± 7 (n=235)	911 ± 28 (n=8)
SH-24	460 ± 21(n=22)	-
SH-29	459 ± 9 (n=81), 923 ± 30 (n=20)	455 ± 5 (n=16)
SH-31c	449 ± 7 (n=256)	-

Table 5: Monazite age data acquired on the LA-ICP MS

	Isotope ratios						Age estimates (Ma)					
Analysis	Pb207/Pb206	2σ	Pb206/U238	2σ	Pb207/U235	2σ	Pb207/Pb206	2σ	Pb206/U238	2σ	Pb207/U235	2σ
madel1	0.05702	0.00065	0.08336	0.00095	0.65648	0.0081	491.7	25.4	516.2	5.63	512.5	4.96
madel2	0.0568	0.00066	0.08394	0.00096	0.65842	0.0082	483.1	25.79	519.6	5.69	513.6	5.04
madel3	0.0583	0.00068	0.08412	0.00096	0.6773	0.0085	540.5	25.87	520.7	5.72	525.1	5.12
madel4	0.05709	0.00067	0.08271	0.00095	0.65217	0.0082	494.5	25.85	512.3	5.65	509.8	5.04
madel5	0.05699	0.00067	0.08178	0.00094	0.64366	0.0082	490.4	26.05	506.8	5.61	504.6	5.04
222a	0.0563	0.00063	0.07104	0.00082	0.5524	0.0068	463.4	24.81	442.4	4.92	446.6	4.44
sh11a	0.09227	0.00132	0.25374	0.00312	3.23377	0.048	1472.9	27.1	1457.7	16.03	1465.3	11.51
sh11d	0.06886	0.00128	0.14851	0.00192	1.4124	0.0264	894.5	37.85	892.6	10.78	894.2	11.1
sh11e	0.06834	0.00155	0.13754	0.00191	1.29832	0.0291	879	46.33	830.7	10.8	845	12.87
sh11f	0.06949	0.0009	0.1269	0.00152	1.21807	0.0169	913.2	26.54	770.2	8.71	808.9	7.74
sh11g	0.06935	0.00117	0.11334	0.00144	1.08537	0.0186	909.2	34.27	692.1	8.32	746.3	9.07
sh11h	0.06962	0.00076	0.146	0.00172	1.40392	0.0172	917.3	22.26	878.5	9.68	890.6	7.26
sh11i	0.06951	0.00089	0.12092	0.00146	1.16088	0.016	913.8	26.06	735.8	8.38	782.4	7.5
sh11j	0.06834	0.00078	0.13234	0.00158	1.24901	0.0159	878.8	23.54	801.2	8.99	823	7.2
sh11l	0.06903	0.0011	0.14428	0.00183	1.37573	0.0228	899.7	32.49	868.8	10.33	878.6	9.72
SH29c	0.05983	0.00066	0.08821	0.00108	0.72886	0.0093	597.4	23.68	544.9	6.4	555.9	5.47
SH29d	0.06097	0.00075	0.09016	0.00112	0.75907	0.0105	638.2	26.39	556.5	6.61	573.5	6.05
SH29f	0.05631	0.00066	0.0761	0.00094	0.5916	0.0079	463.8	25.74	472.8	5.63	471.9	5.01
SH29g	0.05686	0.00064	0.0767	0.00095	0.60196	0.0078	485.4	25.01	476.4	5.68	478.5	4.97
SH29h	0.05645	0.00063	0.07412	0.00092	0.5776	0.0075	469.2	24.69	460.9	5.51	462.9	4.83
SH29i	0.05667	0.00061	0.07743	0.00096	0.60581	0.0078	477.8	23.97	480.8	5.76	480.9	4.9
SH29j	0.0607	0.00072	0.08345	0.00105	0.69953	0.0096	628.8	25.22	516.7	6.27	538.5	5.71
SH29k	0.0563	0.00061	0.07686	0.00096	0.59729	0.0077	463.3	23.98	477.3	5.76	475.5	4.89
SH29l	0.06367	0.00071	0.09068	0.00114	0.79737	0.0105	730.8	23.54	559.6	6.72	595.3	5.92
SH29m	0.05857	0.00074	0.07889	0.00101	0.6381	0.0093	551.2	27.44	489.5	6.06	501.1	5.74
SH29n	0.0584	0.00068	0.08066	0.00103	0.65035	0.0088	544.6	25.12	500.1	6.12	508.7	5.44
sh29p	0.05595	0.0006	0.07825	0.001	0.60429	0.0079	450.2	23.12	485.7	5.99	480	4.98
sh29q	0.05791	0.00067	0.07942	0.00102	0.63475	0.0087	525.9	25.34	492.7	6.12	499	5.39
sh29r	0.05623	0.00064	0.07695	0.001	0.59708	0.0081	460.7	25	477.9	5.97	475.4	5.16
sh29s	0.05621	0.0006	0.07774	0.001	0.60317	0.0079	460	23.57	482.6	6	479.2	5.02
sh29t	0.05659	0.00064	0.07902	0.00103	0.61755	0.0085	474.8	25.2	490.3	6.15	488.3	5.33
sh29u	0.05686	0.00074	0.08122	0.00109	0.6371	0.0096	485.5	28.63	503.4	6.5	500.5	5.96
sh29v	0.05615	0.00065	0.07982	0.00105	0.61876	0.0087	457.8	25.31	495	6.29	489.1	5.47

Table 6: Sm-Nd Isotopic data for Sample SH-16 whole rocks and garnet separates.

Sample	Sm (ppm)	Nd (ppm)	$^{147}Sm/^{144}Nd$	$^{143}Nd/^{144}Nd$	2σ	εNd(0)	2σ	εNd (T)	2σ	TDM (Ma)	2σ
WRR1	3.576	15.916	0.13576	0.5118331	0.0000095	-15.7005	0.185	-8.71427	1.756	2254	17
WRR2	8.073	41.140	0.11860	0.5118988	0.0000086	-14.4198	0.168	-6.45111	1.535	1787	13
R1G1 1	2.408	9.931	0.14655	0.5119195	0.0000151	-14.0156	0.295	-8.91195	1.908	2402	31
R1G1 2	2.330	9.756	0.14434	0.5119199	0.0000089	-14.0086	0.174	-8.67879	1.866	2333	23
R1G2	4.311	21.865	0.11916	0.5118617	0.0000113	-15.1431	0.220	-7.23329	1.550	1851	20
R1G2 HCL	3.062	14.596	0.12677	0.5118544	0.0000120	-15.2865	0.234	-8.15685	1.649	2009	23
R2G1 1	2.758	11.891	0.14015	0.5119266	0.0000105	-13.8776	0.205	-8.11755	1.815	2202	21
R2G12X	2.174	9.412	0.13956	0.5119162	0.0000193	-14.0799	0.376	-8.26003	1.835	2206	37
R2G2	7.894	35.397	0.13480	0.5119103	0.0000089	-14.196	0.174	-7.88759	1.744	2096	22
R2G2 HCL	0.677	2.613	0.15660	0.5120428	0.0000218	-11.6114	0.425	-7.53369	2.059	2484	51

* Assume a 0.3% error

Table 7: Trace element concentrations obtained for a garnet grain from sample SH-16 analysed by LA-ICP MS.

Element	nist610a	bcr1	spot1	spot2	spot3	spot4	spot5	spot6	spot7	spot8	spot9	spot10	spot11	spot12	spot13
Mg24	464.31	20160	9335.47	7181.32	8265.3	9254.51	7561.17	6569.59	6896.11	6740.91	6341.6	4976.47	4875.4	4898.77	6593.69
Si28	325047	251746	92304.1	76506.4	95215.96	120515	119864	116365	117470	128029	124460	120781	112976.1	113444	121660.1
Ca43	11.45	7.12	2.8	2.8	3.5	5	5.6	5.6	5.6	5.6	5.6	5.6	5.6	5.6	5.6
Sc45	443.88	28.81	79.17	67.97	38.74	60.34	146.56	109.15	93.1	151.01	126.73	113.61	112.5	136.97	197.82
Ti47	437.12	14690.1	194.85	211.15	75.14	156.02	420.44	402.86	356.8	382.73	398.74	467.57	441.7	453.26	435.24
Cr53	407.35	14.79	21.6	44.65	54.8	41.81	49.23	44.37	40.73	52.78	68.62	60	46.2	76.65	58.57
Mn55	434.65	1423.12	187.11	217.46	995.8	1591.37	2449.16	5289.02	3469.6	12310.9	18650.7	21163.3	20355.38	19194.9	10634.42
Sr88	496.29	312.84	0.0112	0.0065	0.0923	0.0492	0.0081	0.0261	0.0389	0.835	0.0697	0.799	0.0303	1.053	0.0248
Y89	455.24	28.15	302.94	154.58	409.09	352.6	78.46	72.73	50.15	146.2	179.2	87.33	101.71	145.15	139.34
Zr90	448.16	163.3	3.49	4.38	0.446	0.771	2.32	2.4	10.59	4.76	143.47	6.19	3.25	468.96	14.85
Nb93	420.68	10.98	0.0094	0.00201	<0.0022	0.0032	0.1214	0.0802	0.045	0.056	0.0543	0.094	0.0712	0.1635	0.12
Ba137	423.11	659.66	0.026	<0.0120	<0.0150	<0.0152	<0.0180	<0.0204	0.038	0.205	0.305	0.074	0.024	0.0316	<0.023
La139	459.79	25.22	<0.00178	0.00053	<0.00176	<0.00154	<0.0026	<0.0022	<0.0023	0.439	0.206	<0.0026	<0.0022	0.008	<0.0040
Ce140	442.88	53.95	<0.00137	<0.00160	<0.00169	<0.00132	<0.00240	0.0071	<0.0015	0.881	0.475	0.0033	0.0043	0.0231	0.0065
Pr141	431.06	6.67	<0.0017	0.00125	<0.00106	<0.00132	<0.0020	<0.00190	<0.0014	0.099	0.0589	0.0022	<0.00106	0.0037	<0.00197
Nd146	437.65	28.05	0.074	0.0554	<0.0086	<0.0107	0.0105	0.013	<0.0090	0.402	0.292	0.031	<0.0095	0.014	0.024
Sm147	457.13	6.15	0.479	0.349	0.079	0.104	0.039	0.067	<0.013	0.283	0.159	0.069	0.05	0.104	0.107
Eu153	464.84	2.037	0.433	0.306	0.0623	0.0908	0.0328	0.0477	0.0367	0.13	0.117	0.0513	0.062	0.0962	0.106
Gd157	430.32	5.64	7	4.38	1.151	1.454	0.69	0.724	0.511	1.71	1.77	0.784	1.119	1.324	1.24
Tb159	449.68	0.991	4.96	2.94	1.179	1.534	0.555	0.563	0.375	1.363	1.334	0.574	0.843	1.067	1.212
Dy163	436.03	5.55	54.86	29.98	26.98	30.16	8.59	8.02	5.73	18.51	20.85	8.15	11.79	16.22	17.34
Ho165	456.71	1.191	12.19	6.47	15.66	13.95	3.16	2.92	2.026	6.12	7.3	3.08	3.79	5.6	5.74
Er167	433.76	3.19	25.21	13.39	79.15	56.48	10.99	10.42	6.61	19.37	23.92	10.86	12.82	18.79	20.06
Tm169	426.17	0.481	2.98	1.567	17.33	10.46	1.966	1.936	1.317	3.36	4.1	1.881	2.066	3.26	3.26
Yb173	471.46	3.23	15.2	8.77	144.95	79.04	15.28	16.06	10.12	25.93	33.15	15.2	16.24	26.72	25.75
Lu175	441.02	0.479	1.504	1.011	21.43	11.91	2.41	2.61	1.5	3.86	5.26	2.31	2.54	4.39	4.03
Hf178	424.86	4.32	0.079	0.125	0.013	0.0139	0.0252	0.0396	0.289	0.097	4.13	0.149	0.076	13.03	0.416
Ta181	380.89	0.646	<0.0019	0.0023	<0.00120	0.0083	0.0416	0.0401	0.0155	0.054	0.0511	0.0494	0.0373	0.1138	0.0501
Pb206	413.17	10.61	0.025	0.018	<0.0123	0.06	0.026	0.0224	0.046	0.207	0.566	0.072	0.066	0.96	0.081
Pb207	416.85	9.61	0.022	0.015	<0.0170	0.06	<0.0187	0.0215	0.017	0.16	0.139	0.078	0.096	0.153	0.045
Pb208	410.96	10.07	0.0143	0.0191	0.0211	0.0602	0.0198	<0.0110	0.01	0.208	0.103	0.067	0.066	0.0867	0.042
Th232	452.13	5.76	<0.0023	<0.0030	<0.00161	<0.0040	<0.0044	0.0048	0.0075	0.065	0.091	0.0361	<0.0034	0.169	0.0276
U238	448.19	1.803	0.008	0.0091	<0.00234	<0.0025	<0.0028	<0.0025	0.0316	0.062	0.859	0.0405	0.0087	1.817	0.0666